

Duquesne University

Duquesne Scholarship Collection

Electronic Theses and Dissertations

Summer 8-7-2021

Identification of Fluoxetine-SERT Interactions and APO-SERT Studies via Crosslinking Mass Spectrometry

Elizabeth Castellano

Follow this and additional works at: <https://dsc.duq.edu/etd>



Part of the [Biochemistry Commons](#)

Recommended Citation

Castellano, E. (2021). Identification of Fluoxetine-SERT Interactions and APO-SERT Studies via Crosslinking Mass Spectrometry (Doctoral dissertation, Duquesne University). Retrieved from <https://dsc.duq.edu/etd/2005>

This Immediate Access is brought to you for free and open access by Duquesne Scholarship Collection. It has been accepted for inclusion in Electronic Theses and Dissertations by an authorized administrator of Duquesne Scholarship Collection. For more information, please contact beharyr@duq.edu.

IDENTIFICATION OF FLUOXETINE-SERT INTERACTIONS AND APO-SERT
STUDIES VIA CROSSLINKING MASS SPECTROMETRY

A Dissertation

Submitted to the Bayer School of Natural and Environmental Science

Duquesne University

In partial fulfillment of the requirements for
the degree of Doctor of Philosophy

By

Elizabeth Castellano

August 2021

Copyright by
Elizabeth Castellano

2021

INDENTIFICATION OF FLUOXETINE-SERT INTERACTIONS AND APO-SERT
STUDIES VIA CROSSLINKING MASS SPECTROMETRY

By

Elizabeth Castellano

Approved December 28, 2020

Michael Cascio
Associate Professor of Chemistry and
Biochemistry
(Committee Chair)

Mihaela Rita Mihailescu
Professor of Chemistry and Biochemistry
(Committee Member)

Michael Van Stipdonk
Associate Professor of Chemistry and
Biochemistry
(Committee Member)

Christopher K Surratt
Associate Dean of Research and
Graduate Programs
Long Island University
(Committee Member)

Phillip Reeder
Dean, Bayer School of Natural and
Environmental Sciences
Professor of Chemistry and Biochemistry

Ellen Gawalt
Chair, Chemistry and Biochemistry
Professor of Chemistry and Biochemistry

ABSTRACT

FLUOXETINE-SERT BINDING INTERACTIONS AND APO-SERT STUDIES VIA CROSSLINKING MASS SPECTROMETRY

By

Elizabeth Castellano

August 2021

Dissertation supervised by Michael Cascio

The serotonin transporter (SERT) is a member of the neurotransmitter sodium symporter family of transporters. SERT controls the magnitude and duration of serotonergic neurotransmission by facilitating the reuptake of serotonin back into the pre-synaptic neuron and is thus a target for antidepressants. Selective serotonin re-uptake inhibitors (SSRIs) such as fluoxetine, are commonly prescribed to treat depression. SSRIs act by blocking reuptake and prolonging serotonin signaling. However, significant problems regarding selectivity and mechanisms of action of these drugs remain unresolved. The structures of SERT and related transporters have been determined and serve as useful structural models. However, they are typically mutated for thermostability and typically lack significant regions of the extracellular loops and the amino- and carboxy-termini and are characterized in the absence of a native-like lipid bilayer. To further understand SERT structure and the interactions involved in fluoxetine binding, herein we present two studies. Aim 1 investigates fluoxetine binding sites of SERT using a photo-activatable fluoxetine

analog and LC-MS/MS in crosslinking studies. Some of the crosslinks observed are consistent with regions forming the central and allosteric sites in the crystal structure. While other crosslinks are novel in that they are in areas of SERT that are unresolved such as the terminal tails. Consistent crosslinks were observed on both N and C terminals, suggesting that they are in close association with the lipid bilayer. Given that fluoxetine partitions in bilayers and might interact non-specifically with membrane proteins, control studies with photo-activatable lipids were also conducted to map lipid accessible sites. Thus, allowing us to differentiate between specific and nonspecific fluoxetine binding. Aim 2 directly interrogates the topology of full-length SERT in lipid vesicles in its resting state by coupling photoaffinity labeling with mass spectrometry (MS). The network of identified crosslinks from introduced single cysteine mutants in the extracellular loops (EL) provides distance constraints and topological information regarding SERT structure in the apo state. Some identified crosslinks were consistent with the recently published crystal structure of human SERT such as crosslinks between EL2 and EL4, which suggest proximity between the two loops. Other crosslinks revealed novel structure information, such as consistent crosslinks to the amino and carboxy terminal domains, thus suggesting that both terminal tails are in close association with the lipid bilayer. Other novel structure information includes modest movements in the N-terminus upon dimerization, and intermolecular crosslinks in mutation S252C which suggest it is located near the dimer interface. Taken together, the studies show that crosslinking mass spectrometry allows for the investigation of local protein structure which can serve as a unique compliment to high resolution structures and for which the benefits will bring us closer to the development of efficient and improved therapeutics.

DEDICATION

This dissertation is dedicated to:

My mother, Lucia De La O, who kept me focused and encouraged me through this journey. Thank you mom for always being there for me, you are my role model. My siblings Jacqueline, Viridiana, Vanessa, and Carlos Alexander who have kept me motivated throughout the years. My daughter Diana Evelyn whose smile and happiness has motivated and comforted me during difficult times. My husband David Castellano whose love, patience, and encouragement has kept me motivated throughout the years. My friends and family who always had words of encouragement.

ACKNOWLEDGEMENT

First and foremost, I thank God for His grace, because without it nothing would be possible. I also thank my advisor Michael Cascio, with your guidance we were able to move this project forward. I thank you for your support and for the opportunity to work alongside you and learn from you.

I thank my committee Dr. Michael Van Stipdonk and Dr. Mihaela-Rita Mihailescu for your guidance and time. Dr. David Lapinsky, Dr. Nageswari Yarravarapu, and Dr. Christopher K. Surratt for functional characterization.

I thank past Cascio lab members for their support: Dr. Rathna Veeramachaneni and Nicholas Ferraro. I also thank past undergraduate Cascio lab members who showed an interest in this project and whom I had the pleasure to mentor. Andre Alexis Orbeta, Brandon Caridi, Henry May, Bailey Curran, Sara Luty, Emily Cooper, Zachary Kelly, and Adam Gargano worked on introducing mutations and prepare protein for mass spectrometry studies. I appreciate your dedication and at times long hours at the lab.

Specifically, I performed all the initial steps of molecular cloning prior to introducing mutations. I worked on some mutations while at the same time mentoring and teaching undergraduates how to introduce other single cysteine mutations and produce bacmid DNA. Some mutations were introduced by me, and other mutations by the undergraduates under my guidance. Mutation S190C was introduced by high school student Israa Abdulmuttaleb during a summer research for high school students. The expression of recombinant protein using *Sf9* insect cells was performed by me. I started the cell line and performed transfection to express protein, three independent protein pellets

were expressed from each mutation, and triplicate trials were performed from each protein pellet. I worked with some pellets and assigned others to a group of undergraduates. Andre was assigned protein pellets from mutation S190C, Brandon worked with pellets from mutation Y232C, Henry and I worked together with pellets from mutation R564C, Bailey and I worked together with pellets from mutation S252C and I worked with pellets from mutation A109C. I showed them how to perform every step involved in protein preparation for mass spectrometry studies, from cell lysis to protein digestion. At times we worked together, while I worked on my pellets and other times (once they understood the process and became independent) they worked on their own under my supervision. I ran all the samples on the ESI-QTOF-MS for MS and tandem MS analysis, and analyzed the data. Sara Luty and Zachary Kelly were involved in the fluoxetine study. Specifically, Sara did the rSERT-PC, fluoxetine studies and Zachary worked on isolating and amplifying recombinant baculovirus and expressing the initial pellets, while I performed the hSERT-fluoxetine studies.

TABLE OF CONTENTS

	Page
Abstract.....	iv-v
Dedication.....	vi
Acknowledgement.....	vii-viii
List of Tables	x-xi
List of Figures	xii-xiii
List of Abbreviations.....	xiv-xv
Chapter 1: Introduction.....	1-24
Chapter 2: Methodology	25-40
Chapter 2.1: SERT-Fluoxetine Interactions.....	25-37
Chapter 2.2: Apo-state SERT Structure.....	37-40
Chapter 3: SERT-Fluoxetine Interactions	41-59
Chapter 4: Apo-state SERT Structure	60-80
Chapter 5: Future Directions.....	81-82
Appendix:	97-119

LIST OF TABLES

	Page
Table 1.1 Binding affinity of several SSRIs	7
Table 1.2 SERT structures to date.....	23
Table 2.1 Oligonucleotide primer pair sequences	38
Table 3.1 hSERT-fluoxetine analog crosslinks.....	47
Table 3.2 rSERT-fluoxetine analog crosslinks	49
Table 3.3 SERT-PC analog crosslinks.....	50
Table 4.1 A109C crosslinks	68
Table 4.2 S190C crosslinks.....	69
Table 4.3 Y232C crosslinks	70
Table 4.4 S252C crosslinks.....	71
Table 4.5 R564C crosslinks	72
Table A.1 A109C dimer crosslinks	110
Table A.2 A109C monomer crosslinks.....	110
Table A.3 S190C dimer crosslinks.....	111
Table A.4 S190C monomer crosslinks	111
Table A.5 Y232C dimer crosslinks	112
Table A.6 Y232C monomer crosslinks.....	112
Table A.7 S252C dimer crosslinks	113
Table A.8 S252C monomer crosslinks	113
Table A.9 R564C dimer crosslinks.....	114
Table A.10 R564C monomer crosslinks.....	114

Table A.11 Internal ion fragments.....	125-132
---	---------

LIST OF FIGURES

	Page
Figure 1.1 Structure of monoamine neurotransmitter serotonin	1
Figure 1.2 Alternating access model	2
Figure 1.3 Structural organization of NSS family of proteins	3
Figure 1.4 SERT function	6
Figure 1.5 Psychostimulants	10
Figure 1.6 Peptide fragmentation pattern via collision induced dissociation	16
Figure 3.1 SERT transmembrane domains	42
Figure 3.2 Structure of fluoxetine analog	44
Figure 3.3 Structure of diazirine phosphatidylcholine analog	44
Figure 3.4 Representative MS and MSMS spectrum of precursor and product ion scan.	46
Figure 3.5 hSERT-fluoxetine analog crosslinks	48
Figure 3.6 rSERT-fluoxetine analog crosslinks	49
Figure 3.7 SERT-PC analog crosslinks	50
Figure 3.8 Summary of SERT crosslinks to fluoxetine and PC analog	51
Figure 4.1 Structure of bifunctional crosslinker	61
Figure 4.2 SERT mutations and MS coverage for S252C	62
Figure 4.3 Top-down view of SERT	65
Figure 4.4 A109C crosslinks	68
Figure 4.5 S190C crosslinks	69
Figure 4.6 Y232C crosslinks	70
Figure 4.7 S252C crosslinks	71

Figure 4.8 R564C crosslinks.....	72
Figure 4.9 Network of crosslinks to intracellular and extracellular loops	77
Figure A.1 N1 Trial 1 at retention time 3.477	115
Figure A.2 N1 Trial 1 at retention time 3.557	115
Figure A.3 N1 Trial 2 at retention time 3.733	116
Figure A.4 N1 Trial 2 at retention time 3.822	116
Figure A.5 N1 Trial 3 at retention time 3.47	117
Figure A.6 N1 Trial 3 at retention time 3.62	117
Figure A.7 N1 Trial 3 at retention time 3.735	118
Figure A.8 N1 Trial 3 at retention time 3.873	118
Figure A.9 N2 Trial 2 at retention time 3.855	119
Figure A.10 N2 Trial 2 at retention time 4.035	119
Figure A.11 N2 Trial 3 at retention time 3.765	120
Figure A.12 N2 Trial 3 at retention time 3.796	120
Figure A.13 N3 Trial 1 at retention time 3.385	121
Figure A.14 N3 Trial 1 at retention time 3.518	121
Figure A.15 N3 Trial 2 at retention time 3.445	122
Figure A.16 N3 Trial 2 at retention time 3.557	122
Figure A.17 N3 Trial 3 at retention time 3.6	123
Figure A.18 N3 Trial 3 at retention time 3.741	123
Figure A.19 N3 Trial 3 at retention time 3.483	124
Figure A.20 N3 Trial 3 at retention time 3.515	124

LIST OF ABBREVIATIONS

- CID:** Collision induced dissociation
- Cryo-EM:** Cryo-electron microscopy
- CX-MS:** Crosslinking mass spectrometry
- DAT:** Dopamine transporter
- dDAT:** *Drosophila melanogaster* dopamine transporter
- ECD:** Electron capture dissociation
- EL:** Extracellular loop
- ESI:** Electrospray ionization
- ETD:** Electron transfer dissociation
- FT-ICR:** Fourier transform ion cyclotron resonance
- HEK-293:** Human embryonic kidney cell line 293
- hDAT:** Human dopamine transporter
- HDX-MS:** Hydrogen deuterium exchange mass spectrometry
- HPLC:** High performance liquid chromatography
- hSERT:** Human serotonin transporter
- IL:** Intracellular loop
- K_D:** Equilibrium dissociation constant
- K_i:** Dissociation constant
- LeuT:** Leucine transporter
- LIT:** Linear ion trap
- MALDI:** Matrix assisted laser desorption/ionization

MS: Mass spectrometry

MSMS: Tandem mass spectrometry

MTS: Methanethiosulfonate

nAChR: Nicotinic acetylcholine receptor

NET: Norepinephrine transporter

NHS: N-hydroxysuccinimide

NSS: Neurotransmitter sodium symporter

PA: Phosphatidic acid

PC: Phosphatidylcholine

PIP₂: Phosphatidylinositol 4,5-biphosphate

PPIs: Protein-protein interactions

PS: Phosphatidylserine

PTMs: Post translational modifications

QTOF: Quadrupole time of flight

rSERT: Rat serotonin transporter

SERT: Serotonin transporter

SLC6: Solute carrier 6

SSRIs: Selective serotonin reuptake inhibitors

TCAs: Tricyclic antidepressants

TM: Transmembrane

TOF MS: Time of flight mass spectrometry

5-HT: 5-Hydroxytryptamine

Chapter 1: Introduction

1.1 Serotonin

Serotonin (5-hydroxytryptamine or 5-HT) is a monoamine neurotransmitter (Figure 1.1) that modulates the activity of the central nervous system. Serotonin is synthesized from L-tryptophan, which is catalyzed by enzyme tryptophan 5-hydroxylase to form 5-hydroxytryptophan, which is then converted to serotonin by L-amino acid decarboxylase [2]. In serotonergic neurons, the end-product of the action potential is serotonin exocytosis from pre-synaptic serotonergic neurons into the synapse where it interacts with serotonin receptors, ligand-gated ion channels and a group of G-protein-coupled receptors in the membrane of post-synaptic neurons to propagate the signal [1]. Dysregulation of 5-HT concentration in the synapse is involved with a wide range of physiological functions such as sleep, mood, appetite, cognition, pain, hunger, motor activity, aggression behavior and hormone secretion [3].

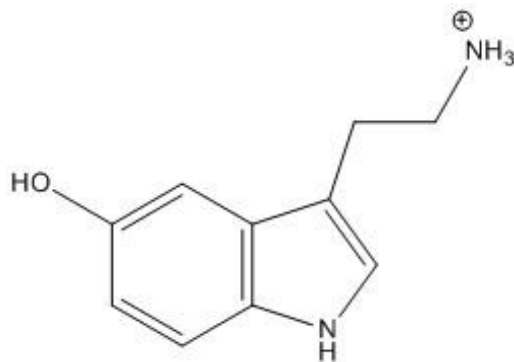


Figure 1.1: Structure of monoamine neurotransmitter serotonin

1.2 Serotonin Transporter

The serotonin transporter (SERT) is a member of the neurotransmitter sodium symporter (NSS) family (also known as SLC6). The SLC6 family of proteins consists of multiple proteins [4-7], however three stand out as a distinct family: the dopamine transporter (DAT), norepinephrine transporter (NET), and the serotonin transporter (SERT). DAT, NET and SERT all share structural and mechanistic properties [8]. They utilize electrochemical gradients to transport their respective monoamine substrates from the synapse to presynaptic neurons, against their concentration gradient [6]. SERT is responsible for serotonin re-uptake [9] by coupling the entry of 5-HT to the entry of Na^+ and Cl^- and the exit of K^+ to move serotonin against its concentration gradient into presynaptic neurons [4, 10]. SERT follows an alternating access mechanism for ion/substrate symport, wherein gates that open intracellularly and extracellularly do so in an alternating fashion. Here, the ion flux is controlled by keeping one of the two gates always closed (Figure 1.2). In the “alternating access” model, the transporter may be outward-facing, occluded or inward-facing [11].

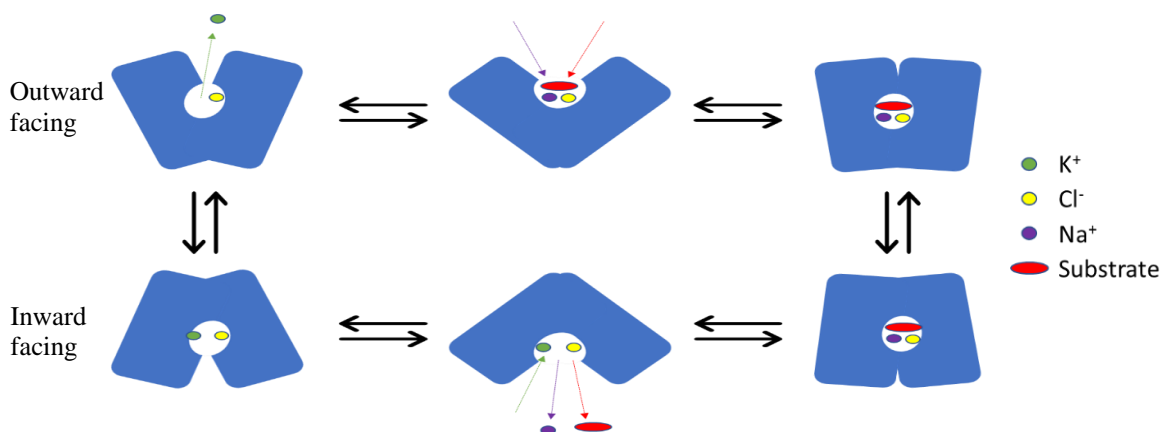


Figure 1.2 Alternating access model

The outward facing conformation allows for the entry of substrate and ions into the binding site. The occluded conformation restricts binding pocket access. The inward facing conformation allows for the release of substrate and ions inside the cell.

Studies have revealed that the NSS family of proteins contain an inverted topology repeat. SERT consists of 12 transmembrane (TM) domains with a pseudo-symmetry arrangement of helices TM 1-5 and TM 6-10 with respect to the plane of the membrane (Figure 1.3) [12] [11]. This pseudo 2-fold symmetry arrangement allows the ligand to enter and exit the binding site thus creating a pathway for transport [13, 14].

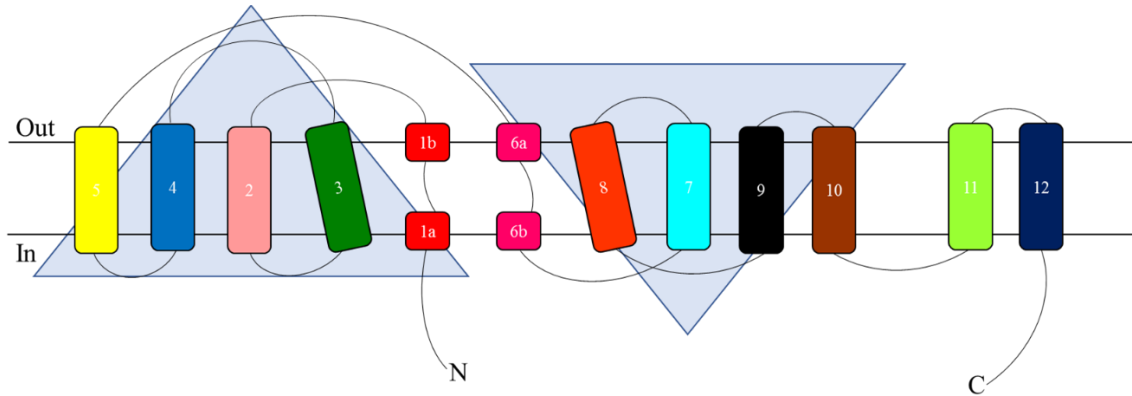


Figure 1.3 Structural organization of NSS family of proteins

Pseudo-symmetrical arrangement of helices 1-5 and 6-10 depicted by inverted blue triangles.

This inverted topology repeat is also observed across a variety of membrane proteins including primary active transporters [15], secondary transporters [16], and channels [17]. Bioinformatic studies have revealed that the pseudo-symmetry arrangement is the result of an evolutionary pathway. Such studies provide evidence that protein topology as we know it today, is the result of amino acid substitutions occurring over evolution, as well as gene fusion, splicing, and deletion events [18].

1.3 Resolved Structures of SERT and its Homologs

Historically, structure information of NSS proteins has been guided by studies on the bacterial homolog *Aquifex aeolicus* leucine transporter (LeuT) and *Drosophila melanogaster* dopamine transporter (dDAT). LeuT, has a 20-25% sequence identity to SERT [14] and was crystallized by Dr. Yamashita and colleagues in 2005 [19]. LeuT has been crystallized in three distinct conformations supporting the alternative access mechanism [19, 20]. dDAT was crystallized bound to the tricyclic antidepressant nortriptyline in 2013 [21]. Nortriptyline stabilizes dDAT in an outward-open conformation by binding halfway across the membrane bilayer and blocking dDAT from adopting the occluded state [21]. dDAT has a greater than 50% sequence identity with mammalian DAT homologs and thus it has served as a powerful tool to understand SERT [21-23]. The norepinephrine transporter (NET) is responsible for the reuptake of epinephrine from the synapse to presynaptic neurons. There is currently no crystal structure of NET however human NET, bovine NET and rat NET have been cloned and studied extensively [24-28].

In 2016, human SERT (hSERT) was crystallized bound to the antidepressant citalopram [29]. Analogous to dDAT bound to nortriptyline, citalopram stabilizes hSERT in an outward-open conformation with the antidepressant drug bound halfway across the membrane bilayer. When bound to the drug, the conformations of TM1 and TM6 are incompatible with the formation of the occluded state thus blocking SERT from adopting the occluded state. The location of the allosteric site was also identified, interposed between extracellular loops 4 and 6 and transmembrane helices 1, 6, 10, and 11.

In 2018, human SERT was crystallized bound to sertraline, fluvoxamine and paroxetine [30]. The study revealed that all three antidepressant drugs bind to the central

binding site and that they stabilize SERT in an outward-open conformation. The structures also show that residues within the central binding site can adopt different conformations to mediate selectivity. The study also revealed that a mutation at Thr³⁷¹ prevents closure of the extracellular gate. Interestingly, this residue is equivalent to Thr³⁵⁶ in DAT, an autism related mutation [30, 31].

In 2019, SERT-ibogaine complexes were captured in outward-open, occluded, and inward-open conformations using cryo-electron microscopy (cryo-EM). The cryo-EM structures revealed that ibogaine, a non-competitive inhibitor of transport, binds to the central binding site and that TM1 and TM6 appear to undergo large movements during the closing of the extracellular gate. Changes to TM1 were also observed during opening of the intracellular gate along with partial unwinding of TM5 [32].

More recently in 2020, the structure of SERT bound to paroxetine analogs was determined using single particle cryo-EM and x-ray crystallography [33]. The exact binding pose of paroxetine in the central site is still a controversy. It is believed that the central binding site is composed of three subsites: A, B, and C [34]. Some studies suggest that paroxetine binds to SERT following an ABC pose mechanism. Here, the piperidine ring binds to subsite A, while the benzodioxol group binds to subsite B and the fluorophenyl groups bind to subsite C [29, 30]. Other studies suggest that binding occurs following an ACB pose mechanism, where the benzodioxol group binds to subsite C, while the fluorophenyl group binds to subsite B [35, 36]. It is believed that the ABC pose is preferred over the ACB pose. However, the possibility that an ACB pose can still occur has not been excluded.

1.4 Selective Serotonin Reuptake Inhibitors (SSRIs)

SERT affects the magnitude and duration of the serotonergic signaling [37] and this makes it a target for the development of antidepressants. Typical depression drug treatments include tricyclic antidepressants (TCAs) and selective serotonin re-uptake inhibitors (SSRIs). TCAs and SSRIs function by binding to SERT to inhibit re-uptake of 5-HT, thus extending serotonergic signaling [30]. As SERT is blocked, the relative 5-HT concentration in the synapse increases (Figure 1.4). TCAs were among the earliest developed antidepressants; they are highly effective, however they are not selective for SERT and act on NET [38] and the acetylcholine receptor which can lead to serious cardiovascular complications [39, 40]. SSRIs are among the most frequently used due to their relatively high selectivity for SERT and limited off target receptors [28]. However, despite SSRIs high selectivity, they can bind to the homologous transporters NET and DAT, although with much lower affinity [24, 41].

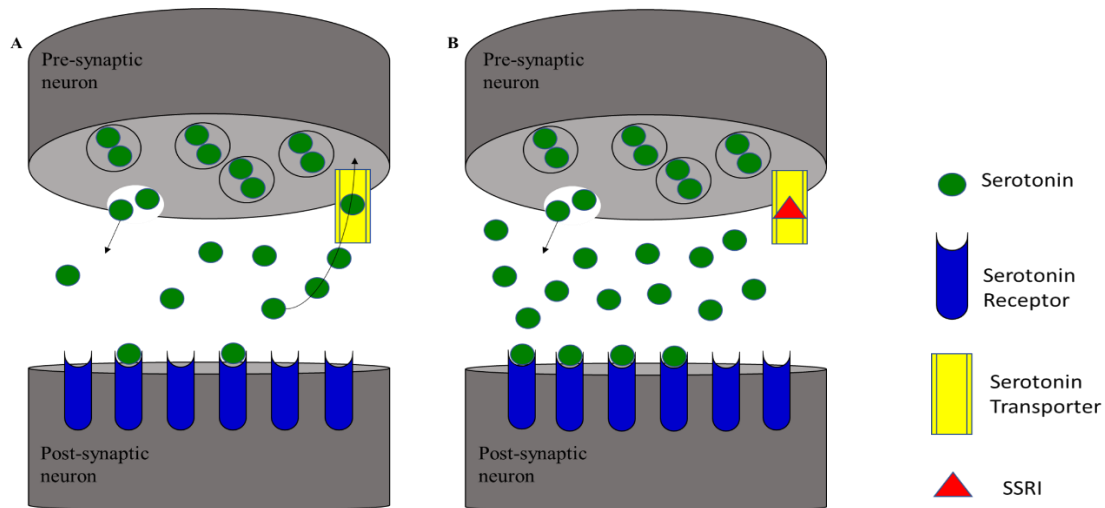
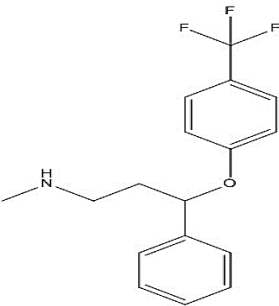
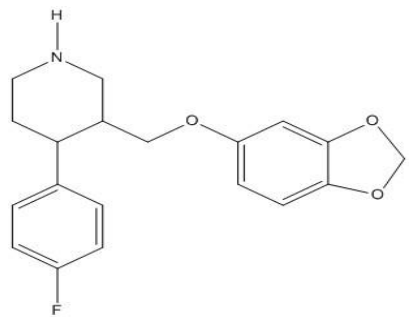
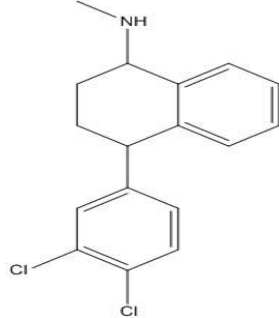
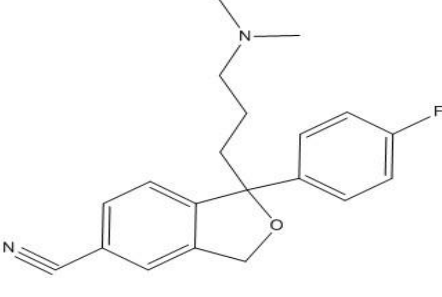


Figure 1.4 SERT function

(A) Serotonin transporter (SERT) reuptakes serotonin from the synapse to the presynaptic cell (B) SSRIs bind to SERT to block reuptake of serotonin causing an increase in serotonin concentration in the synapse.

SSRIs have varying chemical structures (Table 1.1) and as a result they possess substantial pharmacological differences [42]. Paroxetine is the most potent SSRI with the highest known binding affinity for the central binding site [43, 44] (Table 1.1). However, paroxetine is associated with serious side effects such as infertility, cardiovascular issues, birth defects, sexual dysfunction, and suicide [45]. Despite years of research, antidepressants continue to carry serious side effects. Citalopram is associated with insomnia, paroxetine with weight gain, sertraline and fluoxetine cause gastrointestinal problems, anxiety, insomnia. Fluvoxamine is associated with dangerous drug interactions and highest frequency of gastrointestinal problems [46-49]. Fluvoxamine and paroxetine have the highest discontinuation rates due to their side effects in clinical trials [50].

Table 1.1 Binding affinity of several SSRIs

<p>Fluoxetine (Prozac) K_D: 0.81nM, K_i: 1.1nM</p> 	<p>Paroxetine (Paxil) K_D: 0.13nM, K_i: 0.10nM</p> 
<p>Sertraline (Zoloft) K_D: 0.29nM, K_i: 0.26nM</p> 	<p>Citalopram (Celexa) K_D: 1.16nM, K_i: 1.6nM</p> 

Equilibrium dissociation constant (K_D) and inhibition constant (K_i) for various SSRIs to human SERT. K_D and K_i values adapted from Renoir (2013).

Advances in molecular modeling has provided new pathways towards drug discovery and design to improve today's therapeutics. Wasko and co-workers [51] developed computational methods for the purpose of designing new antidepressant drug compounds. This approach utilizes fragment-based drug design methods in which small fragments are introduced into the binding pocket (explained in more detail in section 1.6) to serve as starting points prior to "growing" the drug candidate. This method offers a fast and low-cost alternative for drug discovery. Nolan and co-workers [52] used a virtual screening method followed by *in vitro* pharmacology studies to identify SERT inhibitors, leading to the identification of an inhibitor with a modest affinity for hSERT ($K_i = 284$ nM) and, proving that this approach is a powerful tool for identifying novel inhibitors.

1.5 Psychostimulants

SERT is not only the target for antidepressant medications but also psychostimulants such as cocaine, ibogaine, and methamphetamine (Figure 1.5). Cocaine is derived from the leaves of the *Erythroxylum coca* plant which is indigenous to South America, Indonesia, Mexico and the West Indies [53]. Cocaine is a psychostimulant that increases locomotor activity and euphoria sensation [54] by blocking SERT, NET and DAT to prevent reuptake of their respective monoamines [55]. Cocaine stabilizes SERT in outward-facing conformation [56]. In some cases, users experience paranoia episodes [57]. Cocaine can affect all body systems; among the most severe complications are seizures, aortic dissection, hemorrhagic and ischemic strokes, acute renal injury, myocardial infarction, and multiple organ failure [58]. Ibogaine is a natural occurring psychoactive substance derived from the roots of the African plant *Tabernanthe iboga* [59]. Ibogaine

can interact with numerous brain targets including glutamate receptors, nicotinic receptors, and neurotransmitter transporters such as SERT [60, 61]. Ibogaine stabilizes SERT in an inward-facing conformation [62]. Ibogaine has been reported to have anti-addiction properties and has been used in patients with substance abuse disorders to reduce craving and relapse rates [63]. However, evidence of the safety and efficacy of ibogaine in anti-addiction therapy is lacking. Clinical trials have shown that ibogaine is associated with significant neurologic and cardiac effects such as cardiac dysrhythmias, seizures, hallucinations, and depression [64] and, in some cases, sudden death [65]. Methamphetamine, unlike cocaine and ibogaine, is a man-made substance derived from amphetamine [66]. Amphetamines were commonly used in the 1930s to treat a broad range of disorders such as narcolepsy, depression, and behavioral problems in children (now known as ADHD) [67-69]. Since then, amphetamines have transformed from easily available drugs into highly restricted substances [70]. Methamphetamine is a highly addictive substance that targets many areas in the brain with a high level of neurotoxicity [71]. Studies examining the effects of methamphetamine have identified degeneration of dopamine nerve fibers, loss of tyrosine hydroxylase, tryptophan hydroxylase, loss of serotonin-immunoreactive axons and axon terminals [71-74]. At high levels, methamphetamines can cause anxiety, hallucinations, psychosis, psychomotor impairment, seizures, cerebrovascular hemorrhage, cerebral edema, myocardial infarction due to heatstroke, and death [73, 75, 76].

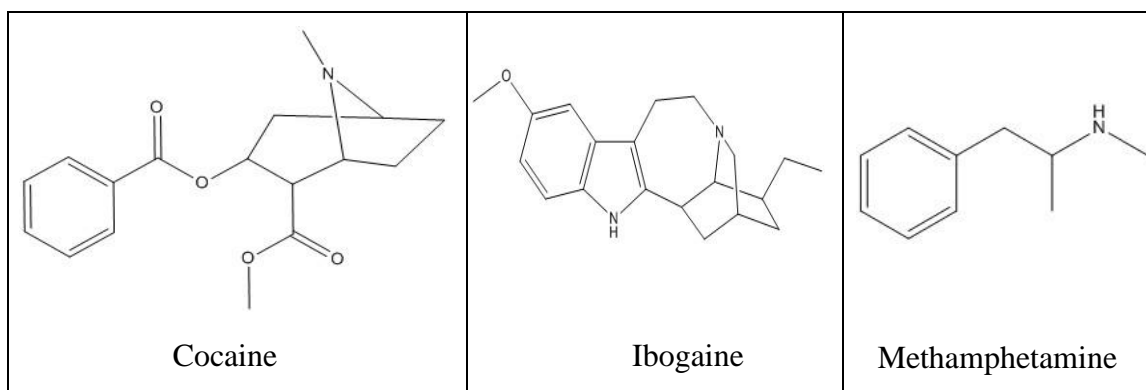


Figure 1.5 Psychostimulants

Structures of psychostimulants that target SERT

1.6 SERT's binding pockets

Prior to the crystallization of SERT, computational models were built to develop the first structure based pharmacophores using the x-ray coordinates of LeuT [77-79]. Ligand docking experiments using cocaine and amphetamine models revealed potential binding pockets [80], and suggested that the binding site for cocaine overlaps with the binding site of dopamine in DAT [81]. DAT molecular modeling studies showed a ligand binding pocket midway through the lipid bilayer, the S1 site [82]. Subsequent mutagenesis and ligand docking studies revealed a second binding site, S2 for DAT located above S1 [79, 83].

The central S1 site is near the midpoint of the lipid bilayer and at the center of the transmembrane domain, while the S2 allosteric site lies in the extracellular vestibule above S1 [84]. Computational studies have suggested that S2 serves as an initial binding site before substrate translocation to S1 via conformational changes [79]. The position of the S1 binding pocket is supported by mutational analysis paired with structure-activity data and drug affinity studies [85-87]. In addition, multiple antidepressants including SSRIs and

certain TCAs have been shown to reach the S1 pocket [38, 88]. Computational studies using the bacterial homolog LeuT, suggested that access to S1 is controlled by TM1-TM10 ionic interactions and TM3-TM6 hydrophobic bridges [84]. hSERT bound to citalopram was crystallized in 2016 by Coleman *et al.* [29] and it was observed that hSERT exhibits an outward-open conformation with the drug bound to the central site, halfway across the membrane lodged into a cavity consisting of residues from TM1, TM3, TM6, TM8 and TM10, with the location of the allosteric site located between EL4 and 6 and TM helices 1, 6, 10 and 11.

1.7 Effects of lipid composition

Lipid composition can greatly affect activity of membrane proteins, and they can modulate transmembrane proteins through a variety of interactions: hydrogen bonding, charge interactions, hydrophobic interactions, altering membrane fluidity, etc. [89]. Multiple studies have shown evidence of lipid interactions with SERT. For instance, studies by Magnani *et al.* show that SERT associates with lipid rafts and that disaggregation of lipids rafts inhibits SERT activity [90]. In addition, computational studies have suggested that phosphatidylinositol 4,5-biphosphate (PIP₂) interact with the terminal tails of the transporter [91]. It is known that lipid interaction is important for activity, but specific sites of interactions are yet to be revealed.

In addition, lipid composition is of great interest for its role on oligomeric state. There is growing evidence that SERT forms a broad distribution of oligomerization ranging from monomers up to pentamers [92, 93]. Single-molecule fluorescence microscopy studies have shown that stabilization of SERT oligomeric complexes are mediated by direct

interactions to phosphatidylinositol-4,5-biphosphate (PIP₂) [92]. Thus, it is essential to conduct studies of SERT in a complete and functional state to fully understand SERT-drug binding sites and structure, and CX-MS allows us to conduct such studies.

1.8 Chemical protein modifications

Chemical modifications of proteins are common in cells and play key roles in cellular processes such as trafficking, differentiation, signaling and migration [94]. The reproduction of chemical modifications of proteins in a highly efficient and controlled way has proven to be an invaluable tool in proteomics. Classic protein modification methods rely on reactions with nucleophilic amino acids such as cysteine and lysine residues. Prior to the elucidation of SERT structure by x-ray crystallography, Chen and coworkers [10] mapped the reactivity of three cysteine residues predicted to be in the extracellular surface of SERT using methanethiosulfonate (MTS) reagents and site-directed mutagenesis. MTS reagents react with free cysteine residues and form a disulfide between the cysteine sulfur and the reagent. Hence, if the cysteine residue were reactive the modification could alter normal protein function. However, if the cysteine were inaccessible, no functional changes would occur. The results of this study predicted the disulfide bond between C200 and C209 in the second extracellular loop. In later years, Androutsellis-Theotokis and coworkers [95] examined cysteine residues in the internal surface of SERT that were responsible for the inactivation of 2- β -carbomethoxy-3- β -(4-[¹²⁵I]iodophenyl)tropane (β -CIT) binding, a high affinity cocaine analog, by MTS reagents in membrane preparations. For this study, a mutant SERT was prepared (X8C), in which eight active cysteines were replaced by other amino acids (at positions 15, 21, 109, 147, 155, 357, 522, and 622), while retaining

significant binding activity and transport. X8C was further modified by restoring each mutated cysteine back into the construct. HeLa cells expressing SERT were assayed for serotonin transport activity or β -CIT binding activity with or without 2-(aminoethyl) methanethiosulfonate hydrobromide (MTSEA). The transport and binding activities of all mutants was assayed. X8C retained $31.9 \pm 3.8\%$ transport activity and $55.8 \pm 6.3\%$ binding activity. The results of the study showed that C357 at the third intracellular loop is a reactive cysteine and that it is sensitive to conformational changes resulting from ligand and ion binding.

1.9 Photo-crosslinking coupled with tandem mass spectrometry

1.9.1 Crosslinking

Structure determination of proteins and identification of protein-protein interactions (PPI) are key to understanding protein function [96]. PPI maps can provide a framework for better understanding all biological systems as it serves as a “skeleton” for its signaling circuitry [97]. Molecular chaperone proteins are an example of a multi-complex assembly where several components work in a coordinated matter to assist in protein folding [98]. For decades, crosslinking methods have been used to study PPI and protein structure [99, 100]. Under physiological conditions PPI are short lived and hence are difficult to study. Crosslinking allows for this short-lived reaction to be captured by covalently binding them together for subsequent characterization [101, 102]. Despite the high complexity of proteins, only a small number of functional groups account for the majority of targets in crosslinking methods: primary amines, carboxyls, carbonyls, and sulfhydryls (thiols) [103].

Crosslinking studies can be performed *in vivo* or *in vitro*. For *in vitro* crosslinking, cells are homogenized and lysed. *In vitro* crosslinking studies on chaperone proteins have revealed how chaperones interact with proteins, and protein complexes to assist in protein folding [104, 105]. For *in vivo* crosslinking, proteins are crosslinked inside the cell. Freinkman *et al.* conducted *in vivo* crosslinking studies to obtain insight into protein interactions in Gram-negative bacteria [106]. Lipopolysaccharides are transported to the outer membrane of gram-negative bacteria, but the process was poorly understood. Freinkman *et al.* used unnatural amino acid mutagenesis and crosslinking to show that LptD and LptE interact. They introduced a UV-photocrosslinker *para*-benzoyl-L-phenylalanine at 27 positions throughout LptE, and subsequent UV light exposure of living cells captured LptE-LptD interactions.

Formaldehyde crosslinking can be used to crosslink DNA-binding proteins to DNA *in vivo* and *in vitro* [107, 108]. However, although the chemistry for formaldehyde crosslinking is well known, the *in vivo* aspects behind the technique are still not fully understood [109]. Nevertheless, it has been shown to successfully crosslink accessible lysine residues, making it a crosslinker of choice for trapping protein-DNA complexes due to lysine residues being common mediators of interactions with DNA [110].

1.9.2 Mass Spectrometry

Major advances in mass spectrometry has transformed this instrument into an indispensable tool for scientists in proteomics research and their efforts to characterize cellular function [111, 112]. Mass spectrometers consist of an ion source that converts analyte molecules into gas-phase ions, a mass analyzer that sorts ionized analytes according to their mass to charge ratio (m/z) and a detector that records the ions [111]. Finally a “mass

spectrum” plot is generated which comprises of ion abundance against m/z [113]. Mass spectrometry (MS)-based proteomics can be performed on intact protein (top-down proteomics) or on digested peptides (bottom-up proteomics), with each method having their own advantages and disadvantages [114]. In general there are 4 stages: protein preparation, chromatographic separation, mass spectrum of peptides is recorded and, a list of peptides is generated [115].

In proteomic research, soft ionization methods are commonly employed such as electrospray ionization (ESI) and matrix-assisted laser desorption/ionization (MALDI) [116, 117]. In MALDI, the analyte is embedded into a UV absorbing matrix, upon radiation by a laser pulse, an analyte-matrix mixture is produced, and vaporization of the matrix carries the analyte with it [118]. In ESI, the analyte is in solution. The volatile liquid is emitted towards an electrode under vacuum, upon solvent evaporation, the drop then decreases in volume producing smaller droplets and finally results in charged ions entering the gas phase [117]. Once the analyte is ionized, ions are separated according to their m/z ratio by the mass analyzer, commonly a quadrupole, time of flight, or orbitrap [119]. In tandem MS, a collision cell is incorporated for fragmentation.

Fragmentation techniques include collision-induced dissociation (CID), electron capture dissociation (ECD), and electron transfer dissociation (ETD) [120]. CID is the most common fragmentation technique employed in the study of peptides and proteins [121]. In CID, precursor ions collide with neutral gas molecules causing bond cleavage and product ion formation [122]. Typically, breakage occurs through the lowest energy pathway at the amide bond, producing “b” and “y” ions (defined as a “b” ion if the charge is at the amino terminal fragment, or “y” if the charge is at the carboxy terminal fragment). In addition,

“a” ions can be formed upon fragmentation (cleavage between the alpha and carbonyl backbone carbons), though this occurs less frequently than by and y ion products (Figure 1.6) [123].

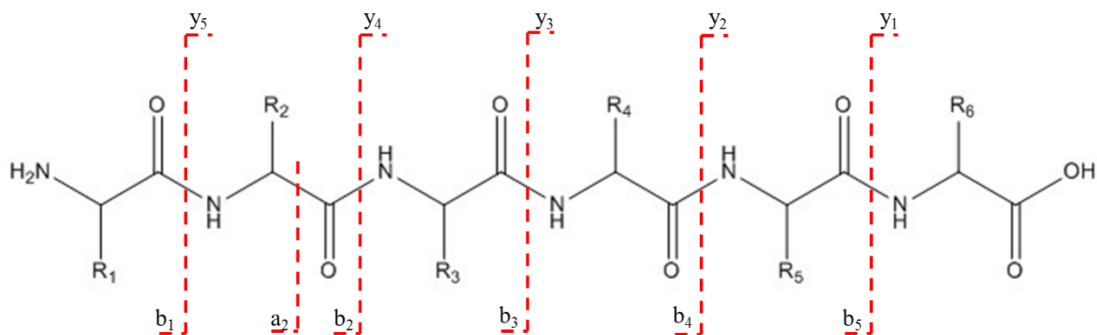


Figure 1.6 Peptide fragmentation pattern via collision induced dissociation.

CID typically forms “b”, “y” ions and, though less occurring, “a” ions.

Mass analyzers commonly used in proteomics are the quadrupole, the ion trap, and time-of-flight (TOF) [111]. They vary in their physical principles and performance. The quadrupole consists of four parallel rods, one pair applies radio frequency (RF) voltage while the other pair applies direct current (DC) voltage. Inside the quadrupole RF and DC voltages are combined and at a given combination ions of a particular m/z ratio are allowed to travel through the quadrupole into the detector while other ions collide against the rods and don’t reach the detector [124]. A linear series of three quadrupoles is known as the triple quadrupole mass spectrometer, where the first and third quadrupoles are used as filters while the second quadrupole is used as a collision cell. The triple quadrupole is an efficient tool for tandem mass spectrometry.

Ion traps utilize oscillating electric field to “trap” ions. There are different types of ion traps such as linear ion trap (LIT), Fourier transform ion cyclotron resonance (FT-ICR), and orbitraps [125]. LIT consist of a quadrupole with hyperbolic rods cut into three

segments. It can be used as mass filter or as a trap. To operate as a trap, the rods apply RF voltage and the electrodes of slightly higher potential located at both ends create a trapping potential well that prevents ions from escaping [126]. To operate as an analyzer, the rods apply a DC voltage to create an axial trapping field, RF voltage is supplied to deliver a radial trapping field, and AC voltage is applied for ion isolation, activation and ejection [127]. Linear ion traps are also capable of precursor ion selection for tandem MS experiments. FT-ICR mass spectrometers consist of an ICR cell composed of two trapping plates, two excitation plates, and two detector plates arranged in a cube-like shape and surrounded by a strong magnetic field [128]. Superconducting magnets are used to provide a strong magnetic field, thus making FT-ICR the most expensive mass spectrometers by far. Ions affected by the magnetic field move in an orbital motion known as “cyclotron motion” and the frequency of this motion is inversely proportional to the m/z ratio of the ion. As the RF voltage is applied, ions accelerate bringing them closer to the detector plates. The image current is then deconvoluted by Fourier transformation and the m/z ratio is determined [128, 129]. Orbitraps are the newest type of mass analyzers that use Fourier transformation technology, and it was invented by Dr. Makarov in 1999 [130]. The orbitrap consists of an outer barrel-like electrode and an inner spindle-like electrode. Voltage is applied between the electrodes creating an electric field that traps ions in an orbital motion around the central spindle. Mass to charge values are measured from the frequency of harmonic ion oscillations by Fourier transformation [131].

Time-of-flight (TOF) mass analyzers separate ions based on the time it takes for them to travel through a flight tube. Ions are accelerated by an electric field into the flight tube. Here all the ions start to travel through the flight tube at the same time with the same

kinetic energy but reach the detector at different times due to their masses. Essentially, lighter ions will arrive to the detector first then the heavier ions [132]. The first TOF mass analyzers were linear and though they offered fast scan rates and an unlimited m/z limit, the resolution was poor. TOF analyzers greatly improved with the incorporation of “delayed extraction” of ions leaving the source, and reflectrons which correct the initial energy spread, hence increasing resolving power [133]. To enhance performance, “hybrid” instruments have been designed. For instance, early quadrupole mass analyzers were capable of only unit resolution, but the coupling of quadrupole and time-of-flight (QTOF) analyzers provide higher resolution up to 0.01 Da [129].

1.9.3 Crosslinking Mass Spectrometry (CX-MS)

CX-MS offers the capability of analyzing three-dimensional structure of proteins and mapping protein-protein interactions [134]. Over the years, many types of crosslinkers have been developed. Conventional crosslinking reagents contain two reactive sites connected through a spacer, typically an alkyl chain [135, 136]. Homobifunctional crosslinkers contain identical functional groups at both reactive sites. Whereas heterobifunctional crosslinkers contain two different reactive groups that target different functional groups. The amine-reactive N-hydroxysuccinimide (NHS) ester crosslinker reacts with nucleophiles to release the NHS and create a stable amide with primary or secondary amines. NHS esters have successfully been used to probe structure of proteins in living cells [137]. Maleimides are sulfhydryl-reactive cross-linkers with little activity to amines thus making them valuable for intramolecular crosslinks [138]. Photoreactive crosslinkers react with their target by exposure to UV light [139]. This tool has been widely

used in drug discovery to identify drug targets, molecular interactions, and for probing binding sites [140]. This is particularly useful in that it can convert short lived interactions between molecular target with a drug candidate into permanent bonds [141]. Benzophenone photoprobes can be activated at safe wavelengths of 350-360 nm, which cause no harm to proteins, and can react in the presence of water and bulk nucleophiles thus making them highly efficient [142]. Benzophenones create a biradical upon UV exposure, which undergoes a hydrogen radical abstraction and form a new C-C bond [136]. Currently, there is a library of crosslinkers available that vary in spacer length and reactive groups. Some crosslinkers contain groups used as purification or detection handles [143-145]. Young *et al.* [146] used an amine specific homobifunctional crosslinker (bis(sulfosuccinimidyl) suberate) to probe the tertiary structure of bovine fibroblast growth factor protein. Lysine residues were crosslinked, trypsinized, and analyzed using HPLC-QTOF-MS and MALDI. The study generated distance constraints that allowed for the refinement of protein models. Analysis of crosslinked peptides by mass spectrometry offers several advantages such as: (1) unlimited protein/protein complex mass because it is the proteolytic peptides that are analyzed, (2) fast analysis, (3) only requires small amounts of sample, (4) the broad range of crosslinking reagents offer varying specificities towards certain functional groups, and a wide range of distances [136]. Advances in chromatography separation and sample enrichment methods has made the study of low abundant crosslinked peptides, compared to unmodified peptides, by crosslinking mass spectrometry (CX-MS) a popular tool in proteomics [99, 147-149]. Recently, CX-MS has found to be suitable for the analysis of an array of *in vivo* and *in vitro* applications of not only large protein complexes but also at the proteome scale [150].

Crosslinking experiments have been used to study not just protein-ligand interactions but also allosteric modulation in proteins and oligomerization [151-153]. Protein dynamics and allostery are difficult to study using high resolution structure methods like crystallography due to their dynamic nature. However, the integration of crosslinking with the high sensitivity, high mass resolution and high mass accuracy advantages in mass spectrometry has emerged CX-MS as a powerful tool in proteomics [154]. CX-MS can serve as a complementary tool to high resolution structure studies and in modeling dynamic regions of proteins. For example, Liu *et al.* analyzed intra- and inter-subunit crosslinks of trypsinized peptides by MALDI-TOF MS to study the extracellular domain of the glycine receptor [155]. The crosslinking constraints were used to validate and refine allosteric models. CX-MS has also proven to be an essential tool in pharmaceutical chemistry. CX-MS studies have been used to probe allosteric changes due to protein-drug interactions [156]. The coupling of crosslinking with mass spectrometry provides advantages that provide insights into complete systems with great degree of detail and sensitivity in a timely manner [157].

CX-MS has also proven to be useful when studying complex post-translational modifications (PTMs). Chavez *et al.* [158] utilized CX-MS to obtain topology measurements on post-translationally modified histone proteins *in vivo*. Proteins on HeLa cells were crosslinked with BDP-NHP-PIR crosslinker which contains a biotin affinity tag for enrichment purposes, and two CID cleavable bonds to release cross-linked peptides. Crosslinked peptides were then trypsinized and analyzed using a UPLC coupled with FTICR Ultra hybrid mass spectrometer. In the study, 115 crosslinks were detected, for which 56 were found to contain at least one post-translational modification. Their results

shine a light into the topology of core histone protein H3 as it is altered with varying PTMs. For instance, some crosslinks were only observed when protein was unmodified, while other residues were only crosslinked when protein was modified by mono-, di-, or trimethylation. Unique crosslinks were also observed when histone H3 was modified by acetylation. The information provided by this study brought to light the structure and orientation of nucleosome complexes *in vivo*.

Affinity-tagged crosslinking reagents have been developed to allow for purification of proteins of interest and enrichment of low abundant crosslinked peptides. Biotin-tagged crosslinkers allow for the isolation of peptides by avidin affinity chromatography [159]. Other affinity-tagged crosslinker reagents include azide-containing crosslinkers, which can be isolated using “click chemistry” [160].

1.10 Rationale

Historically, x-ray crystallography has been widely used to determine protein structure, the atomic details offered by this technique has proven it to be powerful tool to understand chemical details and function [161, 162]. However, this technique does not allow for an investigation of complete protein system. In many cases, proteins are mutagenized and truncated to achieve the thermostability required for crystal formation. The crystal structure of hSERT has served as a useful tool for further understanding SERT function and its drug-binding sites. However, it lacks significant regions of the extracellular loops and the amino- and carboxy-termini which needed to be truncated for thermostability (see Table 1.2). These regions cannot be ignored for they are believed to have functional importance. The external loop regions are suggested to be involved in conformational

changes required for transport [163]. Furthermore, the N-terminus has been shown to be an allosteric modulator of hDAT [91, 164, 165]. A study showed that amphetamine-induced substrate efflux is obstructed when the N-terminal of SERT is tethered to the membrane [166], thus suggesting that the N-terminal is flexible and may be required for conformational rearrangements during transport. The C-terminus of SERT has shown to interact with the first intracellular loop to facilitate folding [167]. Furthermore, several proteins that interact with SERT's N and C termini have been identified [7], demonstrating that these regions are essential for regulation. These proteins include Sec24C which binds to the C-terminal domain of SERT [168, 169], and syntaxin 1A which interacts with the N-terminal domains of SERT, DAT and NET [170-172]. In addition, crystallographic studies are also conducted in membrane-mimetic environments and the structure of the transporter may be affected by the lipid bilayer [173]. In our study we use complete SERT protein with no truncations in lipid vesicles to preserve membrane-like environment.

In the development of specific and effective antidepressants it is vital to understand SERT activity and function. To fully understand SERT, it is necessary to investigate all its conformational states. Currently, there is no information available about the structure of SERT in the apo state. The current crystal structure of hSERT exhibits an outward-open conformation, it has not been crystallized in the apo state. Investigating the apo state is crucial because it will help us understand where allosteric changes occur as it transitions from resting state to an outward-open conformation with the drug bound. The development of efficient therapeutics depends on a full understanding of the target protein. This led us to investigate SERT in the apo state. Although the loops are known to have physiological

importance [10, 167], their topology is not fully characterized. Hence in this study we investigated SERT in its entirety without any truncations.

Table 1.2 SERT structures to date.

Allosteric State	Method	Resolution	Alterations	Activity	Year & PDB Code
(S)-citalopram or paroxetine in Fab complex	X-ray crystallography	3.15 Å	Mutations: I291A, T439S, Y110A, C554A, C580A, C622A. (Residues 1-76 and 618-630 truncated)	No detectable transport activity	2016 PDB Code: 5I71
Sertraline or fluvoxamine or paroxetine in Fab complex	X-ray crystallography	3.5 Å, 3.8 Å	Mutations: Y110A, I291A, T439S, C554A, C580A, C622A. (Residues 1-76 and 618-630 truncated)	No detectable transport activity	2018 PDB Code: 6AWO
Ibogaine in Fab complex	Cryo-EM	3.6 Å, 4.1 Å, and 4.2 Å	Mutations: C109A, C147A, C155A, C166L, C522S, C357L, C369L, I291A, T439S, Y110A, I291A. (Residues 1-72 and 617-630 truncated)	Transport competent	2019 PDB Code: 6DZZ
Paroxetine in Fab complex	Cryo-EM and x-ray crystallography	3.3 Å (cryo) 6.3 Å (x-ray)	Mutations: C109A, C147A, C155A, C166L, C522S, C357L, C369L, I291A, T439S, Y110A, I291A. (Residues 1-72 and 617-630 truncated)	Cryo-EM structure is transport competent; no transport activity in the x-ray crystal	2020 PDB Codes: 6VRH and 6W2C

1.11 Limitations of the study

A limitation of this study is that the peak intensities in mass spectrometry reflect the relative ionization of the mass ions, not their concentration. Hence, the relative abundance of the crosslinks cannot be determined. Quantification of the crosslinks would

differentiate high probability events from low probability events, thus further refining protein-protein interactions. To address this problem, we propose to implement a laser-induced fluorescence microfluidic platform to quantify mass shifted peptides.

Chapter 2: Methodology

2.1 SERT-Fluoxetine Interactions Study

Rat SERT (rSERT)

rSERT plasmid amplification and purification- Blotted rSERT cDNA on filter paper in pBlueScript plasmid (X8C) was kindly provided by Dr. Gary Rudnick from Yale University School of Medicine. The blotted filter paper was resuspended in deionized water and vortexed to extract DNA from the filter paper. The plasmid DNA was transformed and introduced into XL-1 Blue competent cells. Transformation was achieved by heat shock in a water bath for 30 seconds at 42°C, 2 minutes ice incubation, followed by recovery in 0.5 mL of super optimal broth with catabolite repression (SOC) media for 1 hour with gentle shaking at 37°C. Cells were plated overnight on Luria Broth (LB)- amp plates (0.1 mg/ml ampicillin antibiotic) at 37°C overnight. After overnight growth, single colonies were collected and grown overnight in 2 mL of LB-amp growth media (0.05 mg/ml ampicillin antibiotic) with shake incubation at 37°C and 225 rpm. After overnight growth, the plasmid DNA was extracted and purified by miniprep using UltraClean Standard Mini Plasmid Prep Kit following the manufacturer's instructions.

Plasmid X8C in pBlueScript and pFastBac expression vector were digested with Sall and Xba1 at 37°C for 1 hour. Next the restriction enzymes were inactivated at 65°C for 20 minutes. Digested pFastBac was treated with FastAP thermosensitive alkaline phosphatase to prevent re-ligation of the vector. Next the digested X8C and pFastBac were run on an 8% agarose gel to separate the DNA pieces. Gel plugs containing X8C insert at the 2 kilo base pair (kbp) region and pFastBac at the 4.7 kbp region were isolated and purified using Ultra-Sep gel extraction kit by Omega. Next, pFastbac and X8C were ligated

together overnight at different insert to vector ratios (1:1, 2:1, and 3:1) at 16°C. Ligated DNA was transformed into DH-10 competent cells and colonies were grown in LB-agar plates containing 0.1 mg/mL of ampicillin. After overnight growth, single colonies were collected and grown in 2 mL of LB media. Next, the plasmid DNA was extracted and purified using UltraClean Standard Mini Plasmid Prep Kit by MO Bio Laboratories. Purified DNA was then sequenced to verify the presence of cDNA rSERT insert in pFastBac vector.

Production of rSERT Recombinant Virus- Recombinant plasmid DNA was transformed into XL-1 Blue competent cells. Correct orientation of X8C was confirmed by DNA sequencing (GeneWiz). Transformation of recombinant pFastBac in DH10Bac (Invitrogen) competent cells was performed using the manufacturer's instructions. Briefly, transformation was performed by heat shock in a water bath at 42°C for 45 seconds followed by ice incubation for 2 minutes. Next, cells were shake incubated in 900 µl of SOC growth media for 4 hours at 37° C and 225 rpm. Cells were serially diluted by a factor of 10 and each dilution was plated on Luria agar plates containing 50 µg/ml kanamycin, 7 µg/ml gentamicin, 10 µg/ml tetracycline, 100 µg/ml Bluogal, and 40 µg/ml isopropyl β-d-1-thiogalactopyranoside (IPTG). DH10Bac competent cells contain a helper plasmid and a bacmid. Bacmid holds a mini-Tn7 target site and the helper plasmid provides the needed transposition proteins for site-specific transposition from pFastBac into bacmid to take place. The insertion of rSERT in the bacmid results in the disruption of the LacZ operon, which codes to produce β-Galactosidase, this enzyme catalyzes the hydrolysis of lactose into glucose and galactose. Detection of the colonies containing recombinant bacmid was accomplished using the blue-white screening method. Here, if the Lac-Z operon is

functional and not disrupted by a transposed gene, then IPTG will promote the production of β -Galactosidase by the LacZ operon, which hydrolyzes X-gal into 5-Bromo-4-chloro-3-hydroxyindole and galactose. 5-Bromo-4-chloro-3-hydroxyindole then oxidizes into 5,5'-dibromo-4,4'-dichloro-indigo, which is blue in color. The colonies formed by non-recombinant cells will therefore appear blue in color while the recombinant bacmid cells will appear white in color. Plates were incubated at 37°C for ~40 hours. Single white colonies containing recombinant bacmid were inoculated into 2 ml of LB media containing 50 μ g/ml kanamycin, 7 μ g/ml gentamicin, 10 μ g/ml tetracycline and incubated at 37°C with overnight shaking at 250 rpm. Bacmid DNA was extracted and purified. Briefly, growth media was removed by centrifugation at 13,000 g for 2 minutes. Next 300 μ l of resuspension buffer (50 mM of Tris-HCl pH 8, 10 mM ethylenediaminetetraacetic acid (EDTA), and 200 μ g/mL RNase A) was added to the pellet and cells were suspended until homogeneous with no vortex. Next 300 μ l of cell lysis solution (200 mM NaOH, 1% SDS) was added and mixed gently by inverting. Tubes were incubated at room temperature for 5 minutes. Samples were neutralized by adding 300 μ l of 3 M potassium acetate pH 5.5 and mixed by inverting the tubes 5 times. Samples were subsequently incubated on ice, harvested, and suspended in absolute isopropanol at -20°C overnight. Samples were centrifuged, and supernatant was removed. Pellets were washed with 70% ethanol and air dried. Finally, the bacmid was resuspended in 40 μ l of Tris-EDTA (TE) buffer pH 7.5 (1 M Tris, 0.5 M EDTA)

Isolation of recombinant baculovirus- Sf9 cells were purchased from Thermo Fisher Scientific. A frozen vial of Sf9 cells at a concentration of 1×10^7 cells/ml was quickly thawed in a 37°C water bath until only a small frozen piece remained. The vial was then

decontaminated, and cells were transferred into a cell culture flask containing 25 ml of complete media, Grace's Insect Medium (Gibco) supplemented with 10% fetal bovine serum (FBS) (Gibco) and 100 ug/ml penicillin-streptomycin (Gibco). Cells were incubated at 27°C for 45 minutes to allow for cell attachment, and the media was aspirated and replaced with fresh media. *Sf9* cells double every 18-22 hours and at 90-100 percent confluence they were transferred into a 100ml spinner flask. For transfection trials, *Sf9* cells were seeded at 1×10^6 cells/ml on a 35 mm well in 2 ml of complete media. Cells were then stored at 27°C for at least 1 hour to allow for cell attachment. Next, the media was replaced with fresh non-complete Grace's media (no FBS and no antibiotics). 800 ul of non-complete Grace's media was added to a CellFectin/bacmid DNA mixture (1 µg Bacmid DNA in 100 µl non-complete Grace's media, and 6 µl of cationic lipid transfection reagent Cellfectin in 100 µl of non-complete Grace's media) and 160 µl of the CellFectin/bacmid DNA/Grace's media mixture was added into each well and incubated for 5 hours at 27°C. CellFectin lipid solution assists bacmid DNA cross the cell membrane of the *Sf9* cells. After 5 hours, the media was replaced with fresh complete media and stored for 72 hours at 27°C. After the transfected *Sf9* cells showed late-stage infection phenotypes (viral budding, lysis), the media containing amplified virus was harvested after pelleting of intact and dead cells by centrifugation at 500 x g for 5 minutes. The baculovirus was later amplified by infecting 800 ml of cells at 1×10^6 cells/ml with virus in a ProCulture spinner flask. Cells were incubated in a 27°C, non-CO₂, non-humidified incubator on a spinner platform with gentle swirl for a week. The concentration of viral particles was determined with a viral titer plaque assay.

Viral Titer Assay- Titer assay was performed in a sterile 96 well plate. 12 wells were plated with 100 μ l of cells at 3×10^5 cells/ml and incubated at 27°C for 30 minutes to allow cell adherence. Five dilutions of virus were prepared (10^{-2} , 10^{-4} , 10^{-5} , 10^{-6} , and 10^{-7}) by adding 990 μ l of Grace's media to tube 10^{-2} and tube 10^{-4} and 10 μ l of virus stock to 10^{-2} . Next, 10 μ l of the 10^{-2} tube was transferred to tube 10^{-4} . Then 100 μ l of the 10^{-4} and 900 μ l of Grace's media were added to tube 10^{-5} . The remaining dilutions were prepared by serial 10-fold dilutions. The media was removed, and every 2 wells was infected with 100 μ l of each virus dilution, leaving the 1st and 2nd wells as control (no infection), and was incubated for 1 hour at room temperature. Afterwards, the supernatant containing virus was removed and 200 μ l of Grace's media was added to each well. The plate was placed in a sealed bag with a wet paper towel to prevent evaporation of the medium and incubated for 24-30 hours at 27°C. The media was then removed, and wells were washed twice with 100 μ l of PBS (0.01 M pH 7.2) for 1 minute each. Next the cells were washed a third time with 100 μ l of 4% paraformaldehyde. Plates were incubated for 30 minutes at room temperature followed by final rinse with 100 μ l of PBS (0.01 M pH 7.2). The cells were then blocked with 100 μ l of a blocking buffer (5% normal goat serum (NGS), 0.05% polysorbate 20 (Tween), in PBS) for 30 minutes at room temperature. Wells were then washed with 100 μ l of wash buffer (1% NGS, 0.05% Tween in PBS) for 1 minute. Next, 50 μ l of primary antibody solution mouse α GP64 (monoclonal antibody that reacts with the gp64 envelope protein of baculovirus) (Abcam) diluted 1:1000 in PBS containing 5% NGS, and 0.05% Tween) was added to each well and plate was incubated for 1 hour at room temperature. Wells were washed three times with wash buffer for 1 minute each wash. Next, 50 μ l of secondary antibody solution (goat anti-mouse conjugated to β -Galactosidase diluted

1:1000 in PBS, containing 1% NGS, and 0.05% Tween) (Calbiochem) was added to each well and incubated for 1 hour at room temperature. Wells were then washed three times with wash buffer. Next 50 μ l of coloring solution (4 μ l of 50 mg/ml X-gal in dimethylformamide (DMF)), 4 μ l of 83 mg/ml p-nitroblue tetrazolinium in DMF, 5 mM MgCl₂ in 1 ml of PBS was added to each well and plate was incubated at 37°C until cells appeared medium blue to dark purple under light microscope (~2 hours). Once color was established, reaction was stopped by washing three times with PBS. Strongly stained individual cells or cell clusters were counted as 1 unit. Viral titer was determined using the following formula: Titer (pfu/ml) = 10 x (# of infected units) x (viral dilution factor)

rSERT overexpression- A 3L Corning ProCulture spinner flask containing 800 ml of Sf9 cells at a concentration of 1x10⁶ viable cells/ml was infected with virus at a multiplicity of infection (MOI) greater than 5 at 27°C for 3 days. MOI was calculated using the formula below. Cells were harvested 3 days post infection by centrifugation at 500 x g for 5 minutes.

$$\text{Inoculum required (ml): } \frac{\text{desired MOI } \left(\frac{\text{pfu}}{\text{ml}}\right) \times \text{total number of cells}}{\text{titer of viral inoculum } \left(\frac{\text{pfu}}{\text{ml}}\right)}$$

Human SERT (hSERT)

Expression of human SERT- Tetracycline inducible stably expressing hSERT HEK293 cell line was kindly provided by Dr. Hidehito Takayama at Biotechnology Laboratory in Yokohama Japan. This cell line was suspended, inoculated, and grown in complete growth media (Dulbecco's Modified Eagle Medium (DMEM) supplemented with 10% FBS, 1% Penicillin-Streptomycin-Glutamine (PSQ), 100 ug/ml zeocin antibiotic). Cells grown in 75 cm² flask and stored in a 37°C, and 5% CO₂ incubator for 48 hours. Next, the cells washed with Hank's buffered salt solution (HBSS), the supernatant was removed, and the confluent

cells were washed with 10 mL of HBSS. The cells were detached from the flask with 2 mL of trypsin-EDTA, and once detached 8 mL of DMEM growth media was added to inactivate the trypsin-EDTA. The cell suspension was transferred to a 15 mL Falcon tube and centrifuged at 1000 g for 5 minutes. The supernatant was discarded, and the cell pellet was resuspended in 10 mL of DMEM growth media and transferred to 10 cm diameter tissue culturing plates, where the cells were grown for 3 days in a 37°C, and 5% CO₂ incubator in preparation for tetracycline induction. At 90% confluence the media was aspirated, and the cells were tetracycline induced in an induction medium containing DMEM growth media supplemented with 10% FBS, PSQ, 1 ug/ml tetracycline. The cells were grown at 37°C and 5% CO₂ for 24 hours. Afterwards, the cells were centrifuged at 1000g for 5 minutes and the medium was completely removed. The cells were washed in rinse buffer (137mM NaCl, 2.7mM KCl in PBS). Cells were transferred to 50 mL Falcon tubes and centrifuged at 1,000g for 5 minutes and the supernatant was discarded to collect cell pellet.

Purification- Cells were lysed by sonication (microtip set to max, 50% duty cycle, Branson Sonifier 250, VWR) on ice, two times for 15 seconds with a 10 second break in between to prevent the cells from over-heating, in a lysis buffer (10 mM Tris-HCl, 1 mM EDTA in 10 ml of deionized water) containing an anti-proteolytic cocktail (1.6 μunits/ml aprotinin, 100 μM phenylmethanesulfonyl fluoride (PMSF), 1 mM benzamidine, 100 μM benzethonium chloride) to minimize protein degradation. Cell membranes containing SERT were isolated by ultracentrifugation (65,000 rpm in a 70.1 Ti rotor for 30 minutes at 4°C). Cell pellets were washed and procedure was repeated a second time. SERT was solubilized overnight at 4°C in 10 mL solubilization buffer (20 mM Tris-HCl pH 7.4, 500

mM NaCl, 1 mM EDTA, 1 ml of glycerol, 1% digitonin detergent, and anti-proteolytic cocktail). The solubilized SERT was ultra-centrifuged using the same parameters and the supernatant was subjected to affinity chromatography using anti-FLAG antibody beads (Anti-FLAG M2 affinity gel, product number A2220) by Sigma-Aldrich following the manufacturer's instructions. Briefly, 2 ml of resin was transferred to a sterile 15 mL Falcon tube, centrifuged at 3,200 g for 2 minutes at 4°C. The supernatant was removed without discarding any resin and the resin was washed twice with 10 mL of TSB buffer (50 mM Tris HCl, 150 mM NaCl, pH 7.4). The solubilized SERT was then added to the resin and incubated for 2 hours at 4°C with gentle agitation. The tube was centrifuged at 3,200 g for 2 minutes at 4°C and the supernatant was removed. The resin containing SERT was washed twice with 8 mL of wash buffer (25 mM HEPES pH 7.4, 150 mM NaCl, 10% glycerol, 1% digitonin) and centrifuged at 3,200 g for 2 minutes at 4°C. Next, 2 mL of elution buffer (25 mM HEPES pH 7.4, 150 mM NaCl, 10% glycerol, 1% digitonin, 250 ng/ul 3X FLAG-peptide) was added to the resin and incubated at room temperature for 30 with gentle agitation. Finally, the tube was centrifuged at 3,200 g for 2 minutes at 4°C and the eluate (purified SERT) was stored at -20°C.

Isolation of SERT was verified by western immunoblot analysis using anti-FLAG antibody against FLAG-epitope tag. Protein samples were subjected to SDS-PAGE electrophoresis (10% resolving, 5% stacking) and transferred to a nitrocellulose membrane at 90 mA constant current overnight at 4°C. The membrane was treated with Odyssey blocking buffer and incubated for 1 hour at room temperature with gentle agitation. Next, the blocking buffer was discarded and replaced with a primary antibody (monoclonal mouse ANTI-FLAG M2, Sigma-Aldrich) solution with a dilution of 1 µg/mL (5 mL

blocking buffer, 0.1% Tween-20), the membrane was incubated for 2 hours at room temperature. The membrane was washed 4 times with gentle agitation in wash buffer (PBS with 0.1% Tween-20) for 5 minutes each. The membrane was incubated with a solution containing secondary antibody (IR-conjugated 800 CW goat anti-mouse secondary antibody with a dilution of 1:5,000) in PBS with 0.1% Tween-20 for 1 hour. The membrane was again washed 4 times in wash buffer (PBS with 0.1% Tween-20) and scanned on an Odyssey imager.

Lowry Assay- Protein concentration was determined via modified Lowry assay utilizing 1-20 µg/ml bovine serum albumin (BSA) standard curve in duplicates [174]. Protein samples were prepared in duplicates. Precipitation was initiated by adding 150 µL of 1.0% deoxycholate, vortexing, and resting at room temperature for 10 minutes. 0.1 mL of 72% trichloroacetic acid was added, vortexed, and spun at 7000 g for 10 minutes. The samples were aspirated and 0.2 mL of dH₂O was added. 1.0 mL of a Modified Lowry reagent was added to each sample, mixed, and incubated at room temperature for 10 minutes. 100 µL of a 1X Folin-Ciocalteu reagent was added, vortexed, and incubated at room temperature for 30 minutes. Addition of the 1X Folin-Ciocalteu reagent and the 30-minute incubation period were done in the dark. Absorbances were recorded with a UV-Vis spectrophotometer at 750 nm with BSA standards used to determine the protein concentration by performing linear regression analysis on the standard curve.

Removal of affinity tag on hSERT- Removal of FLAG-tag was performed using ProTEV Plus protease (Promega Cat# V6101). ProTEV Plus also contains an HQ tag located at the N-terminus of the protein, which can be removed from the cleavage reaction on affinity resins. The protease reaction was carried out by mixing the following in a 1.5mL centrifuge

tube: 80 μ g of hSERT with 20 μ l of 20X ProTEV buffer, 4 μ l of 100 mM DTT, 4 μ l of ProTEV Plus protease and autoclaved deionized water to a final volume of 400 μ l. The reaction was incubated at 30°C overnight. hSERT was isolated by affinity chromatography in a nickel column using HIS-select nickel affinity gel (Sigma-Aldrich, Cat# P6611). 200 μ l of HIS-select nickel affinity gel was added to a microcentrifuge tube and centrifuge for 30 seconds at 5,000 g. The supernatant was carefully removed and discarded. 800 μ l of equilibration buffer (50 mM sodium phosphate pH 8, and 0.3 M sodium chloride) was added and mixed. The tube was centrifuged for 30 seconds at 5,000 g and the supernatant was discarded. 400 μ l of hSERT/protease solution was added to the column and gently mixed for 2 minutes. ProTEV Plus protease binds to the nickel resin. The mixture was centrifuged for 30 seconds at 5,000 g and the supernatant containing eluted hSERT was collected. The affinity gel column was washed 2 times with 500 μ l of equilibration buffer, the tube was gently mixed for 10 seconds, then centrifuged for 30 seconds at 5,000 g and the supernatant was saved. Next 200 μ l of elution buffer (equilibration buffer with addition of 250 mM imidazole) was added to the tube and centrifuged for 30 seconds at 5,000 g. The elution step was repeated a second time with another 200 μ l of elution buffer to completely remove the protease from the nickel resin.

Reconstitution and addition and photo-crosslinking of pacFA-18:1 PC to rSERT or hSERT- In studies examining crosslinking with photolabeled PC analogs, the addition of the pacFA-18:1 PC analog took place during reconstitution into lipid vesicles. Briefly, 100 μ L of SERT was sonicated in 0.5 ml of lipid solution containing 1.5 mg/ml of 90% plant PC (95% phosphatidylcholine purity), 10% egg PC (60% phosphatidylcholine purity) and 0.004 mg/mL of pacFA-18:1 PC (Avanti) on ice. Samples were then injected into a dialysis

cassette (3500 MW cutoff, Thermo Scientific). The cassettes were incubated at 4°C with gentle spinning three times overnight, in excess 25 mM potassium phosphate buffer, pH 7.4. Final reconstituted protein was harvested and suspended in potassium phosphate buffer (25 mM, pH 7.4).

Agonist crosslinking studies- The fluoxetine analog was kindly provided by Dr. Lapinsky at Duquesne University Pharmacy Department. SERT (100 µL) was transferred to a sterile non-stick 1.5 mL centrifuge tube and mixed with 1 µL of 100 mM fluoxetine analog stock in DMSO. The mixture was incubated on ice for 1 hour in the dark to allow for the fluoxetine analog to bind to SERT. Non-specific crosslink was then induced by photoactivation. The mixture was transferred to a quartz cuvette and exposed to a 420 W Hg Arc lamp (Newport Model 97435-1000-1, 260-320 nm) on ice for 4 sessions of 5 minutes with 5 minutes break of no UV exposure in between each session to prevent sample warming. During UV exposure, the photoactivatable benzophenone moiety activates a radical reaction and undergoes a hydrogen-radical abstraction with the nearest accessible alpha carbon in the protein backbone, forming a covalent linkage.

In-gel trypsin digestion- Crosslinked samples were subjected to SDS-PAGE electrophoresis (10% resolving, 5% stacking) separation. hSERT is approximately 70 kDa, and appropriate gel plugs were excised. Gel plugs containing hSERT were washed with 50:50 absolute methanol: 50 mM ammonium bicarbonate 3 times for 15 minutes each with gentle agitation (VWR Thermal Shake Touch, 800 rpm). Gel plugs were spun down, and supernatant was removed. Gel plugs were dehydrated by adding 100 mM ammonium bicarbonate in 50% acetonitrile and set at room temperature for at least 10 minutes. Once gel plugs turned whitish, supernatant was removed, and gel plugs were dried in an

Eppendorf 5301 Vacufuge Concentrator for 20 minutes. Proteolytic solution containing 10 μ l of trypsin (Promega) at 20 μ g/ml in 50 mM ammonium bicarbonate was added to each gel plug and incubated on ice for 10 minutes, then incubated overnight with gentle shaking (VWR Thermal Shake Touch, 800 rpm) at 37°C. Digested peptides were transferred to VWR nonstick microcentrifuge tubes. Peptide fragments were extracted further by incubating gel plugs for 30 minutes in 300 μ l of elution solution (0.1% MS grade formic acid in 50:50 acetonitrile/ultra-pure water) with gentle agitation at room temperature. The supernatant was combined with initial supernatant. Peptides were dried in Eppendorf 5301 Vacufuge Concentrator.

Mass spectrometry- Dried digested peptides were resuspended in 50 μ l of resuspension solution (50:50 acetonitrile/ultra-pure water with 0.1% MS-grade formic acid). Mass shifted peptides were found using electrospray ionization quadrupole time-of-flight mass spectrometry (ESI-Q-TOF MS) and specific sites of covalent modification were identified using MS/MS. ESI-Q-TOF measurements were taken using an Agilent 6530 Q-TOF MS fitted with an Agilent HPLC-Chip II G424-62006 ProtID-Chip-150, comprised of a 40nL enrichment column and a 75 μ m x 150 mm separation column packed with Zorbax 300 SB-C18 5 μ m material. Studies were run on a positive mode and internal standards (1221.9906 and 299.2944) were provided by Agilent. Mobile phase solvents were Solvent A (95% H₂O, 5% acetonitrile, 0.1% formic acid) and Solvent B (95% acetonitrile, 5% H₂O, 0.1% formic acid). The nanoflow elution gradient was developed as: 0.50 μ L/min of Solvent A (minute: percent A): 0.00: 95%; 4.00: 10%; 6.00: 70%; 9.00:50%; 11.50: 95% and 13.00: 95%. MS data analysis was performed using Mass Hunter Qualitative analysis

software 6.0 (Agilent) with 10 ppm error tolerance allowing for two miss cleavage sites and possible mass shifts of the fluoxetine analog, oxidation, and acrylamide.

Mass shifted peptides found in MS analysis were run again targeting the specific m/z ratio charge and retention time. Collision-induced dissociation (CID) was used for MS/MS fragmentation following a linear increase in collision energy by m/z using the equation: $y=3.7x+2.5$ and performed at ± 0.2 min from the initial MS scan RT. MS/MS data analysis was performed using Mass Hunter Qualitative analysis software 6.0 provided by Agilent in conjunction with ProteinProspector v 5.22.1 available through the University of California San Francisco.

2.2 Apo-state rSERT Structure

Molecular Cloning & Mutagenesis- Rat SERT (rSERT) cDNA in pBlueScript plasmid (X8C) was kindly provided by Dr. Gary Rudnick from Yale University School of Medicine. X8C was moved into the pFastBac transfer vector as described in section 2.1. Single cysteine mutations were introduced at positions 109, 190, 232, 252, and 564 using the QuickChange Lightning site-directed mutagenesis kit (Agilent). Forward and reverse oligonucleotide primers (Eurofins Genomics) containing the desired Cys codon were designed following suggested guidelines are presented in Table 2.1. The mutations were introduced by PCR using the following conditions: 95°C for 1 minute, 95°C for 20 seconds, 62°C for 1 minute, 68°C for 7 minutes. This cycle was repeated 18 times. After Dpn1 digestion to remove parental plasmid, the DNA was transformed into XL-1 Blue competent cells. Briefly, transformation was achieved by heat shock for 30 seconds at 42°C, 2 minutes on ice, followed by recovery in 0.5 mL of SOC growth media for 1 hour with gentle shaking

at 37°C. Cells were plated overnight on LB-amp plates (0.1 mg/ml) of ampicillin antibiotic at 37°C overnight. After overnight growth, single colonies were collected and grown overnight in LB growth media containing 0.05 mg/ml of ampicillin with shake incubation at 37°C and 225 rpm. After overnight growth, the plasmid DNA was extracted and purified by miniprep using UltraClean Standard Mini Plasmid Prep Kit following the manufacturer's instructions. Successful introduction of cysteine codon was confirmed by sequencing (GeneWiz).

Table 2.1 Oligonucleotide primer pair sequences

Mutation	Oligonucleotide primer sequence
A109C	5' CGGTTTCCTTACATA TGC TACCAGAATGGCGGAGGG 3'
A109C-r	5' CCCTCCGCCATTCTGGTAG GCA TATGTAAGGAAACCG 3'
S190C	5' GCGCTCTACTACCTCATCTCC TGC CTCACGGACCGGCTGCCC 3'
S190C-r	5' GGGCAGCCGGTCCGTGAG GCA GGAGATGAGGTAGTAGAGCGC 3'
Y232C	5' CCCGCTGAGGAGTTC TGC TTGCGCCATGTCCTGCAG 3'
Y232C-r	5' CTGCAGGACATGGCGCAA GCA GAACTCCTCAGCGGG 3'
S252C	5' CAGGACCTGGGCACCATC TGC TGGCAGCTGACTCTCTGC 3'
S252C-r	5' GCAGAGAGTCAGCTGCCA GCA GATGGTGCCAGGTCCCTG 3'
R564C	5' GAGCCCACCCAGCTA TGC CTTTTCCAATACTATCCC 3'
R564C-r	5' GGGATAGTTGTATTGGAAAAG GCA TAGCTGGGGTGGGCTC 3'

Designed primer sequences forward and reverse. The yellow highlighted nucleotides code for cysteine.

Production of Recombinant Bacmid DNA- As described in section 2.1

rSERT Expression and Purification- As described in section 2.1

Reconstitution into lipid vesicles- As described in section 2.1 without the addition of pacFA-18:1 PC analog.

Photo-crosslinking of MTS-benzophenone to rSERT- rSERT (100 uL) was mixed with 0.02 mg/ml of heterobifunctional methanethiolsulfonate benzophenone (MTS-benzophenone) crosslinker (Toronto Research Chemicals) in DMSO. To ensure complete labeling excess crosslinker was added (1:5 protein to crosslinker ratio). Protein-crosslinker mixture was placed into quartz cuvettes and incubated on ice for an hour to allow for covalent binding of the cysteine in rSERT to the MTS. Non-specific crosslink was then induced by photoactivation. Cuvettes were exposed to a 420 W Hg Arc lamp (Newport Model 97435-1000-1, 260-320 nm) on ice for 4 sessions of 5 minutes with 5 minutes break of no UV exposure in between each session to prevent sample warming. During UV exposure, the benzophenone activates a radical reaction that undergoes a hydrogen radical abstraction with the nearest accessible alpha carbon in the protein backbone.

In-gel trypsin/Glu-C digestion- Crosslinked rSERT was subjected to SDS-PAGE (10% resolving, 5% stacking) electrophoresis to separate monomeric (~70 kDa) and oligomeric (≥ 140 kDa) bands. Separate gel plugs were excised and washed with 50:50 absolute methanol: 50 mM ammonium bicarbonate three times for 15 minutes each with gentle agitation (VWR Thermal Shake Touch, 800 rpm). Gel plugs were spun down, and supernatant was removed. 500 μ l of 100 mM ammonium bicarbonate and 15 μ l of 200 mM DTT reducing agent was added to the gel plugs and incubated for 1 hour at 56°C to reduce cysteine's disulfide bonds into free sulfhydryl groups. Supernatant was replaced with 500

μl of 100 mM ammonium bicarbonate and 15 μl of 200 mM iodoacetamide alkylation reagent. Gel plugs were incubated for 1 hour at 37°C in the dark for alkylation of the sulfhydryl groups to prevent disulfide bonds from reforming. Supernatant was removed, and gel plugs were dehydrated by adding 100 mM ammonium bicarbonate in 50% acetonitrile. Once gel plugs turned whitish, supernatant was removed, and gel plugs were dried in an Eppendorf 5301 Vacufuge Concentrator for 20 minutes. Proteolytic solution containing 10 μl trypsin at 20 $\mu\text{g}/\text{ml}$, 10 μl Glu-C at 20 $\mu\text{g}/\text{ml}$ in 50 mM ammonium bicarbonate was added to the gel plugs and incubated on ice for 10 minutes. Next, 30 μl of proteolytic solution was added to the gel plugs and incubated overnight at 37°C with gentle agitation. Digested peptides were transferred to VWR nonstick microcentrifuge tubes. Peptide fragments were extracted further by incubating gel plugs for 30 minutes in 300 μl of elution solution (0.1% MS grade formic acid in 50:50 acetonitrile/ultra-pure water) with gentle agitation at room temperature. The supernatant was combined with initial supernatant. Peptides were dried in Eppendorf 5301 Vacufuge Concentrator.

Mass Spectrometry- All MS studies conducted as described previously in section 2.1.

Chapter 3: SERT-Fluoxetine Interactions

3.1 Introduction

In serotonergic neurons, the end-product of the action potential is serotonin exocytosis. In the synaptic cleft, serotonin binds to and activates post-synaptic ionotropic and metabotropic receptors [175]. After this initial signal propagation, the relatively high concentration of serotonin must be reduced to turn off the signal. SERT re-uptakes serotonin, (5-hydroxytryptamine (5-HT)), from the synapse to the pre-synaptic cell. 5-HT is then recycled into storage vesicles or inactivated by deamination by monoamine oxidase [176]. Hence, SERT controls the concentration of serotonin in the synapse and affects the magnitude and duration of the signaling [177]. This serotonergic signaling is affected when serotonin concentration in the synapse is dysregulated leading to several neurological and psychiatric problems such as anxiety, depression, obsessive compulsive disorder, post-traumatic stress and sleep problems, among other physiological problems [29, 37]. This makes SERT is an important target for the development of antidepressants.

Tricyclic antidepressants (TCAs) were among the earliest developed antidepressants drugs. Although they may be effective, they are not selective for SERT and can cause serious side effects such as seizures and cardiovascular problems [178]. Selective serotonin reuptake inhibitors (SSRI) were discovered in the late 1960s and became widely prescribed in the late 1980s [179] due to their relatively high selectivity for SERT and limited off target receptors. However, despite this high selectivity they still bind to the homologous transporters NET and DAT, although with much lower affinity[24, 41].

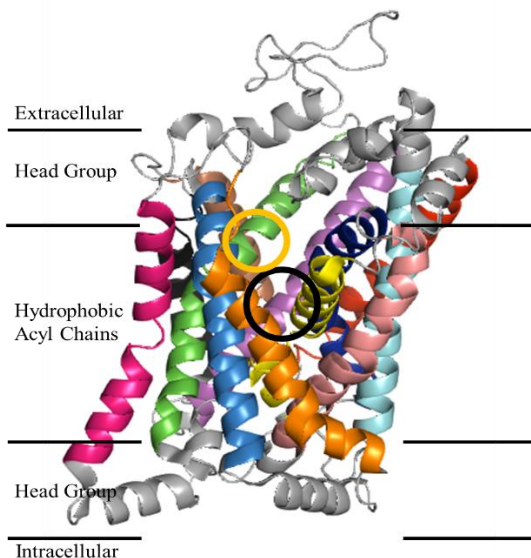


Figure 3.1 SERT transmembrane domains

Structure based on the citalopram bound crystal structure (PDB 5I71) viewed parallel to the membrane with TM1-TM12 shown in blue, salmon, green, brown, red, yellow, cyan, magenta, black, sky blue, orange, and hot pink, respectively. S1 and S2 binding pockets shown as black and gold circles, respectively. Black lines indicate approximate location of bilayer regions.

Two ligand-binding pockets are believed to exist: S1 which is located at the center of the transmembrane domain, and S2 which lies in the extracellular vestibule above S1 [84] (Figure 3.1). The existence and role of the S2 binding pocket remains controversial, as other studies suggest that the S1 site alone accounts for binding of serotonin and inhibitors [180]. The first human SERT crystal structure was crystallized bound to citalopram at both the S1 and S2 binding pockets [29]. However, in this and other high-resolution studies many mutations and deletions of significant regions of the terminal tails must be introduced for thermostability, and these reduce or eliminate the activity of the transporter (see Table 1.2). In addition, these high-resolution structural studies use lipid analogs and/or detergents as membrane mimetics and the structure of the transporter may be affected by the lipid bilayer [173].

Membrane proteins are greatly affected by lipid composition. A study by Magnany *et al.* showed that SERT associates with lipid rafts and that disaggregation of lipids rafts inhibits SERT activity [90]. In addition, interaction between phosphatidylinositol 4,5-biphosphate (PIP₂) and the N-terminus of DAT *in vitro* was observed in lipid binding assays using a GST-fused hDAT N-terminus construct containing the first 64 amino acids [91]. Constructs containing double mutations at positions K3A/K5A and K3N/K5N, show to inhibit the ability of hDAT N-terminus to bind to PIP₂, suggesting that this interaction is driven by electrostatic forces.

To complement these studies, we conducted crosslinking studies of a photoactivatable derivative of fluoxetine and full-length SERT reconstituted in lipid vesicles. Crosslinking mass spectrometry has successfully been used to elucidate protein structure, map protein-protein interactions and to identify protein-drug interactions [96, 136, 156, 181-189]. For example, Yip *et al.* utilized a photolabeling approach coupled with mass spectrometry to successfully identify propofol binding sites on mammalian GABA_A receptors [190]. In this study, SERT was purified from an inducible hSERT overexpressing HEK293 cell line. This system has been shown to produce functional SERT protein [9]. Nolan *et al.* [52] showed that hSERT obtained from HEK293 cells maintains binding affinity ($K_i = 284 \pm 66$ nM) and a high substrate uptake inhibition potency ($IC_{50} = 1167 \pm 26$ nM) when bound to tetrahydropyridinyl compound. Yarravarapu *et al.* [191] used hSERT obtained from HEK293 cells to evaluate hSERT binding affinity to a (*S*)-citalopram derivative containing a photoreactive benzophenone, and was shown to present a high binding affinity ($K_i = 0.16$ nM).

In this study, we similarly investigate the binding of a fluoxetine analog (Figure 3.2) to SERT, but extend these studies to include bottom-up MS to identify the sites of crosslinking. Tandem mass spectrometry provides high sensitivity and mass accuracy allowing us to identify specific amino acid residues involved in crosslinking [192, 193]. This combined with the use of a photoreactive fluoxetine analog will provide further insight into drug-SERT interactions without the need to make any mutation, truncation, or other modification on SERT. Herein, we present fluoxetine-SERT binding sites using a complete and functional hSERT.

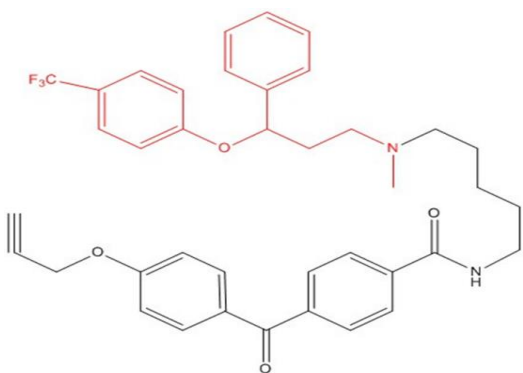


Figure 3.2 Structure of fluoxetine analog

Red region shows fluoxetine, black region shows photoactivatable benzophenone for photocrosslinking.

Given that fluoxetine partitions in bilayers [194] and might interact non-specifically with membrane proteins, control studies with photoactivatable phosphatidylcholine (PC) derivative lipids were also conducted to map lipid accessible sites (Figure 3.2). Comparison of crosslinks between hSERT-fluoxetine analog and hSERT-PC analog allowed us to potentially distinguish non-specific and specific sites of interactions between fluoxetine and SERT.

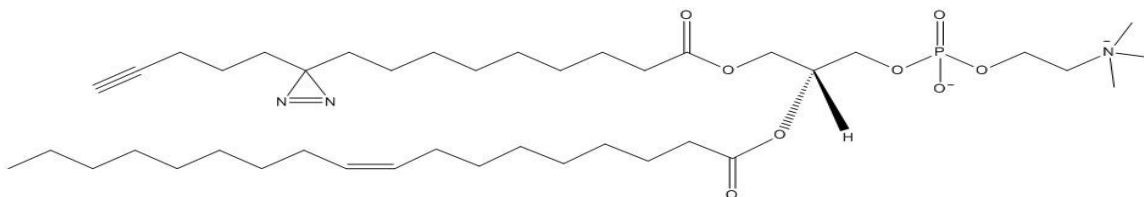


Figure 3.3 Structure of diazirine phosphatidylcholine analog

pacFA-18:1 PC contains a diazirine which serves for photoaffinity labeling.

3.2 Hypothesis

Drug binding sites in SERT can be obtained using MSMS studies on digested peptides bound to fluoxetine analog.

3.3 Results

hSERT was purified via affinity chromatography using a FLAG-epitope on the N-terminus against anti-FLAG affinity beads. The FLAG-tag was later removed using ProTEV Plus protease. After photocrosslinking to fluoxetine analog, hSERT was subjected to SDS-PAGE electrophoresis, and a band at the 70 kDa region was isolated, assuring that the analyzed protein was that of SERT only. Peptides are analyzed by mass spectrometry. MS separates peptides by mass-to-charge and creates a unique spectrum of protein fragments, this fingerprint can then be examined to identify peptides whose mass has been shifted by the mass of the covalently-attached crosslinker.

MS studies were conducted in triplicates from 3 biological replicates, and percent coverages ranged from 15%-35%. Given that peptide fragments can be modified at multiple sites, isobaric precursor ions can be generated. To avoid difficulties in the assignment of isobaric product ion scans, MSMS spectra are not averaged over time, but are strictly matched by retention time to their precursor ion, as in-line liquid C18 chromatography allows for the separation of isobaric peptides via their different chemical properties. CID fragmentation for a given peptide within a retention time window of ± 0.2 minutes produced several product ion fragmentation spectra. Each spectrum was analyzed individually to identify specific sites of photocrosslinking. A representative precursor-product ion spectrum is shown in Figure 3.4.

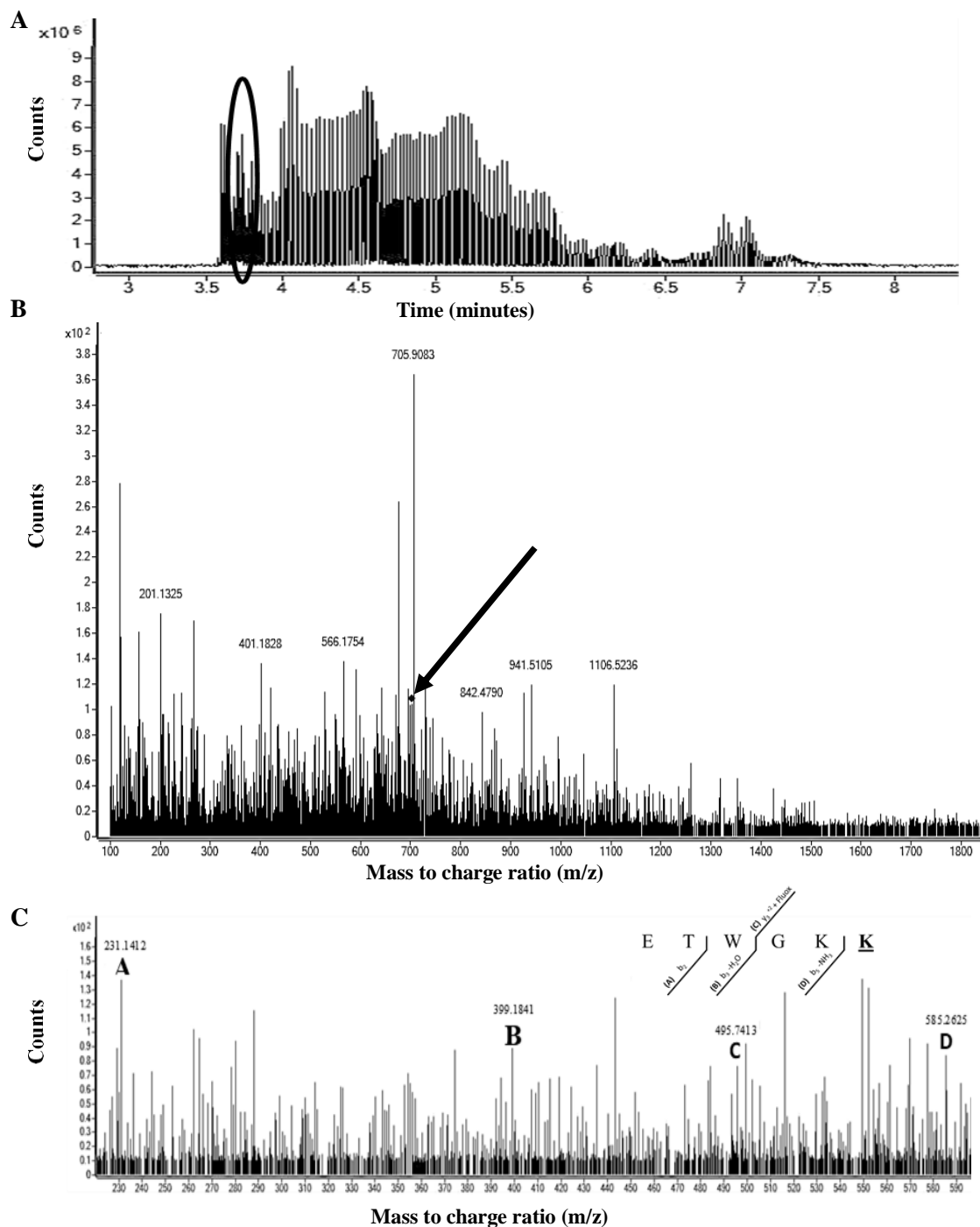


Figure 3.4 Representative MS and MSMS spectrum of precursor and product ion scan. (A). Complete MS ion chromatogram, encircled area indicates region where a mass shifted peptide was observed at retention time 3.862 min (B). A precursor ion with an m/z 703.8514 corresponding to doubly charged peptide $^{80}\text{ETWGKK}^{85}$ mass shifted by fluoxetine analog was identified (peak identified with a black arrow). (C) CID fragmentation of this crosslinked precursor ion. Product ion fragments are labeled (A-D) and specific site of crosslink is bolded and underlined.

In the hSERT-fluoxetine analog study, crosslinking events were identified in the N-terminus, TM2-TM3 intracellular (IC) loop, the extracellular (EC) loop between TM3-TM4, the IC loop between TM4-TM5, the EC loop between TM7-TM8, TM12 and the C-terminus (Table 3.1). The fluoxetine analog contains a fairly long hydrophobic tail (~20Å) therefore, it was possible to see crosslinks to the intracellular loops. These regions are discussed in detail in the “Discussion” in section 3.4.

Table 3.1. hSERT-fluoxetine analog crosslinks

Peptide	Modification	Structural Location
⁸⁰ ETW <u>GK</u> ⁸⁵	⁸⁰⁻⁸⁵ Fluox/ ⁸⁰⁻⁸⁵ Fluox, Oxi	N-Terminus
¹⁵³ <u>KICPIFK</u> ¹⁵⁹	¹⁵³⁻¹⁵⁹ Fluox/ ¹⁵³⁻¹⁵⁹ Fluox, Acryl ¹⁵³⁻¹⁵⁹ Fluox, Acryl	TM2-TM3 IC Loop/TM3
²³⁵ HVL <u>QIHR</u> ²⁴¹	²³⁵⁻²⁴¹ Fluox, Oxi/ ²³⁵⁻²⁴¹ Fluox	TM3-TM4 EC Loop
²⁷³ GVKT <u>SGK</u> ²⁷⁹	²⁷³⁻²⁷⁹ Fluox, Acryl / ²⁷³⁻²⁷⁹ Fluox, Acryl ²⁷⁶⁻²⁷⁹ Fluox	TM4-TM5 IC Loop
³⁹¹ <u>NEDVSEVAK</u> ³⁹⁹	³⁹²⁻³⁹⁹ Fluox	TM7-TM8 EC Loop
⁵⁹⁷ <u>LIITPGTFKERIK</u> ⁶¹⁰	⁵⁹⁷⁻⁶¹⁰ Fluox, Acryl / ⁶⁰⁸⁻⁶¹⁰ Fluox ⁵⁹⁷⁻⁶⁰⁵ Fluox	TM12/C-Terminus
⁶²⁷ <u>LNAV</u> ⁶³⁰	⁶²⁷⁻⁶³⁰ Fluox	C-Terminus

Identified mass-shifted peptides within 10 ppm error. Specific sites of covalent crosslink identified via CID fragmentation analysis are bolded and underlined.

Sites of crosslinking were mapped onto a model of hSERT-citalopram crystal structure (PDB#5I71) for visualization purposes (Figures 3.5-3.7).

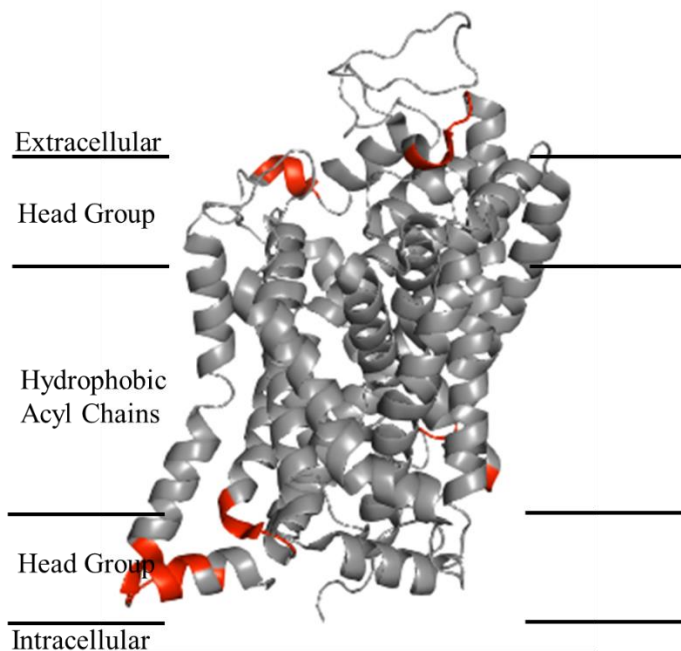


Figure 3.5 hSERT-fluoxetine analog crosslinks.

Red regions indicate fluoxetine crosslinks. Black lines indicate approximate location of bilayer regions.

Crosslinks are mapped on structure of hSERT bound to citalopram (PDB# 5I71) [1]. Not all crosslinking data can be shown as some regions are missing in the crystal structure.

In the hSERT-fluoxetine studies, the FLAG-tag located at the N-terminus was cleaved off. However, in the rSERT (rat SERT) studies (Chapter 4) the FLAG-tag located in the C-terminus was not removed due to missing cleavage site. Therefore, to test for any possible artifacts attributable to the sites of chimeric tags, additional CX-MS studies were conducted using baculovirus overexpression of rSERT. In the rSERT-fluoxetine analog study, crosslinks corresponding to the following regions were found: N-terminus, TM 2-TM 3 IC loop, TM 3-TM 4 EC loop, and TM 5-TM 6 EC loop (Table 3.2). In both studies, we observed crosslinking to the N-terminus, TM 2-TM 3 IL, TM 3-TM 4 EL however, no crosslinks to the C-terminus and TM 7-TM 8 EL were observed in the rSERT-fluoxetine study.

Table 3.2 rSERT-fluoxetine analog crosslinks

Peptide	Modification	Structural Location
¹¹ VLSEAK <u>K</u> DR ¹⁸	¹¹⁻¹⁸ Fluox	N-Terminus
¹⁵⁴ <u>I</u> APIFK ¹⁵⁹	¹⁵⁴⁻¹⁵⁹ Fluox	TM2-TM3 IC Loop/TM3
²³⁵ HVLQ <u>I</u> HQSK ²⁴³	²³⁵⁻²⁴³ Fluox, Acry, Oxi	TM3-TM4 EC Loop
²⁹⁹ GATLPG <u>A</u> WR ³⁰⁷	²⁹⁹⁻³⁰⁷ Fluox	TM5-TM6 EC Loop

Identified mass-shifted peptides within 10 ppm. Specific sites of covalent crosslinks identified via CID fragmentation analysis are bolded and underlined.

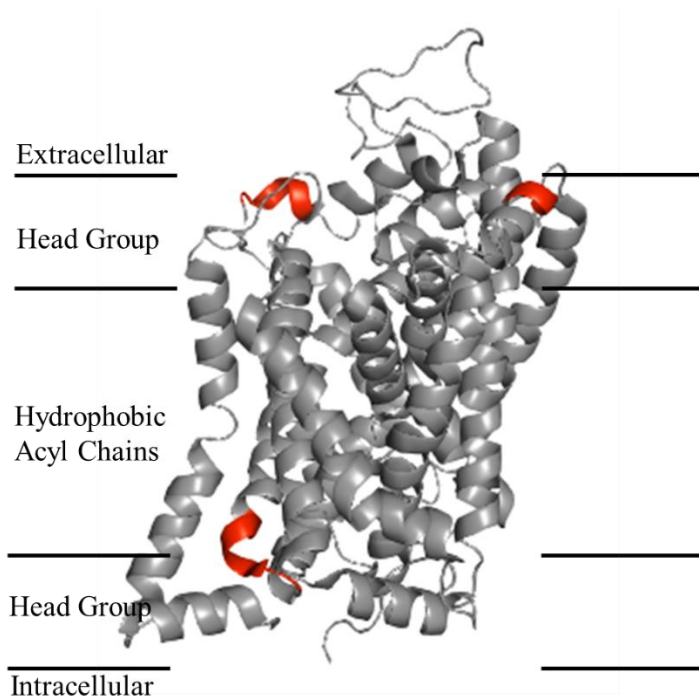


Figure 3.6 rSERT-fluoxetine analog crosslinks.

Red regions indicate fluoxetine crosslinks. Black lines indicate approximate location of bilayer regions. See Fig. 3.5 for analogous details.

Fluoxetine can partition in the lipid bilayer [194-196] as well as neurotransmitters including dopamine [197] and serotonin [198]. Hence, fluoxetine might interact non-specifically with membrane proteins. Since these presumably low abundant non-specific interactions might be detected by this highly sensitive MS approach, control studies with photoactivatable lipids were also conducted to map lipid accessible sites. Here, both the

fluoxetine analog and a phosphatidylcholine (PC) derivative were used. In the hSERT-fluoxetine/PC study, we observed PC crosslinks to TM4-TM5 IC loop and on the rSERT-fluoxetine/PC study we observed PC crosslinks to the N-terminus, TM3-TM4 EC loop, TM4-TM5 IC loop, and TM5-TM6 EC loop (Table 3.3).

Table 3.3 SERT-PC analog crosslinks

Peptide	Modification	Structural Location
¹¹ <u>VLSEAKDR</u> ¹⁸	¹¹⁻¹⁸ PC ⁺⁺ / ¹⁷⁻¹⁸ PC, 2 Acry ⁺⁺	N-Terminus
⁷⁶ <u>QGERETWGK</u> ⁸⁴	⁷⁶⁻⁸⁴ PC ⁺⁺	
²³⁵ <u>HVLQIHQSK</u> ²⁴³	²³⁵⁻²⁴³ PC, Acry, Oxi ⁺⁺	TM3-TM4 EC Loop
²⁷³ <u>GVKTSQK</u> ²⁷⁹	²⁷³⁻²⁷⁵ PC ⁺ / ²⁷³⁻²⁷⁵ PC, 2 Acry ⁺ / ²⁷³⁻²⁷⁵ PC ⁺⁺ ²⁷⁶⁻²⁷⁹ PC, Acry ⁺⁺	TM4-TM5 IC Loop
²⁹⁹ <u>GATLPGAWR</u> ³⁰⁷	²⁹⁹⁻³⁰⁷ PC ⁺⁺	TM5-TM6 EC Loop

Identified mass-shifted peptides within 10 ppm error. Specific sites of covalent crosslinks identified via CID fragmentation analysis are bolded and underlined. ⁺ Indicates hSERT, ⁺⁺ indicates rSERT

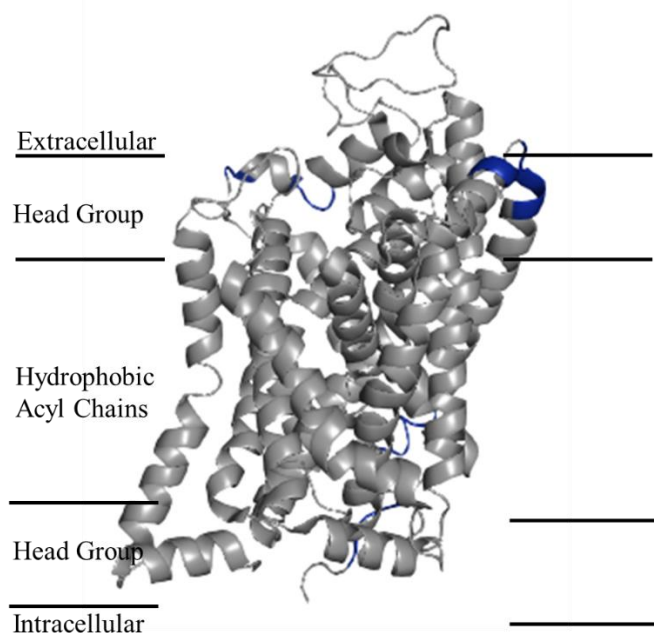


Figure 3.7 SERT-PC analog crosslinks.

Blue regions indicate PC crosslinks, black lines indicate approximate location of bilayer regions.

See Fig. 3.5 for analogous details

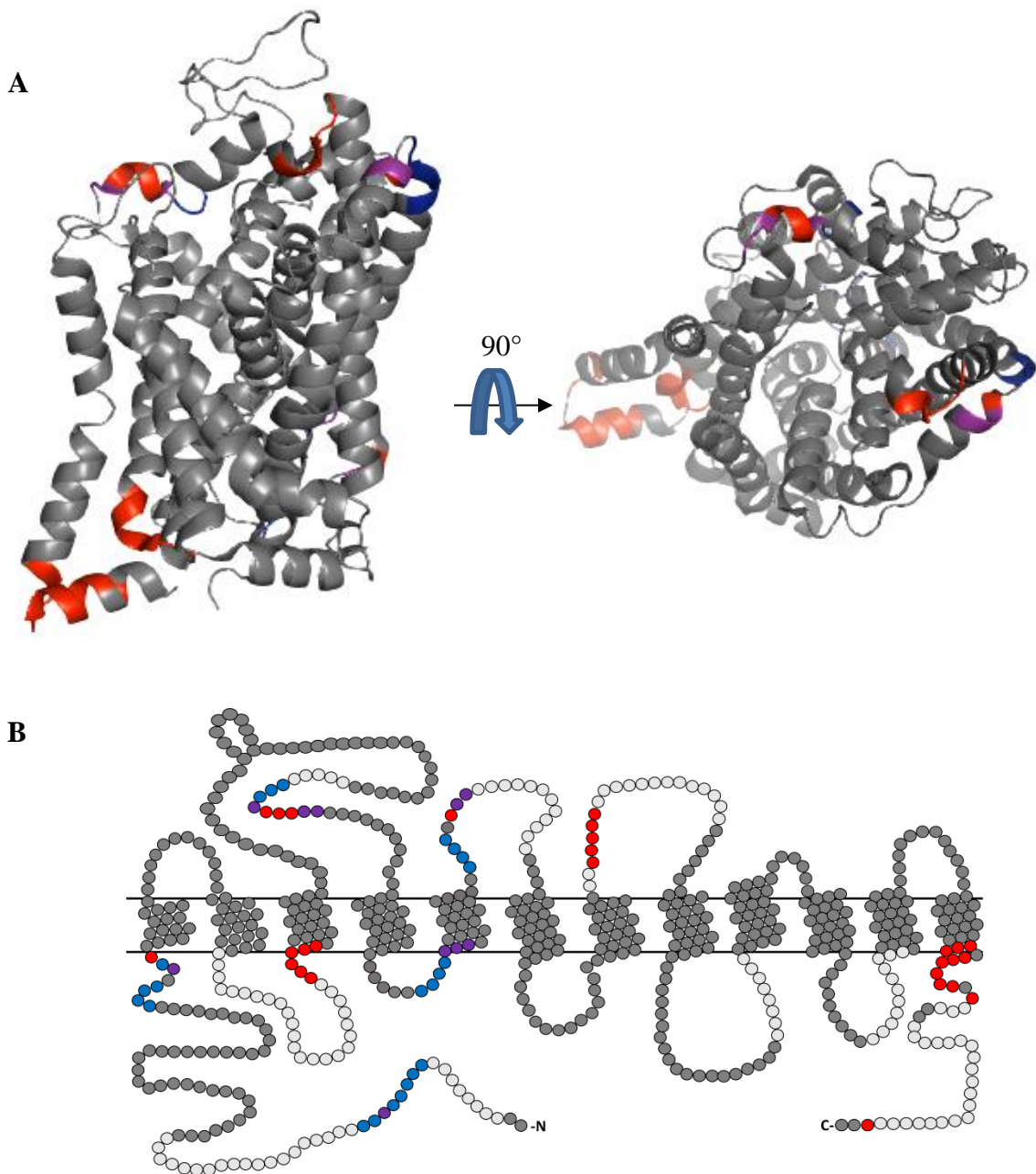


Figure 3.8 Summary of SERT crosslinks to fluoxetine and PC analog

(A) Crosslinks illustrated using the citalopram-bound human crystal structure of hSERT (PDB# 5I71). Red regions represent crosslink to fluoxetine analog, blue regions represent crosslink to PC, purple represents crosslink to both fluoxetine and PC. (B) Bead model of SERT crosslinks. Red regions represent crosslink to fluoxetine analog, blue regions represent crosslink to PC, purple represents crosslink to both fluoxetine and PC. Light grey indicates regions observed without the crosslinker, dark grey indicates regions not observed.

Not all fluoxetine crosslinking data can be shown in (A) as some regions are missing in the crystal structure

Crosslinks to regions located in the S1 and S2 binding pockets were observed. However, given that the distance between S1 and S2 (13 Å) is shorter than the distance between the crosslinking moiety and the drug itself (20 Å), the exact binding location of the fluoxetine analog remained inconclusive. However, other novel results were observed. Below are key points to take from the observed crosslinks; these points are explained in more detail in the “Discussion” (Section 3.4).

Terminal tails appear to be closely associated with the membrane

Crosslinks to the terminal tails is interesting as they are missing from the crystal structures. Both hSERT-fluoxetine and rSERT-fluoxetine studies showed crosslinks to both the N-terminus and C-terminus, suggesting they are closely associated with the membrane. The fluoxetine analog can only bind to either S1 or S2 binding pockets and as mentioned earlier, S2 is located midway the bilayer and S1 is located just above S2. The hydrophobic core of the lipid bilayer is approximately 30 Å thick while the hydrophilic head group regions are approximately 15 Å each. Given that the photoactivatable moiety can crosslink to amino acids within a distance of 20 Å, it is possible for the analog to bind to S1 or S2, and crosslink to regions of the protein near the membrane facing the intracellular side. This observation was also found in another study done in our laboratory by Andrew DeMarco, where he identified hSERT crosslinks to azi-cholesterol. In addition, crosslinks to the terminal tails were also observed in the protein-protein study in chapter 4. The fact that the SERT-fluoxetine study, the protein-protein study and the SERT-azi cholesterol study all showed crosslinks to the terminal tails show that there is consistency and support this observation.

A region of extracellular loop 2 is closely associated with the membrane

The EC 2 is the largest loop, and its structure is unknown. Fluoxetine and PC crosslink to peptide ²³⁵HVLQIHQSK²⁴³ suggests there is non-specific binding, and that this is a lipid accessible region. Crosslinking to this peptide was also observed in our laboratory by DeMarco *et al.* in analogous studies using photoactivatable cholesterol [199]. Further supporting that this region of the loop comes in proximity with the membrane.

The lower region of TM12 shows movements/rearrangement

Unlike LeuT but reminiscent of DAT, SERT has a kink in TM12. This kink is halfway across the membrane and angled ~20 degrees away from the protein [21]. The functionality of this kink is unknown, but studies have suggested that there is mobility in the lower region of TM12. Hydrogen deuterium exchange studies by Moller *et al.* [177] showed that 5-HT induces changes in the dynamics of hSERT in regions of EL4 and TM12. In this study, we observed crosslinking to ⁵⁹⁹ITPGTFKERIIK⁶¹⁰ located in the lower region of TM12. The fluoxetine analog used in this study has a distance of ~20Å between the crosslinking moiety and the drug itself, limiting crosslinking to regions within this range. PyMOL visualization software analysis was used to measure distances between position 597 and Asp98 in subsite A, Tyr176 in subsite B, and Thr497 in subsite C, using the citalopram bound SERT crystal structure (PDB # 5I71). The distances found were 43.6 Å, 39.7 Å, 31.5 Å, respectively. This observation suggests that there is movement in the apo form not observed in the drug bound crystal structure. One possibility is that when fluoxetine is bound, the lower region of TM12 tilts inward, hence becoming available for crosslink.

Other crosslinks are consistent with the literature. PC crosslinks in TM4-TM5 IL and TM5-TM6 EL overlap with known cholesterol binding sites known as cholesterol recognition/interaction amino acid consensus sequence or CRAC and its mirror motif, CARC [200]. Mutagenesis studies by Laursen *et al.* [201] show that there is cholesterol binding to TM1 and TM5 (adjacent to TM4-TM5 IL and TM5-TM6 EL), supporting the observation that those regions are in proximity with the membrane. This observation suggest that this study does not produce random crosslinks. Instead, it shows that CX-MS is a powerful tool that can provide accurate results which can be used as a complement to other biophysical methods to provide structure information of regions not available in other high-resolution methods.

Some sites of crosslinking are not shown as they are missing from the model such as the terminal tails. Crosslinks to areas not seen in the crystal structure show that current models need refinements and that those regions play a key role and thus need to be considered when studying SERT and its binding sites. The observation also highlights the utility of CX-MS based approach which can provide local structure information of regions not available in other high-resolution structures.

3.4 Discussion

As the cases of anxiety and depression continue to grow [202], the need to understand how antidepressants act is much greater. It is crucial to understand the structural and mechanistic details underlying the binding process to develop new, improved, and efficient antidepressants. The x-ray crystallography and cryo-EM structures of SERT offer great insight into ligand interaction sites. However, they lack important regions that are

known to play key roles in activity such as the terminal tails. In addition, these structures contain many mutations needed to achieve thermostability. In this study, we identify sites of interaction of SERT with a photoactivatable fluoxetine analog in the presence of an intact bilayer as a unique complement to current high-resolution structures.

The presence of crosslinking sites on the periphery of the transporter near the lipid accessible surface raised concerns whether these sites might be due to non-specific interactions due to the partitioning of fluoxetine analog in the reconstituted bilayer. It has been reported that many neurotransmitters and drugs, including SSRIs, partition in the bilayer [194-198]. To control for this, parallel studies were conducted with photoactivable PC included in the composition of the vesicles.

The PC analog showed crosslinks to peptide ²³⁵HVLQIHQSK²⁴³ in TM3-TM4 extracellular loop overlapping with regions of labeling in fluoxetine-hSERT studies (See Tables 3.1-3.3). The TM3-TM4 loop is the largest extracellular loop whose structure is not fully resolved as this loop is often truncated and mutated for thermostability in crystallographic and cryo-EM studies of SERT and other MATs. We propose that the fluoxetine-crosslinks that overlap with the PC-crosslinks observed in these CXMS studies, might be due to non-specific lipid binding regions (See Tables 3.1-3.3). Given the sensitivity of the MS platform, it would not be unexpected to see low frequency crosslinking events. Interestingly, this same region of SERT was found to crosslink with azi-cholesterol in previous studies conducted in our laboratory [199]. The two observations suggest that this region is associating with the bilayer and represents a step towards understanding the structure/function of this loop. PC-crosslinks were also observed to ²⁷³GVKTS²⁷⁹ in IL2 and ²⁹⁹GATLPGAWR³⁰⁷ in EL3. These peptides also crosslinked

with azi-cholesterol, further supporting the idea that these regions are also associating with the bilayer and are being labeled non-specifically.

The PC crosslinks to the N-terminus at ⁷⁸ERETWVK⁸⁴ and ¹¹VLSEAKDR¹⁸ suggest that the crosslink observed between fluoxetine and hSERT to the N-terminus is also a nonspecific lipid binding site. Interestingly, ⁷⁸ERETWVK⁸⁴ also crosslinked to cholesterol in studies by DeMarco *et al.* [199]. This observation is interesting, as the N-terminus is believed to interact with phosphatidylinositol 4,5-bisphosphate (PIP₂) lipids [165], and this interaction has been shown to be prerequisite for amphetamines action on SERT [203]. It is interesting to note that the PC crosslinked regions at ¹¹VLSEAKDR¹⁸ in the N-terminus and the ²⁷⁶TSGK²⁷⁹ in the TM4-TM5 intracellular loop contain sites of phosphorylation (Ser 13, Ser 277) [204]. This observation suggests the possibility that this lipid interaction and its electrostatics may result in remodeling of the region upon phosphorylation.

In our study we observed novel crosslinks as well as crosslinks consistent with known structure information of SERT. The fluoxetine crosslinks to peptide ¹⁵⁴ICPI¹⁵⁷ which is in the intracellular loop between TM2-TM3 and a portion of TM3, is consistent with a section of the central binding site which according to Coleman *et al.* [1] is defined to reside in TM1, TM3, TM6, TM8, and TM10. Fluoxetine crosslinking was also observed to EL4 (TM7-TM8 extracellular loop), specifically ³⁹¹NEDVS³⁹⁵. This is consistent with a section of the allosteric binding site which resides in TM1, TM6, TM10, TM11, EL4 and EL6 [1]. Fluoxetine analog crosslinks were also observed to EL2. EL2 participates in extensive interactions with EL4 and EL6 and together they sculpt a portion of the allosteric site [1]. We did not observed crosslinks to EL6 and the other regions that compose the

allosteric and central binding sites. However, we note that the percent coverage was ~35%, so negative results such as the absence of mass-shifted peptides detected cannot be interpreted.

The crosslinks to the N and C-termini regions were surprising as their observance suggests that these regions, absent from known structures and often drawn as intracellular loops in schematics of the transporter, are closely associated with the membrane. This is of special interest since these regions are known to be physiologically important in activity [7, 166-169]. Sucic *et al.* found that the N-terminal of SERT can be found tethered in the membrane [166] and other studies have suggested a close interaction of the N-terminus with the membrane in hDAT [164]. Surprisingly, not only did we observe crosslinking to the N-terminus but also the C-terminus, thus suggesting that regions in both termini may be associated with the membrane in the apo structure. This observation questions the accuracy of the SERT models currently used. In other corroborating studies conducted in our lab by DeMarco *et al.*, the terminal tails were also crosslinked by azi-cholesterol [199] suggesting that these regions of the transporter are closely associated with the membrane.

The fluoxetine-hSERT crosslink to peptide ⁵⁹⁹ITPGTFK⁶⁰⁵ in the lower region of TM12 was unique. TM12 has a kink at the center causing the lower half to turn away from the transporter, and it is conserved among hDAT, hNET and hSERT [21, 151]. The role of TM12 is unclear, simulations studies suggest that it plays a role in dimerization [205], however SERT structure has not been captured in an oligomeric state. HDX-MS studies on dDAT suggest that TM12 may play a role in transport mechanism and/or regulation of transporter activity [206]. The crystal structure of dDAT bound to antidepressant nortriptyline and locked in an outward open conformation shows that the lower region of

TM12 is approximately angled ~20 degrees away from TM12 of LeuT [21]. An x-ray crystallography study of hSERT bound to varying antidepressants revealed that though they all stabilize SERT in an outward-open conformation, some residues can adopt different conformations to mediate selectivity [30]. Furthermore HDX-MS studies on hSERT detected differences between 5-HT and K⁺ bound states in the lower region of TM12 [177], suggesting movement on TM12 during transport. In the citalopram-bound structure [1] distances between position 597 in the lower region of TM12 and position 98 in subsite A, position 497 in subsite C and position 176 in subsite B that constitute the S1 site located at the center of the transmembrane domain were 43.6 Å, 31.5 Å, and 38.7 Å, respectively. S2 is located above S1, therefore the distance between any amino acid within S2 and position 597 is even longer. For the 20 Å long crosslinker to crosslink to the lower region of TM12, this region had to come into proximity. We propose that this region is dynamic and is oriented differently in the apo state of the transporter.

The crosslinks that align with known information about SERT structure and the novel crosslinks were very promising. However, we could not determine the exact binding site of fluoxetine due to the long distance between the photoactivatable moiety and the fluoxetine moiety. The distance between the allosteric and central binding sites is approximately 13 Å [1], and the distance between the benzophenone and the fluoxetine active site is approximately 20 Å. Hence, not only can we observe the regions lining the central and allosteric sites, but we can also observe regions located even further from the binding site. As a result, the exact binding location of the fluoxetine analog remained inconclusive.

Overall, this study highlights the power of CX-MS to identify crosslinks directly and sensitivity on SERT. The fluoxetine analog showed to be an innovative approach and although we could not determine the exact binding location of fluoxetine, we were able to provide new information about SERT structure which can aid in expanding our current understanding of SERT. For instance, we were able to identify lipid accessible sites which are probably assisting in protein stabilization. We were able to shine light into regions that may be associating with the membrane bilayer including regions, including the terminal tails which are not visible in other high-resolution structures. In addition, we were able to shine light into a possible role of TM12.

This approach is particularly advantageous in that it allows the studies to be performed in a complete and functional SERT without any mutations, truncations, or deletions. The results presented herein give an insight into local structure of protein regions that are not available in other high-resolution structures and serves as a unique compliment to current structures.

3.5 Acknowledgements

I thank Sara Luty and Zachary Kelly who assisted in the fluoxetine study. Specifically, Sara did the rSERT-PC, fluoxetine studies- this included expressing protein, crosslinking, mass spectrometry, and data analysis- and Zachary worked on isolating and amplifying recombinant baculovirus and expressing the initial pellets. I performed the hSERT-fluoxetine studies which also included expressing protein, crosslinking, mass spectrometry, and data analysis.

Chapter 4: Apo-state SERT Structure

4.1 Introduction

Currently there is a wealth of high-resolution structures of SERT and other NSS members available from crystallographic and cryo-EM studies [1, 30, 32, 33]. While these studies provide tremendous insights into the structure of NSS members, these static images have caveats in that the transporters are typically mutagenized for thermostability to reduce sample heterogeneity and often have truncations of significant regions. Often such alterations cause a loss of activity and/or binding affinity. As a result, many of today's available models are of inactive protein. In addition, these studies are also conducted in membrane-mimetic environments and the structure of the transporter may be affected by the lipid bilayer [173]. Multiple studies have shown evidence of lipid interactions with SERT. Such as the necessity of lipid rafts in SERT's activity [90] and the suggested interactions between PIP₂ lipids with the terminal tails [91]. Furthermore, lipid composition is of great interest for its role on oligomeric state. There is growing evidence that SERT forms a broad distribution of oligomeric states ranging from monomers up to pentamers [92, 93]. Thus, it is essential to conduct studies of full-length SERT in a physiologically-relevant membrane to fully understand SERT structure and function.

A novel approach to assess complete structural information is by coupling chemical crosslinking with mass spectrometry. Crosslinking mass spectrometry (CX-MS) studies do not require truncations, allowing us to potentially identify distance constraints and generate refined models of the entire functional transporter. CX-MS makes it possible to investigate local structure of protein regions that are not available in other high-resolution structures. CX-MS has been widely used to elucidate protein structure and to identify binding sites.

For example, the structure of the mitochondrial prohibitin complex [182] and bovine serum albumin [186] were investigated using lysine specific cross-linkers and MS to map spatial distance constraints.

The loops and terminal tails of SERT play key functional roles in transport therefore it is critical to refine current models and investigate these unmapped regions [163, 167]. The extracellular loops (EL) are not fully resolved in crystal structures yet are known to play key roles in SERT activity. EL4 can modulate inhibitor binding and plays a crucial role in controlling the conformational equilibrium of SERT [207]. Thus, to fully understand SERT it is necessary to map its loops.

In this study, we probe the extracellular loops using a heterobifunctional methanethiosulfonate (MTS) benzophenone reagent (Figure 4.1) to crosslink single cysteine mutants to nearby amino acids and MS to identify the sites of crosslinked residues and provide distance constraints. The photoactivatable benzophenone allows for non-specific crosslinking, typically at backbone alpha C, within the crosslinking radius.

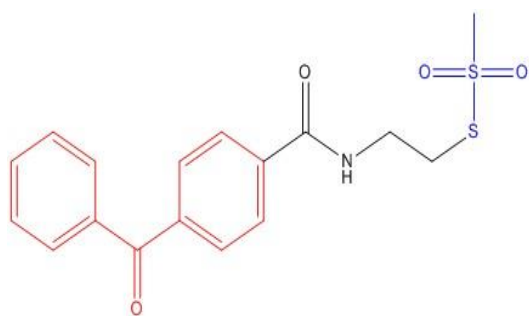


Figure 4.1 Structure of bifunctional crosslinker Benzophenone-4-carboxamidoethyl methanethiosulfonate. It includes a methanethiosulfonate moiety shown in blue for SH coupling and a photoactivatable benzophenone moiety shown in red for photo-crosslinking.

The current SERT models available are those of hSERT bound to different SSRIs which lock SERT in an outward-open conformation [29]. At present there is no information about SERT in the apo state, and to fully understand SERT it is imperative to investigate all its conformations during serotonin transport. This led us to investigate SERT in the apo state. In this study, we specifically interrogate the topology of the EL1, 2 and 6. Given our

need to systematically introduce specific single cysteine mutations and covalently bind the given cysteine to a heterobifunctional crosslinker, single cysteines were introduced into a *Cys-null* construct. In this construct, (provided by Dr. Rudnick at Yale University School of Medicine) eight reduced cysteine residues were mutated –C15A, C21A, C109A, C147A, C155A, C357I, C522S, and C622A– to produce an X8C rSERT. This construct was reported to retain 32% of wild type transport activity and 56% of wild type binding activity [95]. A109C was introduced to investigate topology of EL1. EL2 is the longest loop and S190C, Y232C, and S252C were introduced separately, one at a time. Mutation R564C was introduced to investigate EL6 (Figure 4.2).

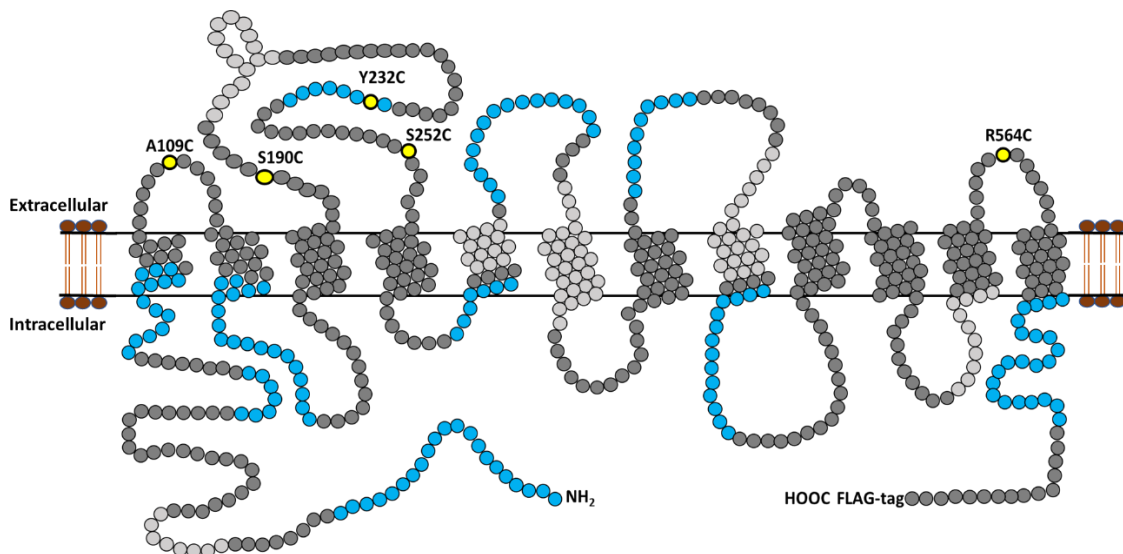


Figure 4.2 SERT mutations and MS coverage for S252C

Mutations were introduced one at a time and are shown as yellow spheres. Pellet 3 trial 2 oligomer study for mutation S252C showed nearly 50% coverage. Blue regions represent crosslink to MTS-benzophenone crosslinker, light grey represent regions observed without the crosslinker, dark grey represent regions not observed.

Oligomerization of NSS proteins is believed to be crucial for their trafficking to the membrane and substrate transport [208]. In numerous studies, DAT has been shown to exist as a dimer or higher oligomer [152, 208-213] and there is growing evidence

suggesting oligomeric formation in SERT [92, 93, 214]. Liu *et al.* used MALDI-TOF MS to identify and differentiate intra- from intermolecular Lys-Lys crosslinks in the extracellular domain of the glycine receptor in comparative footprinting studies of monomeric and oligomeric SDS-PAGE gel plugs [155]. Crosslinks observed in monomeric bands must be intramolecular crosslinks, while crosslinks identified in studies of oligomeric bands might be due to intra- or inter-molecular crosslinks. In this study, to distinguish intermolecular from intramolecular crosslinking, comparative CX-MS footprinting studies were conducted on monomeric and oligomeric bands.

4.2 Hypothesis

Structural information of SERT can be obtained by coupling photoaffinity labeling and mass spectrometry.

4.3 Results

Single cysteine mutations were introduced in extracellular loops 1, 2, and 6 into a cysteine-null rSERT cDNA (X8C). The commercially available bifunctional crosslinker (benzophenone-4-carboxamidoethyl methanethiosulfonate) contains a methanethiosulfonate (MTS) moiety for SH coupling to the introduced cysteine, and a photo-crosslinking benzophenone moiety for non-specific binding to amino acids within 20 Å. Upon photoactivation, SDS-PAGE gel-plus containing monomeric and oligomeric peptides were isolated, and proteolyzed to differentiate intra from intermolecular crosslinks. Mass shifted peptides containing the crosslinker mass were identified by electrospray ionization quadrupole time-of-flight mass spectrometry (ESI-Q-TOF MS) and

tandem MS studies identified specific sites of non-specific covalent attachment of the photocrosslinker.

Initially, trypsin digests were performed, but these studies did not result in acceptable levels of sequence coverage (only 5%-12% of rSERT was identified in control and experimental samples). This is attributed to significantly large regions of the sequence that do not contain arginine or lysine for trypsin digestion, with this being further exacerbated by any missed cleavages. Therefore, a double digest was performed using trypsin and Glu-C. The combination of the two produced percent coverages up to nearly 60%.

Pellets from 3 independent cell infections were prepared for each mutation, and each pellet was analyzed in triplicates. Mass shifted peptides are only reported if observed in at least 2 replicates. Given that peptide fragments can be modified at multiple sites, isobaric precursor ions are expected. To correctly pair precursor and product ion scans to allow for unambiguous product ion assignments, MSMS spectra are matched by retention time to their precursor ion as in-line liquid chromatography allows for the separation of isobaric peptides via their different chemical properties. CID fragmentation for a given peptide within a retention time window of ± 0.2 minutes produced several product ion fragmentation spectra. Each spectrum was analyzed individually to identify specific sites of crosslink. Sites of crosslinking were mapped using the crystal structure model of hSERT bound to citalopram (PDB#5I71) for visualization purposes (Figures 4.3-4.7). All hSERT crystal structures are bound to SSRIs that stabilize SERT in an outward-open conformation. Our studies were performed in the apo state, therefore the spatial crosslinking mapped onto the structure model may not represent the conformation of the transporter in its apo state.

For instance, in the citalopram-bound structure, positions Y232C and R564C (see figure 4.3) might seem inaccessible from the TM1 region, but become accessible for crosslink in the apo state.

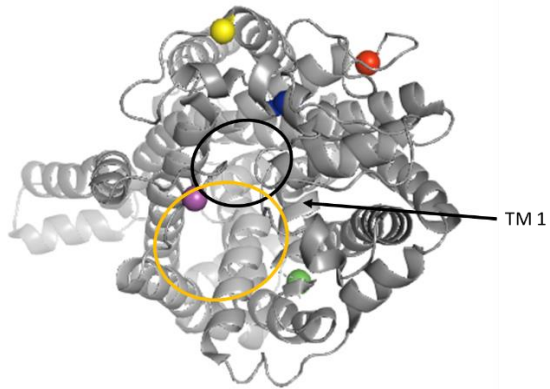


Figure 4.3 Top-down view of SERT Mutations A109C, S190C, Y232C, S252C, and R564C are represented in green, red, blue, yellow, and magenta spheres, respectively. Black and gold ovals represent location of S1 and S2 binding pockets, respectively.

The crosslinks observed for each introduced cysteine mutant are described below:

Mutation A109C- In the X8C plasmid, cysteine at position 109 was one of eight active cysteine, hence it was replaced with alanine. Here it was returned it to active cysteine, hence this mutation does not affect function. In the monomer study we observed crosslinking to the N-terminus, TM2-TM3 IL, TM4-TM5 IL, TM5-TM6 EL, TM8-TM9 IL, and the C-terminus (Table 4.1). It is important to note that residues 20-37 in the N-terminus were observed in the oligomer only, this could suggest a N-terminus movement upon dimerization of SERT. This observation agrees with previous studies which have suggested that the N-terminus is flexible and that this flexibility is necessary for function [91, 164-166]. On the other hand, it might be due to structure differences between the apo state and the outward-open state.

Mutation S190C- In the monomer study we observed crosslinking to the N-terminus, TM2-TM3 IL, TM3-TM4 EL, TM5-TM6 EL, TM8-TM9 IL, and the C-terminus (Table 4.2). No unique crosslinks in the oligomer compared to the monomer were observed. This shows no intermolecular crosslinks which could indicate that S190C is not within proximity of the dimer interface.

Mutation Y232C- In the monomer study we observed crosslinking to the N-terminus, TM1, TM2-TM3 IL, TM4-TM5 IL, TM5-TM6 EL, TM8-TM9 IL, and the C-terminus (Table 4.3). Residues 20-39 in the N-terminus were only observed in the oligomer crosslinks. This observation also suggests slight movements in the N-terminus upon dimerization.

Mutation S252C- In the monomer study we observed crosslinking to the N-terminus, TM2-TM3 IL, TM4-TM5 IL, TM5-TM6 EL, TM7-TM8 EL, TM8-TM9 IL, and the C-terminus (Table 4.4). Crosslinks to the TM3-TM4 EL were unique to the oligomer suggesting it is due to intermolecular crosslinks. This observation suggests that mutation S252C (located near TM4) is close to the dimer interface. This agrees with previous studies in which cysteine crosslinking experiments suggest that TM4 is involved in dimer formation in DAT [152, 210]. Coleman *et al.* suggested that EL2 participates in interactions with EL4 and EL6 and together sculpt a portion of the allosteric site [29]. There was no coverage to EL6, hence we did not see crosslinks to this region (See Fig. 4.2). Interestingly, mutation S252C is in EL2 and although we did not see crosslinking to EL6 we observed crosslinking in both the monomer and dimer studies to EL4.

Mutation R564C- In the monomer study we observed crosslinking to the N-terminal, TM1, TM2-TM3 IL, TM3-TM4 EL, TM5-TM6 EL, TM8-TM9 IL, and the C-terminus (Table 4.5). No difference was observed between the monomer and the oligomer study, in other words no indication of intermolecular crosslinks. This suggests that mutation R564C is also not within proximity to the dimer interface.

Table 4.1 A109C Crosslinks

Peptide	Structural Location	Molecular Crosslink	n
¹ <u>ME</u> T <u>TP</u> LNSQK <u>VLSEAKDR</u> ¹⁸	N-Terminal	Intramolecular	10
²⁰ D <u>AO</u> ENGVLQK <u>GVPTTADR</u> ³⁷		Intermolecular	2
⁵⁹ ASH <u>SIPA</u> ATTTLVAEIR <u>QGERETWGGK</u> ⁸⁵		Intramolecular	5
¹⁴⁵ N <u>GAI</u> S <u>IWRK</u> IAP <u>IFK</u> ¹⁵⁹	TM2-TM3 IC Loop		13
²⁹⁹ GAT <u>LP</u> G <u>AWR</u> GV <u>VFYLKP</u> NWQK <u>LE</u> ³²²	TM5-TM6 EC Loop		19
⁴⁴⁵ G <u>VITAV</u> LDEF <u>PHI</u> WAK <u>RR</u> ⁴⁶²	TM8/TM8-TM9 IC Loop		13
⁵⁹⁷ L <u>I</u> ST <u>PG</u> TL <u>KER</u> I <u>IK</u> ⁶¹⁰	TM12/C-Terminal		5
⁶⁰⁶ ER <u>I</u> IK <u>SIT</u> PE <u>I</u> PT <u>EIPA</u> GDIR ⁶²⁶	C-Terminal		10

Identified crosslinked peptides observed in mutation A109C. Peptides were observed within 10ppm error. The superscript numbers in the “Peptide” column represent the sequence position of the peptide. The underlined amino acids represent sites of crosslink. Blue font represents crosslinks from the monomeric bands, red font represents crosslinks from the oligomeric bands, purple font indicates crosslinks observed in both monomeric and oligomeric bands. The “Oligomeric Crosslink” column shows whether the peptide is an intermolecular or intramolecular crosslink. Peptides are defined as intermolecular if only observed in oligomeric bands. The “n” column represents the number of trials the peptide was observed in both dimer and monomeric studies.

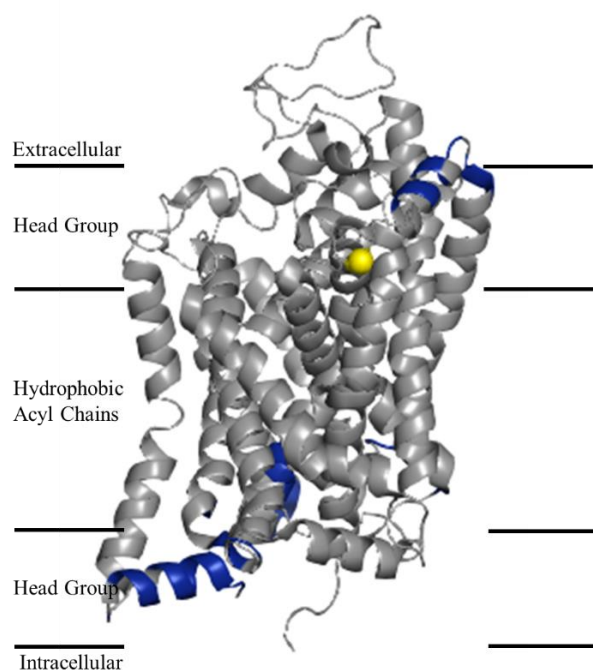


Figure 4.4 A109C crosslinking studies

Yellow sphere represents site of C109 attachment and sites of crosslinking are shown in blue. Residues 1-76 and 618-630 are truncated. Black lines represent location of lipid membrane head group region.

Data is mapped on crystal structure of hSERT bound to citalopram PDB# 5I71 [1]. Not all crosslinking data can be shown as some regions are missing in the crystal structure.

Table 4.2 S190C Crosslinks

Peptide	Structural Location	Molecular Crosslink	n
¹ METPLNSQKVLSEAKDR ¹⁸	N-Terminal	Intramolecular	29
¹⁵ AKDREDAQENGVLQK ²⁹			15
¹⁹ EDAQENGVLQKGVPTTADRAE ³⁹			13
⁵⁹ ASHSPAATTLLVAEIRQGER ⁷⁹			8
⁷⁴ IRQGERETWGKK ⁸⁵			14
¹³⁷ LALGQYHRNGAISWRK ¹⁵³	TM2/TM2-TM3 IC Loop		8
¹⁴⁵ NGAISWRKIAPFK ¹⁵⁹	TM2-TM3 IC Loop		15
²³¹ FYLRHVLQIHQSK ²⁴³	TM3-TM4 EC Loop		7
²⁹⁹ GATLPGAWRGVVFYLNWQKLE ³²²	TM5-TM6 EC Loop		18
⁴⁴⁵ GVITAVLDEFPHIWAKRR ⁴⁶²	TM8-TM9 IC Loop		13
⁵⁹⁷ LISLTPGILKERIK ⁶¹⁰	TM12/C-Terminal		16
⁶⁰⁶ ERIKSITPE ⁶¹⁵	C-Terminal	9	
⁶⁰⁷ RIKSITPETPEIPAGDIR ⁶²⁶		17	
⁶²⁰ IPAGDIRMNAV ⁶³⁰		5	

Identified crosslinked peptides observed in mutation S190C. Description of columns described in table 4.1.

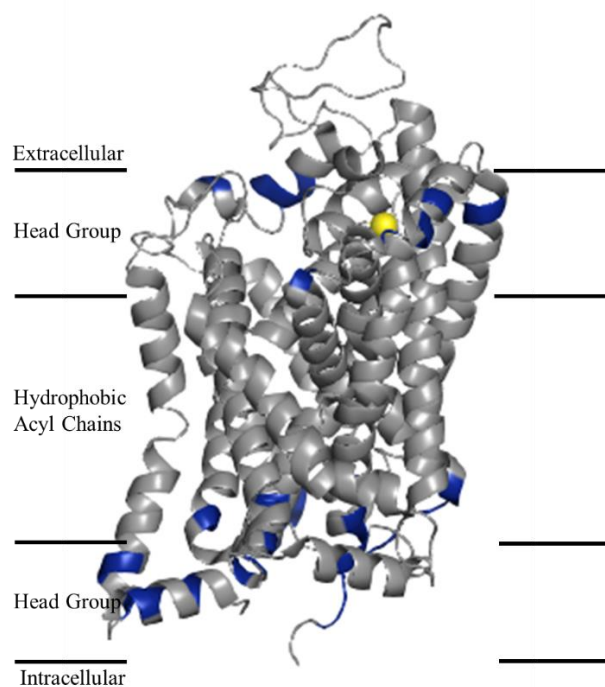


Figure 4.5 S190C crosslinking studies
 Yellow sphere represents site of C190 attachment and sites of crosslinking are shown in blue. See Fig. 4.3 for analogous details.

Table 4.3 Y232C Crosslinks

Peptide	Structural Location	Molecular Crosslink	n
³ ITPLNSQKVLSEAK ¹⁶	N-Terminal	Intramolecular	25
²⁰ DAQENGVLQKGVPTADRAE ³⁹		Intermolecular	2
⁵⁹ ASHSIPAATTTLVAEIRQGER ⁷⁹		Intramolecular	5
⁷⁴ IRQGERETWGGK ⁸⁵			12
⁸⁶ MDFLLSVIGYAVDLGNIWR ¹⁰⁴	TM1		4
¹⁴⁵ NGAISIWRKIPIFK ¹⁵⁹	TM2-TM3 IC Loop		7
²⁷³ GVKTS ^{GK} ²⁷⁹	TM4-TM5 IC Loop		3
²⁹⁹ GATLPGAWRGVV ^{FY} LKPNWQK ³¹⁹	TM5-TM6 EC Loop		10
⁴⁴⁵ GVITAVLDEFFHIWAKR ⁴⁶¹	TM8/TM8-TM9 IC Loop		13
⁴⁵⁴ FPHIWAKRR ⁴⁶²	TM8-TM9 IC Loop		36
⁵⁹⁷ LSTPGTLKER ⁶⁰⁷	TM12/C-Terminus		5
⁶⁰⁶ ERIKSITPETPTE ⁶¹⁹	C-Terminus		18
⁶⁰⁸ IKSITPETPTEIPAGDIRMNAV ⁶³⁰			9

Identified crosslinked peptides observed in mutation Y232C. Description of columns as described in table 4.1.

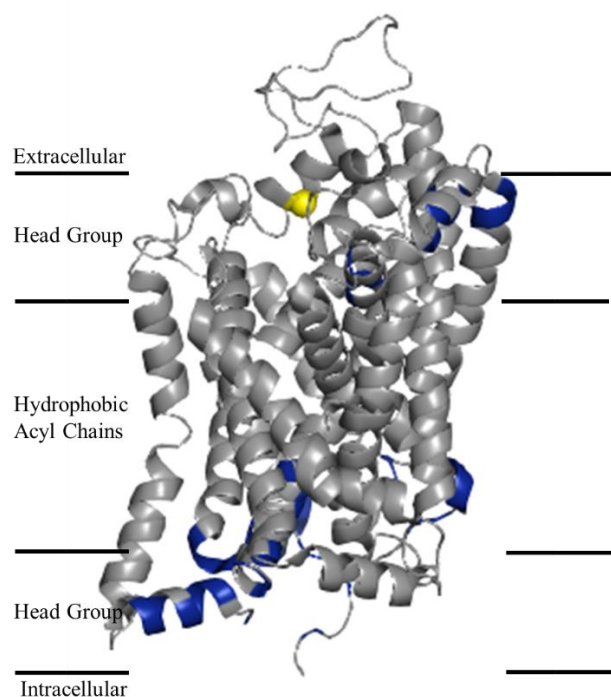


Figure 4.6 Y232C crosslinking studies. Yellow sphere represents site of C232 attachment and sites of crosslinking are shown in blue. See Fig. 4.3 for analogous details.

Table 4.4 S252C Crosslinks

Peptide	Structural Location	Molecular Crosslink	n	
¹ METPLNSQKVLSEAKDR ¹⁸	N-Terminal	Intramolecular	31	
¹⁷ DREDAQENGLQK ²⁹			2	
⁵⁹ ASHSIPAA ⁷⁹ TTLVAEIRQGER ⁷⁹			6	
⁷⁹ RETWGKK ⁸⁵			12	
⁸¹ TWGKKMDFLLSVIGYAVDLGN ¹⁰⁴ IWR ¹⁰⁴	N-Terminal/TM1	Intramolecular	7	
¹³⁷ LALGQYHRNGAIS ¹⁵⁹ IWRKIAP ¹⁵⁹ IFK ¹⁵⁹	TM2/TM2-TM3 IC Loop		11	
²³¹ FYLRHVLQIHQSK ²⁴³	TM3-TM4 EC Loop		Intermolecular	3
²⁷³ GVK ²⁷⁹ ISGK ²⁷⁹	TM4-TM5 IC Loop/TM5		Intramolecular	4
²⁹⁹ GATLPGAWRGV ³¹⁹ VFYLKPNWQK ³¹⁹	TM5-TM6 EC Loop	Intramolecular	23	
³⁸⁹ MRNEDVSEVAKDAGPSLLFIT ⁴¹² YAE ⁴¹²	TM7-TM8 EC Loop		5	
⁴⁴⁵ GVI ⁴⁶¹ AVLDEFPHI ⁴⁶¹ WAKR ⁴⁶¹	TM8/TM8-TM9 IC Loop		13	
⁴⁵⁴ FPHI ⁴⁶² WAKR ⁴⁶²	TM8-TM9 IC Loop		12	
⁵⁹⁷ L ⁶¹⁹ ISTPG ⁶¹⁹ TLKERI ⁶¹⁹ KSIT ⁶¹⁹ PETPTE ⁶¹⁹	C-Terminal		Intramolecular	13
⁶⁰⁷ RI ⁶²⁶ KSIT ⁶²⁶ PE ⁶²⁶ TP ⁶²⁶ I ⁶²⁶ EIPAGDIR ⁶²⁶				14

Identified crosslinked peptides observed in mutation S252C. Description of columns as described in table 4.1.

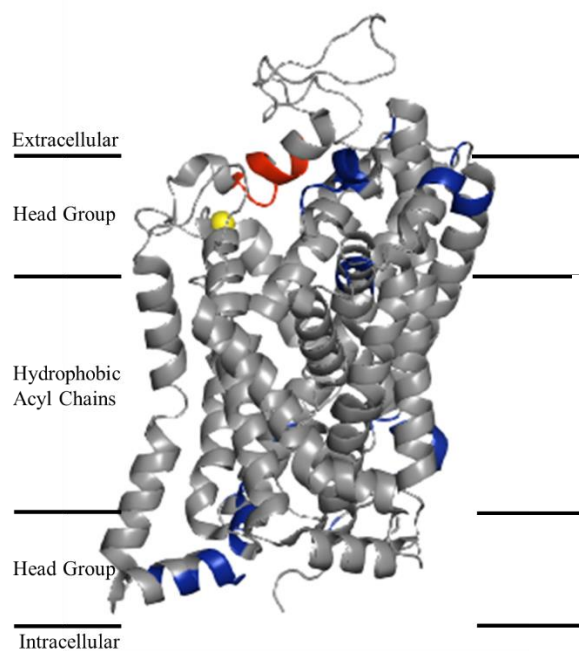


Figure 4.7 S252C crosslinking data
 Yellow sphere represents site of C252 attachment and sites of crosslinking are shown in blue. See Fig. 4.3 for analogous details.

Table 4.5 R564C Crosslinks

Peptide	Structural Location	Molecular Crosslink	n
¹ ME <u>T</u> PLNSQKVLSEAK ¹⁶	N-Terminal	Intramolecular	15
¹¹ VLSEAKDREDAQE ²³			7
¹⁵ AKDREDAQENGVLOK ²⁹			6
¹⁹ EDAQENGVLQKGVPTIADR ³⁷			15
⁵⁹ ASHSIPAAFTTLVAEIROQE ⁷⁸			9
⁷⁶ QGERETWGGK ⁸⁵			8
⁸¹ TWGGKMDFLLSVIGYAVDLGNIWR ¹⁰⁴	TM1		5
¹³⁷ LALGQYHRNGAISWRK ¹⁵³	TM2/TM2-TM3 IC Loop		13
¹⁵³ KIAPIFK ¹⁵⁹	TM2-TM3 IC Loop		9
²³¹ FYLRHVLQIHQSK ²⁴³	TM3-TM4 EC Loop		9
³⁰⁸ GVVFFYLPNWQK ³¹⁹	TM5-TM6 EC Loop		11
⁴⁴⁵ GVITAVLDEFPHIWAARR ⁴⁶²	TM8/TM8-TM9 IC Loop		20
⁵⁹⁷ LISTPGTLKE ⁶⁰⁶	TM12/C-Terminal		12
⁶⁰⁸ IKSITPTEIPAGDIRMNAV ⁶³⁰	C-Terminal	15	

Identified crosslinked peptides observed in mutation R564C. Description of columns as described in table 4.1.

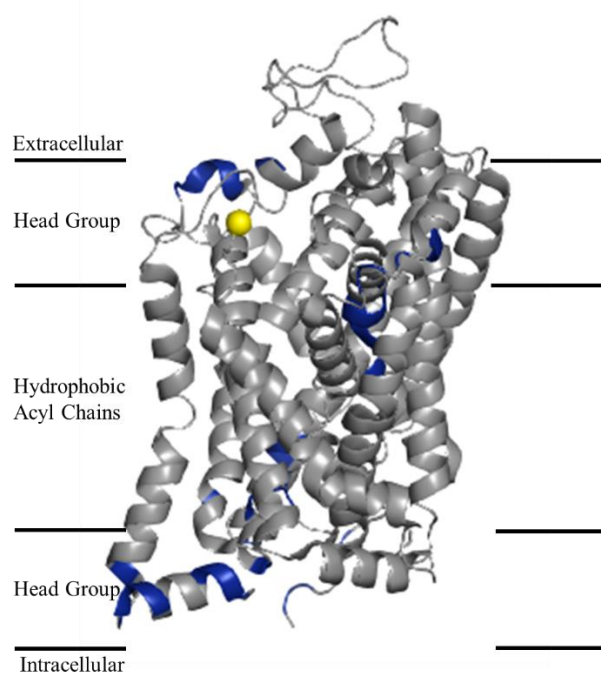


Figure 4.8 R564C crosslinking studies. Yellow sphere represents site of C564 attachment and sites of crosslinking are shown in blue. See Fig. 4.3 for analogous details.

Crosslinks from mutations V310C, L406C, and V489C in EL3, EL4, and EL5 respectively, are currently being analyzed by Warren Lowther in our laboratory. The network of all crosslinks from all EL is needed to create a more complete set of distance constraints and map a thorough analysis of the structure of all the EL. Although this report lacks comprehensive crosslinking data from every loop, the resulting unique and interesting observations to date assist in our understanding of SERT structure. Below are key points to take from the observed crosslinks; these points are explained in more detail in the “Discussion” (Section 4.4).

The N- and C- terminals are closely associated with the membrane.

Crosslinks were observed to both termini from every mutation located in EL1, EL2, and EL6. This observation was also observed in azi-cholesterol crosslinks performed in our laboratory by Andrew Demarco, and in the SERT-fluoxetine study in chapter 3. The fact that this study, the SERT-fluoxetine study, and the SERT-azi cholesterol study all showed crosslinks to the terminal tails show that there is consistency and support this observation.

Regions within IL1, IL2 and IL4 are closely associated with the membrane.

Mutations Y232C and S252C showed crosslinks to the IL2, while all mutations showed crosslinks to IL1 and IL4. Given that our crosslinker has a highly nonpolar benzophenone there is a possibility for the crosslinker to travel into the hydrophobic acyl-chains in the lipid bilayer and crosslink to intracellular regions if they come into proximity. Therefore, this observation suggests that regions of IL1, IL2, and IL4 are closely associated with the membrane.

Position S252 is located near the dimer interface.

Mutation S252C showed intermolecular crosslinks to region 231-243. Crosslinks to this region was not observed in the monomeric crosslinks. The dimer interface has not been elucidated and although more studies are needed to define this region, our results show that position 252 and region 231-243 are located at or near the dimer interface.

There are slight movements in the N-terminus.

Mutations A109C and Y232C showed intermolecular crosslinks in the N-terminus. In mutation A109C, we see intermolecular crosslinks to ²¹AQ²², ²⁹K, and ³²P, and intramolecular crosslinks to ¹¹VLSEAKDR¹⁸. These intermolecular crosslinks are evidence of movements in different regions within the same peptide. This observation may indicate slight changes due to dynamics. Similarly, in mutation Y232C, we observed intermolecular crosslinks to ²⁰DAQE²³ and ³⁴TADR³⁷, and intramolecular crosslinks to ¹¹VLSEAK¹⁶.

4.4 Discussion

To fully understand SERT it is imperative to investigate all its conformations during serotonin transport. In this study, we provide unique information about SERT structure in the apo state, which has not been resolved to date, thus providing new structural information. Investigating the apo state is crucial because it will help us understand where allosteric changes occur as it transitions from resting state to an outward-open conformation with the drug bound. In this study, not only do we provide structure information in a new state to which little is known about, but we also present crosslinks to regions that are currently not resolved in the SERT structure. Altogether, our results serve

as a unique complement to high resolution structures and can enhance current models. This might bring more insight into SERT's mechanism, which is of utmost importance to the refinement and improvement of therapeutics.

It is important to note that the observed crosslinks were mapped using the crystal structure of SERT bound to citalopram, which as previously mentioned is missing the terminal tails, was crystallized in a membrane mimetic environment, and is bound to the drug and is locked in the outward-open state. We performed our studies in the apo state. Hence, the images are not an absolute representation of SERT in the apo state. There could be movements which allow for the crosslinker to crosslink to areas that would seem inaccessible in the outward-open state but that become accessible for crosslink in the apo state.

Given that we used lipid vesicles where voltage gradient cannot be controlled, one might suggest that the crosslinker reached the intracellular regions due to the protein being positioned in the reverse orientation, that is with the intracellular regions facing out. However, regardless of orientation, the EL and IL are separated by a lipid bilayer whose acyl chains are about 30 Å across. The crosslinker used in this study can crosslink to any amino acid within approximately 20 Å, from the carbonyl carbon in the benzophenone to the alpha carbon of the rSERT backbone.

Crosslinking to the intracellular region of the protein was unexpected. Interestingly we saw crosslinks to the IL from all five cysteines introduced in the ELs. Since the crosslinker contains a highly non-polar benzophenone moiety there is a possibility that it can travel into the hydrophobic tail regions of the membrane, and crosslink to intracellular regions within 20Å. On one hand, the crosslinks to the intracellular regions might suggest

protein flexibility. Ryl *et al.* [215] used crosslinking mass spectrometry to identify structural restraints in human mitochondria using a non-cleavable crosslinker disuccinimidyl suberate. Ryl *et al.* proved that crosslinking mass spectrometry can generate enough data to unravel protein structure by identifying hundreds of distance restraints between protein residues and comparing them to protein data bank structures. Overall, they obtained crosslinks consistent with protein data bank structures, but some crosslinks suggest protein flexibility occurring *in situ* [215]. The influence that the phospholipid bilayer has on the structure and function of membrane proteins is well established. However, the role it plays on membrane protein flexibility is understudied. Lipids are not rigid but highly deformable molecules, this gives the lipid bilayer fluidity, and it may give SERT a level of flexibility. To our knowledge SERT flexibility within the lipid bilayer and its exact impact on protein structure has not been studied.

IL crosslinks may also indicate that such regions of the intracellular loops come in close contact with the membrane. Peptide ¹⁴⁵NGAISIWRK¹⁵³ in IL1 and peptide ⁴⁴⁹AVLDEFPHIW⁴⁵⁸ in IL4 crosslinked from all mutations, suggesting that these regions are closely associated with the membrane. Crosslinks to peptide ²⁷⁵KTSG²⁷⁸ in IL2 were observed in mutations Y232C and S252C. Interestingly, this peptide also crosslinked to PC using both hSERT and rSERT (chapter 3) and by azi-cholesterol in studies performed in our laboratory by DeMarco *et al.* using hSERT [199]. This suggests that this region is closely associated with the membrane.

The crosslinker can crosslink to any amino acid within approximately 20 Å, this helps us map distance constraints. We propose that peptide ¹⁴⁵NGAISIWRKIAPIFK¹⁵⁹ in IL1 and peptide ⁴⁴⁵GVITAVLDEFPHIWAKRR⁴⁶² in IL4 are within 20 Å from each

mutation. Whereas peptide $^{273}\text{GVKTSKG}^{279}$ is 20 Å from mutations Y232C and S252C and at a distance greater than 20 Å from mutations A109C, S190C and R564C. (See Figure 4.8). Crosslinks to EL3 was observed in all mutations, peptide $^{299}\text{GATLPGAWRGVVFYLYKPNWQK}^{319}$ crosslinked to mutations A109C, S190C, Y232C and S252C and peptide $^{308}\text{GVVFYLYKPNWQK}^{319}$ crosslinked to mutation R564C. This suggests that this region of EL3 is accessible to the mutations introduced in EL1, EL2, and EL6 and is within 20 Å from each mutation. Crosslinks to peptide $^{231}\text{FYLRHVLQIHQSK}^{243}$ in EL2 was observed in mutations S190C, S252C and R564C. Hence this region of EL2 is within 20 Å of these mutations, no crosslinks were observed to mutations A109C, Y232C suggesting this region of the EL2 is possibly further out at a distance greater than 20 Å from mutations A109C and Y232C. Crosslinks to EL4 were only observed in mutation S252C. (Figure 4.8)

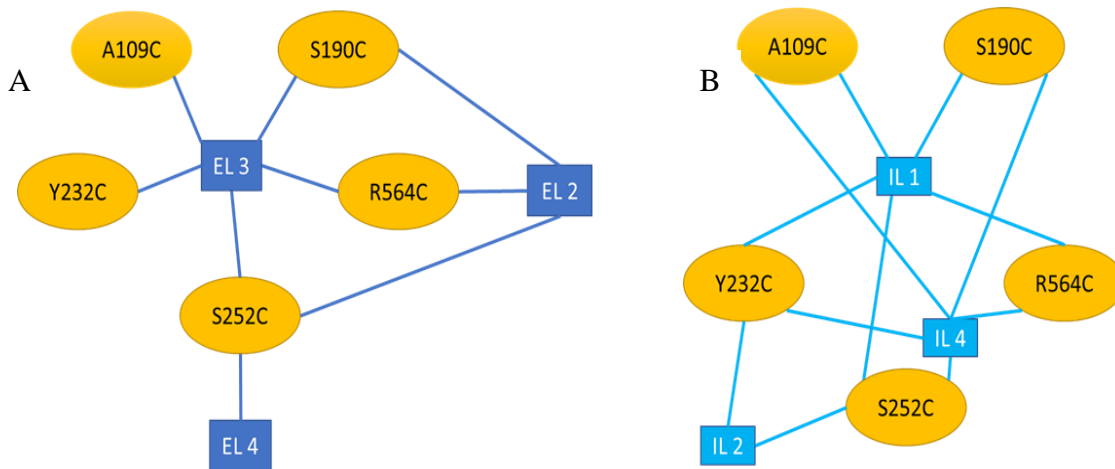


Figure 4.9 Network of crosslinks to intracellular and extracellular loops

(A) Network of crosslinks to the extracellular loops. (B) Network of crosslinks to the intracellular loops. Yellow ovals represent the mutations, dark blue boxes represent extracellular loops, light blue boxes represent intracellular loops, lines represent crosslinks within 20 Å.

The crosslinks to the terminal tails question the accuracy of the SERT models currently used. Our results suggest that both the N and C-termini are closely associated with the membrane. This is of special interest since those regions are not refined in the models yet are known to be physiologically important in activity [7, 166-169]. Sucic *et al.* found that the N-terminal of SERT can be found tethered in the membrane [166] and other studies have suggested a close interaction of the N-terminus with the membrane in hDAT [164]. Interestingly, in all mutations we observe crosslink to or near position 13 in the N-terminus, Ser13 is a phosphorylation site [204]. Possibly this lipid interaction and its electrostatics results in remodeling of the region upon phosphorylation and/or perhaps it is required for protein stability. Surprisingly, not only did we observe crosslinking to the N-terminus but also the C-terminus, thus suggesting that both terminal tails can be found associated with the membrane. This was also observed in the fluoxetine-SERT study in chapter 3, and in corroborating studies conducted in our lab by DeMarco *et al.*, where the terminal tails were also crosslinked by azi-cholesterol [199]. Previous studies have suggested that the N-terminal interacts with the membrane and that this interaction is necessary for transport, but here we provide evidence that both may be associated with the membrane. The exact role of the C-terminal is not fully known and there is still much to learn about the C-terminus, but our observation is a step forward towards understanding the structure of the C-terminus.

Other crosslinks to the N-terminus are evidence of potential subtle changes due to dynamics. In mutation A109C, we see intermolecular crosslinks to ²¹AQ²², ²⁹K, and ³²P, and intramolecular crosslinks to ¹¹VLSEAKDR¹⁸. These intermolecular crosslinks are evidence of movements in different regions within the same peptide. Similarly, in mutation

Y232C, we observed intermolecular crosslinks to ²⁰DAQE²³ and ³⁴TADR³⁷, and intramolecular crosslinks to ¹¹VLSEAK¹⁶. These are the first observations of dynamic movements within the N-terminus.

SERT dimerization is still an area of investigation, but by comparing monomeric and oligomeric crosslinks we were able to identify unique intermolecular crosslinks. S252C showed intermolecular crosslinks to the EL2. This observation suggests that position EL2-EL2 interactions occur across a dimer interface, placing both 252 and 231-243 as close enough to crosslink intermolecularly. This observation is significant as SERT's dimerization interface has not been elucidated. Although, more studies are needed to map the dimer interface more closely, these are the first observations of a direct interaction between SERT monomers.

Altogether, this study provides novel SERT structure information and shows the capability of CX-MS to map protein-protein interactions. This study also serves as a platform for future studies of SERT in other conformational states which could shine a light into SERT's allostery. This would enhance our current understanding of SERT and bring us closer to the development of improved therapeutics for not only depression but for numerous other disorders associated with SERT. This study highlights the power of CX-MS, it allows for insight into local structure of protein regions that are not available in other high-resolution structures and thus serves as a unique complement to current structures.

4.5 Acknowledgements

I thank every student involved in this project. Specifically, mutation S190C was introduced by high school student Israa Abdulmuttaleb during a summer research for high school students. The expression of all recombinant protein pellets using *Sf9* insect cells was performed by me, 3 protein pellets were expressed from each mutation, and 3 trials were performed from each protein pellet. I worked with some pellets and assigned others to a group of undergraduates. Andre Alexis Orbeta was assigned protein pellets from mutation S190C, Brandon Caridi worked with pellets from mutation Y232C, Henry May and I worked together with pellets from mutation R564C, Bailey Curran and I worked together with pellets from mutation S252C, and I worked with pellets from mutation A109C. I showed them how to perform every step involved in protein preparation for mass-spectrometry studies, from cell lysis to protein digestion. At times we worked together, while I worked on my pellets and other times (once they understood the process and became independent) they worked on their own under my supervision. I ran all the samples on the ESI-QTOF-MS for MS and tandem MS analysis, and analyzed the data.

Chapter 5: Future Directions

This study successfully shows that CX-MS can accurately provide distance constraints of the full-length transporter in a native-like lipid environment. This method can produce a wealth of information to complement current structures and enhance today's understanding of SERT's function and structure. Protein pellets containing single cysteine mutations V310C in EL3, L406 in EL4, and V489C in EL5 were MS analyzed by former undergraduate student Adam Gargano. The mass shifted peptides found will be targeted to determine specific sites of crosslink. The network of crosslinks from all EL will help us further map the structure of SERT by creating more distance constraints in every EL. This will shine light to more regions that cannot be characterized using high-definition structural tools such as x-ray crystallography due to the dynamic nature of the loops. Additionally, the complete network of distance constraints could help us map the dimer interface. The intermolecular crosslinks found in specific single cysteine mutants, and the lack of intermolecular crosslinks in other mutants might help us identify the region where two subunits come together.

In addition, to further characterize distance constrains, analogous crosslinking studies can be performed on the same point mutations but using crosslinkers of varying lengths. Increasing or decreasing the "diameter" of the area within crosslinking reach, would allow us to restrict the number of nearby crosslinks and further refine distances between residues.

Creating distance constraints of SERT at different conformational states would provide insight into SERT's allostery. Warren Lowther is currently conducting crosslinking studies using the same point mutations as in this study but in the inward-facing

conformational state that is stabilized by binding of ibogaine. Comparing his data with the data reported herein, will shine light into peptide movements occurring between the two states using full length SERT. This information can complement x-ray crystallography and cryo-EM structures, and offer a better understanding of the mechanistic changes that occur during transition between states.

Given that the peak intensities in mass spectrometry reflect the relative ionization of the mass ions not their concentration, the relative abundance of the crosslinks cannot be determined. Quantification of the crosslinks would differentiate high probability events from low probability events, thus further refining protein-protein interactions. The Cascio lab has developed a laser-induced fluorescence microfluidic platform to quantify mass shifted peptides (Andrew Davic, PhD Thesis, 2018). This method has the potential to detect ultra-trace amounts of sample using fluorescence detection. Microdroplets containing peptides are formed within a polyurethane microfluidic chip. Peptides are fluorescently tagged, and the resulting fluorescence response is directly proportional to sample concentration.

Membrane composition is known to influence protein structure and function. Phospholipids vary in tail length, degree of saturation and head groups all of which have an effect on the physical properties of membranes [216]. Studies on the nicotinic acetylcholine receptor (nAChR) show that there are differences in transport mechanism in relationship with nAChR interactions with phosphatidyl choline (PC) and phosphatidic acid (PA). This study was performed using PC lipids, potential crosslinking differences could be detected by performing analogous studies in PA lipids. Hence, showing the effect that different lipid compositions have on SERT structure.

References

1. Coleman, J.A., E.M. Green, and E. Gouaux, *X-ray structures and mechanism of the human serotonin transporter*. *Nature*, 2016. **532**(7599): p. 334-9.
2. Lin, T.W. and Y.M. Kuo, *Exercise benefits brain function: the monoamine connection*. *Brain Sci*, 2013. **3**(1): p. 39-53.
3. Kema, I.P., E.G. de Vries, and F.A. Muskiet, *Clinical chemistry of serotonin and metabolites*. *J Chromatogr B Biomed Sci Appl*, 2000. **747**(1-2): p. 33-48.
4. Tavoulari, S., A.N. Rizwan, L.R. Forrest, and G. Rudnick, *Reconstructing a chloride-binding site in a bacterial neurotransmitter transporter homologue*. *J Biol Chem*, 2011. **286**(4): p. 2834-42.
5. Beuming, T., L. Shi, J.A. Javitch, and H. Weinstein, *A comprehensive structure-based alignment of prokaryotic and eukaryotic neurotransmitter/Na⁺ symporters (NSS) aids in the use of the LeuT structure to probe NSS structure and function*. *Mol Pharmacol*, 2006. **70**(5): p. 1630-42.
6. Kristensen, A.S., et al., *SLC6 neurotransmitter transporters: structure, function, and regulation*. *Pharmacol Rev*, 2011. **63**(3): p. 585-640.
7. Torres, G.E. and S.G. Amara, *Glutamate and monoamine transporters: new visions of form and function*. *Curr Opin Neurobiol*, 2007. **17**(3): p. 304-12.
8. Rudnick, G. and J. Clark, *From synapse to vesicle: the reuptake and storage of biogenic amine neurotransmitters*. *Biochim Biophys Acta*, 1993. **1144**(3): p. 249-63.

9. Takayama, H. and S. Sugio, *Functional expression of milligram quantities of the synthetic human serotonin transporter gene in a tetracycline-inducible HEK293 cell line*. *Protein Expr Purif*, 2011. **76**(2): p. 211-20.
10. Chen, J.G., S. Liu-Chen, and G. Rudnick, *External cysteine residues in the serotonin transporter*. *Biochemistry*, 1997. **36**(6): p. 1479-86.
11. Boudker, O. and G. Verdon, *Structural perspectives on secondary active transporters*. *Trends Pharmacol Sci*, 2010. **31**(9): p. 418-26.
12. Forrest, L.R., Y.W. Zhang, M.T. Jacobs, J. Gesmonde, L. Xie, B.H. Honig, and G. Rudnick, *Mechanism for alternating access in neurotransmitter transporters*. *Proc Natl Acad Sci U S A*, 2008. **105**(30): p. 10338-43.
13. Torres-Altora, M.I., C.P. Kuntz, D.E. Nichols, and E.L. Barker, *Structural analysis of the extracellular entrance to the serotonin transporter permeation pathway*. *J Biol Chem*, 2010. **285**(20): p. 15369-79.
14. Rudnick, G., *Cytoplasmic permeation pathway of neurotransmitter transporters*. *Biochemistry*, 2011. **50**(35): p. 7462-75.
15. Locher, K.P., A.T. Lee, and D.C. Rees, *The E. coli BtuCD structure: a framework for ABC transporter architecture and mechanism*. *Science*, 2002. **296**(5570): p. 1091-8.
16. Dutzler, R., E.B. Campbell, M. Cadene, B.T. Chait, and R. MacKinnon, *X-ray structure of a ClC chloride channel at 3.0 Å reveals the molecular basis of anion selectivity*. *Nature*, 2002. **415**(6869): p. 287-94.

17. Murakami, S., R. Nakashima, E. Yamashita, T. Matsumoto, and A. Yamaguchi, *Crystal structures of a multidrug transporter reveal a functionally rotating mechanism*. Nature, 2006. **443**(7108): p. 173-9.
18. Saier, M.H., Jr., *Tracing pathways of transport protein evolution*. Mol Microbiol, 2003. **48**(5): p. 1145-56.
19. Yamashita, A., S.K. Singh, T. Kawate, Y. Jin, and E. Gouaux, *Crystal structure of a bacterial homologue of Na⁺/Cl⁻-dependent neurotransmitter transporters*. Nature, 2005. **437**(7056): p. 215-23.
20. Krishnamurthy, H. and E. Gouaux, *X-ray structures of LeuT in substrate-free outward-open and apo inward-open states*. Nature, 2012. **481**(7382): p. 469-74.
21. Penmatsa, A., K.H. Wang, and E. Gouaux, *X-ray structure of dopamine transporter elucidates antidepressant mechanism*. Nature, 2013. **503**(7474): p. 85-90.
22. Wang, K.H., A. Penmatsa, and E. Gouaux, *Neurotransmitter and psychostimulant recognition by the dopamine transporter*. Nature, 2015. **521**(7552): p. 322-7.
23. Penmatsa, A., K.H. Wang, and E. Gouaux, *X-ray structures of Drosophila dopamine transporter in complex with nisoxetine and reboxetine*. Nat Struct Mol Biol, 2015. **22**(6): p. 506-508.
24. Tatsumi, M., K. Groshan, R.D. Blakely, and E. Richelson, *Pharmacological profile of antidepressants and related compounds at human monoamine transporters*. Eur J Pharmacol, 1997. **340**(2-3): p. 249-58.

25. Bruss, M., P. Porzgen, L.J. Bryan-Lluka, and H. Bonisch, *The rat norepinephrine transporter: molecular cloning from PC12 cells and functional expression*. Brain Res Mol Brain Res, 1997. **52**(2): p. 257-62.
26. Miller, G.M., S.M. Yatin, R. De La Garza, 2nd, M. Goulet, and B.K. Madras, *Cloning of dopamine, norepinephrine and serotonin transporters from monkey brain: relevance to cocaine sensitivity*. Brain Res Mol Brain Res, 2001. **87**(1): p. 124-43.
27. Xhaard, H., V. Backstrom, K. Denessiouk, and M.S. Johnson, *Coordination of Na(+) by monoamine ligands in dopamine, norepinephrine, and serotonin transporters*. J Chem Inf Model, 2008. **48**(7): p. 1423-37.
28. Andersen, J., A.S. Kristensen, B. Bang-Andersen, and K. Stromgaard, *Recent advances in the understanding of the interaction of antidepressant drugs with serotonin and norepinephrine transporters*. Chem Commun (Camb), 2009(25): p. 3677-92.
29. Coleman, J.A., E.M. Green, and E. Gouaux, *X-ray structures and mechanism of the human serotonin transporter*. Nature, 2016. **532**(7599): p. 334-339.
30. Coleman, J.A. and E. Gouaux, *Structural basis for recognition of diverse antidepressants by the human serotonin transporter*. Nat Struct Mol Biol, 2018. **25**(2): p. 170-175.
31. Hamilton, P.J., et al., *De novo mutation in the dopamine transporter gene associates dopamine dysfunction with autism spectrum disorder*. Mol Psychiatry, 2013. **18**(12): p. 1315-23.

32. Coleman, J.A., D. Yang, Z. Zhao, P.C. Wen, C. Yoshioka, E. Tajkhorshid, and E. Gouaux, *Serotonin transporter-ibogaine complexes illuminate mechanisms of inhibition and transport*. *Nature*, 2019. **569**(7754): p. 141-145.
33. Coleman, J.A., V. Navratna, D. Antermite, D. Yang, J.A. Bull, and E. Gouaux, *Chemical and structural investigation of the paroxetine-human serotonin transporter complex*. *Elife*, 2020. **9**: p. e56427.
34. Wang, H., A. Goehring, K.H. Wang, A. Penmatsa, R. Ressler, and E. Gouaux, *Structural basis for action by diverse antidepressants on biogenic amine transporters*. *Nature*, 2013. **503**(7474): p. 141-5.
35. Abramyan, A.M., R.D. Slack, S. Meena, B.A. Davis, A.H. Newman, S.K. Singh, and L. Shi, *Computation-guided analysis of paroxetine binding to hSERT reveals functionally important structural elements and dynamics*. *Neuropharmacology*, 2019. **161**: p. 107411.
36. Slack, R.D., et al., *A Novel Bromine-Containing Paroxetine Analogue Provides Mechanistic Clues for Binding Ambiguity at the Central Primary Binding Site of the Serotonin Transporter*. *ACS Chem Neurosci*, 2019. **10**(9): p. 3946-3952.
37. Neubauer, H.A., C.G. Hansen, and O. Wiborg, *Dissection of an allosteric mechanism on the serotonin transporter: a cross-species study*. *Mol Pharmacol*, 2006. **69**(4): p. 1242-50.
38. Sinning, S., et al., *Binding and orientation of tricyclic antidepressants within the central substrate site of the human serotonin transporter*. *J Biol Chem*, 2010. **285**(11): p. 8363-74.

39. Glassman, A.H., *Cardiovascular effects of tricyclic antidepressants*. *Annu Rev Med*, 1984. **35**: p. 503-11.
40. Pacher, P., Z. Ungvari, P.P. Nanasi, S. Furst, and V. Kecskemeti, *Speculations on difference between tricyclic and selective serotonin reuptake inhibitor antidepressants on their cardiac effects. Is there any?* *Curr Med Chem*, 1999. **6**(6): p. 469-80.
41. Eshleman, A.J., M. Carmolli, M. Cumbay, C.R. Martens, K.A. Neve, and A. Janowsky, *Characteristics of drug interactions with recombinant biogenic amine transporters expressed in the same cell type*. *J Pharmacol Exp Ther*, 1999. **289**(2): p. 877-85.
42. Vetulani, J. and I. Nalepa, *Antidepressants: past, present and future*. *Eur J Pharmacol*, 2000. **405**(1-3): p. 351-63.
43. Cool, D.R., F.H. Leibach, and V. Ganapathy, *High-affinity paroxetine binding to the human placental serotonin transporter*. *Am J Physiol*, 1990. **259**(2 Pt 1): p. C196-204.
44. Renoir, T., *Selective serotonin reuptake inhibitor antidepressant treatment discontinuation syndrome: a review of the clinical evidence and the possible mechanisms involved*. *Front Pharmacol*, 2013. **4**: p. 45.
45. Nevels, R.M., S.T. Gontkovsky, and B.E. Williams, *Paroxetine-The Antidepressant from Hell? Probably Not, But Caution Required*. *Psychopharmacol Bull*, 2016. **46**(1): p. 77-104.
46. Ferguson, J.M., *SSRI Antidepressant Medications: Adverse Effects and Tolerability*. *Prim Care Companion J Clin Psychiatry*, 2001. **3**(1): p. 22-27.

47. Kennedy, S.H., H.F. Andersen, and R.W. Lam, *Efficacy of escitalopram in the treatment of major depressive disorder compared with conventional selective serotonin reuptake inhibitors and venlafaxine XR: a meta-analysis*. J Psychiatry Neurosci, 2006. **31**(2): p. 122-31.
48. Schellander, R. and J. Donnerer, *Antidepressants: clinically relevant drug interactions to be considered*. Pharmacology, 2010. **86**(4): p. 203-15.
49. Preskorn, S.H., *Comparison of the tolerability of bupropion, fluoxetine, imipramine, nefazodone, paroxetine, sertraline, and venlafaxine*. J Clin Psychiatry, 1995. **56 Suppl 6**: p. 12-21.
50. Dewan, M.J. and V.S. Anand, *Evaluating the tolerability of the newer antidepressants*. J Nerv Ment Dis, 1999. **187**(2): p. 96-101.
51. Wasko, M.J., K.A. Pellegrine, J.D. Madura, and C.K. Surratt, *A Role for Fragment-Based Drug Design in Developing Novel Lead Compounds for Central Nervous System Targets*. Front Neurol, 2015. **6**: p. 197.
52. Nolan, T.L., et al., *Identification of a novel selective serotonin reuptake inhibitor by coupling monoamine transporter-based virtual screening and rational molecular hybridization*. ACS Chem Neurosci, 2011. **2**(9): p. 544-552.
53. Goldstein, R.A., C. DesLauriers, and A.M. Burda, *Cocaine: history, social implications, and toxicity--a review*. Dis Mon, 2009. **55**(1): p. 6-38.
54. Uhl, G.R., F.S. Hall, and I. Sora, *Cocaine, reward, movement and monoamine transporters*. Mol Psychiatry, 2002. **7**(1): p. 21-6.

55. Han, D.D. and H.H. Gu, *Comparison of the monoamine transporters from human and mouse in their sensitivities to psychostimulant drugs*. BMC Pharmacol, 2006. **6**: p. 6.
56. Rudnick, G. and W. Sandtner, *Serotonin transport in the 21st century*. J Gen Physiol, 2019. **151**(11): p. 1248-1264.
57. Satel, S.L., S.M. Southwick, and F.H. Gawin, *Clinical features of cocaine-induced paranoia*. Am J Psychiatry, 1991. **148**(4): p. 495-8.
58. Zimmerman, J.L., *Cocaine intoxication*. Crit Care Clin, 2012. **28**(4): p. 517-26.
59. Popik, P., R.T. Layer, and P. Skolnick, *100 years of ibogaine: neurochemical and pharmacological actions of a putative anti-addictive drug*. Pharmacol Rev, 1995. **47**(2): p. 235-53.
60. Glick, S.D. and I.S. Maisonneuve, *Mechanisms of antiaddictive actions of ibogaine*. Ann N Y Acad Sci, 1998. **844**: p. 214-26.
61. Alper, K.R., *Ibogaine: a review*. Alkaloids Chem Biol, 2001. **56**: p. 1-38.
62. Jacobs, M.T., Y.W. Zhang, S.D. Campbell, and G. Rudnick, *Ibogaine, a noncompetitive inhibitor of serotonin transport, acts by stabilizing the cytoplasm-facing state of the transporter*. J Biol Chem, 2007. **282**(40): p. 29441-7.
63. Brown, T.K., *Ibogaine in the treatment of substance dependence*. Curr Drug Abuse Rev, 2013. **6**(1): p. 3-16.
64. Grogan, J., R. Gerona, J.W. Snow, and L. Kao, *Ibogaine Consumption With Seizure-Like Episodes, QTc-Prolongation, and Captured Cardiac Dysrhythmias*. J Emerg Med, 2019. **57**(4): p. e99-e104.

65. Koenig, X. and K. Hilber, *The anti-addiction drug ibogaine and the heart: a delicate relation*. *Molecules*, 2015. **20**(2): p. 2208-28.
66. Anglin, M.D., C. Burke, B. Perrochet, E. Stamper, and S. Dawud-Noursi, *History of the Methamphetamine Problem*. *Journal of Psychoactive Drugs*, 2000. **32**(2): p. 137-141.
67. Bett, W.R., *Benzedrine sulphate in clinical medicine; a survey of the literature*. *Postgrad Med J*, 1946. **22**: p. 205-18.
68. Guttmann, E. and W. Sargant, *Observations on Benzedrine*. *Br Med J*, 1937. **1**(3984): p. 1013-5.
69. Bradley, C., *The behavior of children receiving benzedrine*. *American journal of Psychiatry*, 1937. **94**(3): p. 577-585.
70. Heal, D.J., S.L. Smith, J. Gosden, and D.J. Nutt, *Amphetamine, past and present-- a pharmacological and clinical perspective*. *J Psychopharmacol*, 2013. **27**(6): p. 479-96.
71. Itzhak, Y. and C. Achat-Mendes, *Methamphetamine and MDMA (ecstasy) neurotoxicity: 'of mice and men'*. *IUBMB Life*, 2004. **56**(5): p. 249-55.
72. Axt, K.J. and M.E. Molliver, *Immunocytochemical evidence for methamphetamine-induced serotonergic axon loss in the rat brain*. *Synapse*, 1991. **9**(4): p. 302-13.
73. Cadet, J.L., S. Jayanthi, and X. Deng, *Speed kills: cellular and molecular bases of methamphetamine-induced nerve terminal degeneration and neuronal apoptosis*. *FASEB J*, 2003. **17**(13): p. 1775-88.

74. McCann, U.D. and G.A. Ricaurte, *Amphetamine neurotoxicity: accomplishments and remaining challenges*. *Neurosci Biobehav Rev*, 2004. **27**(8): p. 821-6.
75. Perez, J.A., Jr., E.L. Arsura, and S. Strategos, *Methamphetamine-related stroke: four cases*. *J Emerg Med*, 1999. **17**(3): p. 469-71.
76. Salanova, V. and R. Taubner, *Intracerebral haemorrhage and vasculitis secondary to amphetamine use*. *Postgrad Med J*, 1984. **60**(704): p. 429-30.
77. Macdougall, I.J. and R. Griffith, *Pharmacophore design and database searching for selective monoamine neurotransmitter transporter ligands*. *J Mol Graph Model*, 2008. **26**(7): p. 1113-24.
78. Chang, C., S. Ekins, P. Bahadduri, and P.W. Swaan, *Pharmacophore-based discovery of ligands for drug transporters*. *Adv Drug Deliv Rev*, 2006. **58**(12-13): p. 1431-50.
79. Indarte, M., J.D. Madura, and C.K. Surratt, *Dopamine transporter comparative molecular modeling and binding site prediction using the LeuT(Aa) leucine transporter as a template*. *Proteins*, 2008. **70**(3): p. 1033-46.
80. Indarte, M., Y. Liu, J.D. Madura, and C.K. Surratt, *Receptor-Based Discovery of a Plasmalemmal Monoamine Transporter Inhibitor via High Throughput Docking and Pharmacophore Modeling*. *ACS Chem Neurosci*, 2010. **1**(3): p. 223-233.
81. Beuming, T., et al., *The binding sites for cocaine and dopamine in the dopamine transporter overlap*. *Nat Neurosci*, 2008. **11**(7): p. 780-9.
82. Quick, M., A.M. Winther, L. Shi, P. Nissen, H. Weinstein, and J.A. Javitch, *Binding of an octylglucoside detergent molecule in the second substrate (S2) site*

- of LeuT establishes an inhibitor-bound conformation. Proc Natl Acad Sci U S A*, 2009. **106**(14): p. 5563-8.
83. Shi, L., M. Quick, Y. Zhao, H. Weinstein, and J.A. Javitch, *The mechanism of a neurotransmitter:sodium symporter--inward release of Na⁺ and substrate is triggered by substrate in a second binding site. Mol Cell*, 2008. **30**(6): p. 667-77.
84. Nolan, T.L., L.M. Geffert, B.J. Kolber, J.D. Madura, and C.K. Surratt, *Discovery of novel-scaffold monoamine transporter ligands via in silico screening with the S1 pocket of the serotonin transporter. ACS Chem Neurosci*, 2014. **5**(9): p. 784-92.
85. Andersen, J., et al., *Mutational mapping and modeling of the binding site for (S)-citalopram in the human serotonin transporter. J Biol Chem*, 2010. **285**(3): p. 2051-63.
86. Barker, E.L., M.A. Perlman, E.M. Adkins, W.J. Houlihan, Z.B. Pristupa, H.B. Niznik, and R.D. Blakely, *High affinity recognition of serotonin transporter antagonists defined by species-scanning mutagenesis. An aromatic residue in transmembrane domain I dictates species-selective recognition of citalopram and mazindol. J Biol Chem*, 1998. **273**(31): p. 19459-68.
87. Henry, L.K., et al., *Tyr-95 and Ile-172 in transmembrane segments 1 and 3 of human serotonin transporters interact to establish high affinity recognition of antidepressants. J Biol Chem*, 2006. **281**(4): p. 2012-23.
88. Plenge, P., et al., *Steric hindrance mutagenesis in the conserved extracellular vestibule impedes allosteric binding of antidepressants to the serotonin transporter. J Biol Chem*, 2012. **287**(47): p. 39316-26.

89. Lee, A.G., *How lipids affect the activities of integral membrane proteins*. Biochim Biophys Acta, 2004. **1666**(1-2): p. 62-87.
90. Magnani, F., C.G. Tate, S. Wynne, C. Williams, and J. Haase, *Partitioning of the serotonin transporter into lipid microdomains modulates transport of serotonin*. J Biol Chem, 2004. **279**(37): p. 38770-8.
91. Khelashvili, G. and H. Weinstein, *Functional mechanisms of neurotransmitter transporters regulated by lipid-protein interactions of their terminal loops*. Biochim Biophys Acta, 2015. **1848**(9): p. 1765-74.
92. Anderluh, A., et al., *Single molecule analysis reveals coexistence of stable serotonin transporter monomers and oligomers in the live cell plasma membrane*. J Biol Chem, 2014. **289**(7): p. 4387-94.
93. Kilic, F. and G. Rudnick, *Oligomerization of serotonin transporter and its functional consequences*. Proc Natl Acad Sci U S A, 2000. **97**(7): p. 3106-11.
94. Walsh, C.T., S. Garneau-Tsodikova, and G.J. Gatto, Jr., *Protein posttranslational modifications: the chemistry of proteome diversifications*. Angew Chem Int Ed Engl, 2005. **44**(45): p. 7342-72.
95. Androutsellis-Theotokis, A., F. Ghassemi, and G. Rudnick, *A conformationally sensitive residue on the cytoplasmic surface of serotonin transporter*. J Biol Chem, 2001. **276**(49): p. 45933-8.
96. Sinz, A., *Chemical cross-linking and mass spectrometry for mapping three-dimensional structures of proteins and protein complexes*. J Mass Spectrom, 2003. **38**(12): p. 1225-37.

97. Silverbush, D. and R. Sharan, *A systematic approach to orient the human protein–protein interaction network*. Nature Communications, 2019. **10**(1): p. 3015.
98. Hartl, F.U., A. Bracher, and M. Hayer-Hartl, *Molecular chaperones in protein folding and proteostasis*. Nature, 2011. **475**(7356): p. 324-32.
99. Leitner, A., T. Walzthoeni, A. Kahraman, F. Herzog, O. Rinner, M. Beck, and R. Aebersold, *Probing native protein structures by chemical cross-linking, mass spectrometry, and bioinformatics*. Mol Cell Proteomics, 2010. **9**(8): p. 1634-49.
100. Brunner, J., *New photolabeling and crosslinking methods*. Annu Rev Biochem, 1993. **62**: p. 483-514.
101. Hur, G.H., J.L. Meier, J. Baskin, J.A. Codelli, C.R. Bertozzi, M.A. Marahiel, and M.D. Burkart, *Crosslinking studies of protein-protein interactions in nonribosomal peptide biosynthesis*. Chem Biol, 2009. **16**(4): p. 372-81.
102. Pham, N.D., R.B. Parker, and J.J. Kohler, *Photocrosslinking approaches to interactome mapping*. Curr Opin Chem Biol, 2013. **17**(1): p. 90-101.
103. Kluger, R. and A. Alagic, *Chemical cross-linking and protein-protein interactions-a review with illustrative protocols*. Bioorg Chem, 2004. **32**(6): p. 451-72.
104. Schlieker, C., et al., *Substrate recognition by the AAA+ chaperone ClpB*. Nat Struct Mol Biol, 2004. **11**(7): p. 607-15.
105. Liu, C., et al., *Coupled chaperone action in folding and assembly of hexadecameric Rubisco*. Nature, 2010. **463**(7278): p. 197-202.

106. Freinkman, E., S.S. Chng, and D. Kahne, *The complex that inserts lipopolysaccharide into the bacterial outer membrane forms a two-protein plug-and-barrel*. Proc Natl Acad Sci U S A, 2011. **108**(6): p. 2486-91.
107. Solomon, M.J. and A. Varshavsky, *Formaldehyde-mediated DNA-protein crosslinking: a probe for in vivo chromatin structures*. Proc Natl Acad Sci U S A, 1985. **82**(19): p. 6470-4.
108. Hecht, A., T. Laroche, S. Strahl-Bolsinger, S.M. Gasser, and M. Grunstein, *Histone H3 and H4 N-termini interact with SIR3 and SIR4 proteins: a molecular model for the formation of heterochromatin in yeast*. Cell, 1995. **80**(4): p. 583-92.
109. Gavrillov, A., S.V. Razin, and G. Cavalli, *In vivo formaldehyde cross-linking: it is time for black box analysis*. Brief Funct Genomics, 2015. **14**(2): p. 163-5.
110. Rohs, R., X. Jin, S.M. West, R. Joshi, B. Honig, and R.S. Mann, *Origins of specificity in protein-DNA recognition*. Annu Rev Biochem, 2010. **79**: p. 233-69.
111. Han, X., A. Aslanian, and J.R. Yates, 3rd, *Mass spectrometry for proteomics*. Curr Opin Chem Biol, 2008. **12**(5): p. 483-90.
112. Trauger, S.A., W. Webb, and G. Siuzdak, *Peptide and protein analysis with mass spectrometry*. Spectroscopy, 2002. **16**: p. 320152.
113. Griffiths, W.J. and Y. Wang, *Mass spectrometry: from proteomics to metabolomics and lipidomics*. Chem Soc Rev, 2009. **38**(7): p. 1882-96.
114. Resing, K.A. and N.G. Ahn, *Proteomics strategies for protein identification*. FEBS Lett, 2005. **579**(4): p. 885-9.
115. Aebersold, R. and M. Mann, *Mass spectrometry-based proteomics*. Nature, 2003. **422**(6928): p. 198-207.

116. Kriwacki, R., N. Reisdorph, and G. Siuzdak, *Protein structure characterization with mass spectrometry*. Spectroscopy, 2004. **18**: p. 407960.
117. Nadler, W.M., D. Waidelich, A. Kerner, S. Hanke, R. Berg, A. Trumpp, and C. Rösli, *MALDI versus ESI: The Impact of the Ion Source on Peptide Identification*. Journal of Proteome Research, 2017. **16**(3): p. 1207-1215.
118. Dreisewerd, K., *The desorption process in MALDI*. Chem Rev, 2003. **103**(2): p. 395-426.
119. Haag, A.M., *Mass Analyzers and Mass Spectrometers*. Adv Exp Med Biol, 2016. **919**: p. 157-169.
120. Jones, A.W. and H.J. Cooper, *Dissociation techniques in mass spectrometry-based proteomics*. Analyst, 2011. **136**(17): p. 3419-3429.
121. Wells, J.M. and S.A. McLuckey, *Collision-induced dissociation (CID) of peptides and proteins*. Methods Enzymol, 2005. **402**: p. 148-85.
122. Sleno, L. and D.A. Volmer, *Ion activation methods for tandem mass spectrometry*. J Mass Spectrom, 2004. **39**(10): p. 1091-112.
123. Steen, H. and M. Mann, *The ABC's (and XYZ's) of peptide sequencing*. Nat Rev Mol Cell Biol, 2004. **5**(9): p. 699-711.
124. Savaryn, J.P., T.K. Toby, and N.L. Kelleher, *A researcher's guide to mass spectrometry-based proteomics*. Proteomics, 2016. **16**(18): p. 2435-43.
125. Douglas, D.J., A.J. Frank, and D. Mao, *Linear ion traps in mass spectrometry*. Mass Spectrom Rev, 2005. **24**(1): p. 1-29.
126. Mao, D. and D.J. Douglas, *H/D exchange of gas phase bradykinin ions in a linear quadrupole ion trap*. J Am Soc Mass Spectrom, 2003. **14**(2): p. 85-94.

127. Hager, J.W., *A new linear ion trap mass spectrometer*. Rapid Communications in Mass Spectrometry, 2002. **16**(6): p. 512-526.
128. Marshall, A.G., C.L. Hendrickson, and G.S. Jackson, *Fourier transform ion cyclotron resonance mass spectrometry: a primer*. Mass Spectrom Rev, 1998. **17**(1): p. 1-35.
129. Parker, C.E., M.R. Warren, and V. Mocanu, *Mass Spectrometry for Proteomics*. 2010.
130. Makarov, A., *Electrostatic axially harmonic orbital trapping: a high-performance technique of mass analysis*. Anal Chem, 2000. **72**(6): p. 1156-62.
131. Hu, Q., R.J. Noll, H. Li, A. Makarov, M. Hardman, and R. Graham Cooks, *The Orbitrap: a new mass spectrometer*. J Mass Spectrom, 2005. **40**(4): p. 430-43.
132. Boesl, U., *Time-of-flight mass spectrometry: Introduction to the basics*. Mass Spectrom Rev, 2017. **36**(1): p. 86-109.
133. Mamyrin, B., V. Karataev, D. Shmikk, and V. Zagulin, *The mass-reflectron, a new nonmagnetic time-of-flight mass spectrometer with high resolution*. Zh. Eksp. Teor. Fiz, 1973. **64**(1): p. 82-89.
134. Sinz, A., C. Arlt, D. Chorev, and M. Sharon, *Chemical cross-linking and native mass spectrometry: A fruitful combination for structural biology*. Protein Sci, 2015. **24**(8): p. 1193-209.
135. Sinz, A., *Cross-Linking/Mass Spectrometry for Studying Protein Structures and Protein-Protein Interactions: Where Are We Now and Where Should We Go from Here?* Angew Chem Int Ed Engl, 2018. **57**(22): p. 6390-6396.

136. Sinz, A., *Chemical cross-linking and mass spectrometry to map three-dimensional protein structures and protein-protein interactions*. Mass Spectrom Rev, 2006. **25**(4): p. 663-82.
137. Chen, F., S. Gerber, V.M. Korkhov, S. Mireku, M. Bucher, K.P. Locher, and R. Zenobi, *On the efficiency of NHS ester cross-linkers for stabilizing integral membrane protein complexes*. J Am Soc Mass Spectrom, 2015. **26**(3): p. 493-8.
138. Partis, M.D., D.G. Griffiths, G.C. Roberts, and R.B. Beechey, *Cross-linking of protein by ω -maleimido alkanoylN-hydroxysuccinimido esters*. Journal of Protein Chemistry, 1983. **2**(3): p. 263-277.
139. Preston, G.W. and A.J. Wilson, *Photo-induced covalent cross-linking for the analysis of biomolecular interactions*. Chem Soc Rev, 2013. **42**(8): p. 3289-301.
140. Smith, E. and I. Collins, *Photoaffinity labeling in target- and binding-site identification*. Future Med Chem, 2015. **7**(2): p. 159-83.
141. Herner, A., et al., *2-Aryl-5-carboxytetrazole as a New Photoaffinity Label for Drug Target Identification*. J Am Chem Soc, 2016. **138**(44): p. 14609-14615.
142. Dorman, G. and G.D. Prestwich, *Benzophenone photophores in biochemistry*. Biochemistry, 1994. **33**(19): p. 5661-73.
143. Novak, P. and G.H. Kruppa, *Intra-molecular cross-linking of acidic residues for protein structure studies*. Eur J Mass Spectrom (Chichester), 2008. **14**(6): p. 355-65.
144. Liu, F. and M.B. Goshe, *Combinatorial electrostatic collision-induced dissociative chemical cross-linking reagents for probing protein surface topology*. Anal Chem, 2010. **82**(14): p. 6215-23.

145. Zybailov, B.L., G.V. Glazko, M. Jaiswal, and K.D. Raney, *Large Scale Chemical Cross-linking Mass Spectrometry Perspectives*. J Proteomics Bioinform, 2013. **6**(Suppl 2): p. 001.
146. Young, M.M., et al., *High throughput protein fold identification by using experimental constraints derived from intramolecular cross-links and mass spectrometry*. Proc Natl Acad Sci U S A, 2000. **97**(11): p. 5802-6.
147. Schmidt, R. and A. Sinz, *Improved single-step enrichment methods of cross-linked products for protein structure analysis and protein interaction mapping*. Anal Bioanal Chem, 2017. **409**(9): p. 2393-2400.
148. Mitulovic, G. and K. Mechtler, *HPLC techniques for proteomics analysis--a short overview of latest developments*. Brief Funct Genomic Proteomic, 2006. **5**(4): p. 249-60.
149. Mitulovic, G., M. Smoluch, J.P. Chervet, I. Steinmacher, A. Kungl, and K. Mechtler, *An improved method for tracking and reducing the void volume in nano HPLC-MS with micro trapping columns*. Anal Bioanal Chem, 2003. **376**(7): p. 946-51.
150. Yu, C. and L. Huang, *Cross-Linking Mass Spectrometry: An Emerging Technology for Interactomics and Structural Biology*. Anal Chem, 2018. **90**(1): p. 144-165.
151. Cheng, M.H., J. Garcia-Olivares, S. Wasserman, J. DiPietro, and I. Bahar, *Allosteric modulation of human dopamine transporter activity under conditions promoting its dimerization*. J Biol Chem, 2017. **292**(30): p. 12471-12482.

152. Hastrup, H., N. Sen, and J.A. Javitch, *The human dopamine transporter forms a tetramer in the plasma membrane: cross-linking of a cysteine in the fourth transmembrane segment is sensitive to cocaine analogs*. J Biol Chem, 2003. **278**(46): p. 45045-8.
153. Tian, M. and S. Ye, *Allosteric regulation in NMDA receptors revealed by the genetically encoded photo-cross-linkers*. Scientific Reports, 2016. **6**: p. 34751.
154. Zhao, L., et al., *Smart Cutter: An Efficient Strategy for Increasing the Coverage of Chemical Cross-Linking Analysis*. Anal Chem, 2020. **92**(1): p. 1097-1105.
155. Liu, Z., A. Szarecka, M. Yonkunas, K. Speranskiy, M. Kurnikova, and M. Cascio, *Crosslinking constraints and computational models as complementary tools in modeling the extracellular domain of the glycine receptor*. PLoS One, 2014. **9**(7): p. e102571.
156. Muller, M.Q. and A. Sinz, *Chemical cross-linking and high-resolution mass spectrometry to study protein-drug interactions*. Methods Mol Biol, 2012. **803**: p. 205-18.
157. Iacobucci, C., M. Gotze, and A. Sinz, *Cross-linking/mass spectrometry to get a closer view on protein interaction networks*. Curr Opin Biotechnol, 2020. **63**: p. 48-53.
158. Chavez, J.D., C.R. Weisbrod, C. Zheng, J.K. Eng, and J.E. Bruce, *Protein interactions, post-translational modifications and topologies in human cells*. Mol Cell Proteomics, 2013. **12**(5): p. 1451-67.

159. Kang, S., L. Mou, J. Lanman, S. Velu, W.J. Brouillette, and P.E. Prevelige, Jr., *Synthesis of biotin-tagged chemical cross-linkers and their applications for mass spectrometry*. Rapid Commun Mass Spectrom, 2009. **23**(11): p. 1719-26.
160. Nessen, M.A., et al., *Selective enrichment of azide-containing peptides from complex mixtures*. J Proteome Res, 2009. **8**(7): p. 3702-11.
161. Shi, Y., *A glimpse of structural biology through X-ray crystallography*. Cell, 2014. **159**(5): p. 995-1014.
162. Smyth, M.S. and J.H. Martin, *x ray crystallography*. Mol Pathol, 2000. **53**(1): p. 8-14.
163. Smicun, Y., S.D. Campbell, M.A. Chen, H. Gu, and G. Rudnick, *The role of external loop regions in serotonin transport. Loop scanning mutagenesis of the serotonin transporter external domain*. J Biol Chem, 1999. **274**(51): p. 36058-64.
164. Khelashvili, G., M. Doktorova, M.A. Sahai, N. Johner, L. Shi, and H. Weinstein, *Computational modeling of the N-terminus of the human dopamine transporter and its interaction with PIP2 -containing membranes*. Proteins, 2015. **83**(5): p. 952-69.
165. Khelashvili, G., et al., *Spontaneous inward opening of the dopamine transporter is triggered by PIP2-regulated dynamics of the N-terminus*. ACS Chem Neurosci, 2015. **6**(11): p. 1825-37.
166. Sucic, S., et al., *The N terminus of monoamine transporters is a lever required for the action of amphetamines*. J Biol Chem, 2010. **285**(14): p. 10924-38.

167. Koban, F., et al., *A salt bridge linking the first intracellular loop with the C terminus facilitates the folding of the serotonin transporter*. J Biol Chem, 2015. **290**(21): p. 13263-78.
168. Sucic, S., A. El-Kasaby, O. Kudlacek, S. Sarker, H.H. Sitte, P. Marin, and M. Freissmuth, *The serotonin transporter is an exclusive client of the coat protein complex II (COPII) component SEC24C*. J Biol Chem, 2011. **286**(18): p. 16482-90.
169. Sucic, S., F. Koban, A. El-Kasaby, O. Kudlacek, T. Stockner, H.H. Sitte, and M. Freissmuth, *Switching the clientele: a lysine residing in the C terminus of the serotonin transporter specifies its preference for the coat protein complex II component SEC24C*. J Biol Chem, 2013. **288**(8): p. 5330-41.
170. Quick, M.W., *Regulating the conducting states of a mammalian serotonin transporter*. Neuron, 2003. **40**(3): p. 537-49.
171. Sung, U., et al., *A regulated interaction of syntaxin 1A with the antidepressant-sensitive norepinephrine transporter establishes catecholamine clearance capacity*. J Neurosci, 2003. **23**(5): p. 1697-709.
172. Lee, K.H., M.Y. Kim, D.H. Kim, and Y.S. Lee, *Syntaxin 1A and receptor for activated C kinase interact with the N-terminal region of human dopamine transporter*. Neurochem Res, 2004. **29**(7): p. 1405-9.
173. Zhou, H.X. and T.A. Cross, *Influences of membrane mimetic environments on membrane protein structures*. Annu Rev Biophys, 2013. **42**: p. 361-92.
174. Lowry, O.H., N.J. Rosebrough, A.L. Farr, and R.J. Randall, *Protein measurement with the Folin phenol reagent*. J Biol Chem, 1951. **193**(1): p. 265-75.

175. Berumen, L.C., A. Rodriguez, R. Miledi, and G. Garcia-Alcocer, *Serotonin receptors in hippocampus*. ScientificWorldJournal, 2012. **2012**: p. 823493.
176. Wong, D.T., K.W. Perry, and F.P. Bymaster, *Case history: the discovery of fluoxetine hydrochloride (Prozac)*. Nat Rev Drug Discov, 2005. **4**(9): p. 764-74.
177. Moller, I.R., M. Slivacka, A.K. Nielsen, S.G.F. Rasmussen, U. Gether, C.J. Loland, and K.D. Rand, *Conformational dynamics of the human serotonin transporter during substrate and drug binding*. Nat Commun, 2019. **10**(1): p. 1687.
178. Feighner, J.P., *Mechanism of action of antidepressant medications*. J Clin Psychiatry, 1999. **60 Suppl 4**: p. 4-11; discussion 12-3.
179. Hillhouse, T.M. and J.H. Porter, *A brief history of the development of antidepressant drugs: from monoamines to glutamate*. Exp Clin Psychopharmacol, 2015. **23**(1): p. 1-21.
180. Piscitelli, C.L., H. Krishnamurthy, and E. Gouaux, *Neurotransmitter/sodium symporter orthologue LeuT has a single high-affinity substrate site*. Nature, 2010. **468**(7327): p. 1129-32.
181. Back, J.W., L. de Jong, A.O. Muijsers, and C.G. de Koster, *Chemical cross-linking and mass spectrometry for protein structural modeling*. J Mol Biol, 2003. **331**(2): p. 303-13.
182. Back, J.W., et al., *A structure for the yeast prohibitin complex: Structure prediction and evidence from chemical crosslinking and mass spectrometry*. Protein Sci, 2002. **11**(10): p. 2471-8.

183. Chang, Z., J. Kuchar, and R.P. Hausinger, *Chemical cross-linking and mass spectrometric identification of sites of interaction for UreD, UreF, and urease*. J Biol Chem, 2004. **279**(15): p. 15305-13.
184. Egnaczyk, G.F., K.D. Greis, E.R. Stimson, and J.E. Maggio, *Photoaffinity cross-linking of Alzheimer's disease amyloid fibrils reveals interstrand contact regions between assembled beta-amyloid peptide subunits*. Biochemistry, 2001. **40**(39): p. 11706-14.
185. Giron-Monzon, L., L. Manelyte, R. Ahrends, D. Kirsch, B. Spengler, and P. Friedhoff, *Mapping protein-protein interactions between MutL and MutH by cross-linking*. J Biol Chem, 2004. **279**(47): p. 49338-45.
186. Huang, B.X., H.Y. Kim, and C. Dass, *Probing three-dimensional structure of bovine serum albumin by chemical cross-linking and mass spectrometry*. J Am Soc Mass Spectrom, 2004. **15**(8): p. 1237-47.
187. Muller, M.Q., C.H. Ihling, and A. Sinz, *Analyzing PPARalpha/ligand interactions by chemical cross-linking and high-resolution mass spectrometry*. Methods Mol Biol, 2013. **952**: p. 287-99.
188. Vasilescu, J., X. Guo, and J. Kast, *Identification of protein-protein interactions using in vivo cross-linking and mass spectrometry*. Proteomics, 2004. **4**(12): p. 3845-54.
189. Bennett, K.L., M. Kussmann, P. Bjork, M. Godzwon, M. Mikkelsen, P. Sorensen, and P. Roepstorff, *Chemical cross-linking with thiol-cleavable reagents combined with differential mass spectrometric peptide mapping--a novel approach to assess intermolecular protein contacts*. Protein Sci, 2000. **9**(8): p. 1503-18.

190. Yip, G.M., et al., *A propofol binding site on mammalian GABAA receptors identified by photolabeling*. Nat Chem Biol, 2013. **9**(11): p. 715-20.
191. Yarravarapu, N., L. Geffert, C.K. Surratt, M. Cascio, and D.J. Lapinsky, *Clickable photoaffinity ligands for the human serotonin transporter based on the selective serotonin reuptake inhibitor (S)-citalopram*. Bioorg Med Chem Lett, 2018. **28**(21): p. 3431-3435.
192. Chen, Z.A., et al., *Architecture of the RNA polymerase II-TFIIF complex revealed by cross-linking and mass spectrometry*. EMBO J, 2010. **29**(4): p. 717-26.
193. Kaake, R.M., et al., *A new in vivo cross-linking mass spectrometry platform to define protein-protein interactions in living cells*. Mol Cell Proteomics, 2014. **13**(12): p. 3533-43.
194. Pham, V.T., T.Q. Nguyen, U.P.N. Dao, and T.T. Nguyen, *On the interaction between fluoxetine and lipid membranes: Effect of the lipid composition*. Spectrochim Acta A Mol Biomol Spectrosc, 2018. **191**: p. 50-61.
195. Do, T.T.T., U.P.N. Dao, H.T. Bui, and T.T. Nguyen, *Effect of electrostatic interaction between fluoxetine and lipid membranes on the partitioning of fluoxetine investigated using second derivative spectrophotometry and FTIR*. Chem Phys Lipids, 2017. **207**(Pt A): p. 10-23.
196. Kapoor, R., T.A. Peyear, R.E. Koeppe, 2nd, and O.S. Andersen, *Antidepressants are modifiers of lipid bilayer properties*. J Gen Physiol, 2019. **151**(3): p. 342-356.
197. Jodko-Piorecka, K. and G. Litwinienko, *First experimental evidence of dopamine interactions with negatively charged model biomembranes*. ACS Chem Neurosci, 2013. **4**(7): p. 1114-22.

198. Peters, G.H., C. Wang, N. Cruys-Bagger, G.F. Velardez, J.J. Madsen, and P. Westh, *Binding of serotonin to lipid membranes*. J Am Chem Soc, 2013. **135**(6): p. 2164-71.
199. DeMarco, A.G., N.A. Ferraro, K. Sweigard, and M. Cascio, *Characterizing the lipid-protein interface of the human serotonin transporter by crosslinking mass spectrometry*. bioRxiv, 2020: p. 2020.06.01.128025.
200. Fantini, J. and F.J. Barrantes, *How cholesterol interacts with membrane proteins: an exploration of cholesterol-binding sites including CRAC, CARC, and tilted domains*. Front Physiol, 2013. **4**: p. 31.
201. Laursen, L., et al., *Cholesterol binding to a conserved site modulates the conformation, pharmacology, and transport kinetics of the human serotonin transporter*. J Biol Chem, 2018. **293**(10): p. 3510-3523.
202. Galea, S., R.M. Merchant, and N. Lurie, *The Mental Health Consequences of COVID-19 and Physical Distancing: The Need for Prevention and Early Intervention*. JAMA Intern Med, 2020.
203. Buchmayer, F., et al., *Amphetamine actions at the serotonin transporter rely on the availability of phosphatidylinositol-4,5-bisphosphate*. Proc Natl Acad Sci U S A, 2013. **110**(28): p. 11642-7.
204. Sorensen, L., K. Stromgaard, and A.S. Kristensen, *Characterization of intracellular regions in the human serotonin transporter for phosphorylation sites*. ACS Chem Biol, 2014. **9**(4): p. 935-44.

205. Periole, X., T. Zeppelin, and B. Schiott, *Dimer Interface of the Human Serotonin Transporter and Effect of the Membrane Composition*. Sci Rep, 2018. **8**(1): p. 5080.
206. Nielsen, A.K., I.R. Moller, Y. Wang, S.G.F. Rasmussen, K. Lindorff-Larsen, K.D. Rand, and C.J. Loland, *Substrate-induced conformational dynamics of the dopamine transporter*. Nat Commun, 2019. **10**(1): p. 2714.
207. Rannversson, H., P. Wilson, K.B. Kristensen, S. Sinning, A.S. Kristensen, K. Stromgaard, and J. Andersen, *Importance of the Extracellular Loop 4 in the Human Serotonin Transporter for Inhibitor Binding and Substrate Translocation*. J Biol Chem, 2015. **290**(23): p. 14582-94.
208. Sitte, H.H., H. Farhan, and J.A. Javitch, *Sodium-dependent neurotransmitter transporters: oligomerization as a determinant of transporter function and trafficking*. Mol Interv, 2004. **4**(1): p. 38-47.
209. Sorkina, T., S. Doolen, E. Galperin, N.R. Zahniser, and A. Sorkin, *Oligomerization of dopamine transporters visualized in living cells by fluorescence resonance energy transfer microscopy*. J Biol Chem, 2003. **278**(30): p. 28274-83.
210. Hastrup, H., A. Karlin, and J.A. Javitch, *Symmetrical dimer of the human dopamine transporter revealed by cross-linking Cys-306 at the extracellular end of the sixth transmembrane segment*. Proc Natl Acad Sci U S A, 2001. **98**(18): p. 10055-60.

211. Li, Y., S.Y. Cheng, N. Chen, and M.E. Reith, *Interrelation of dopamine transporter oligomerization and surface presence as studied with mutant transporter proteins and amphetamine*. J Neurochem, 2010. **114**(3): p. 873-85.
212. Torres, G.E., A. Carneiro, K. Seamans, C. Fiorentini, A. Sweeney, W.D. Yao, and M.G. Caron, *Oligomerization and trafficking of the human dopamine transporter. Mutational analysis identifies critical domains important for the functional expression of the transporter*. J Biol Chem, 2003. **278**(4): p. 2731-9.
213. Zhen, J., T. Antonio, S.Y. Cheng, S. Ali, K.T. Jones, and M.E. Reith, *Dopamine transporter oligomerization: impact of combining protomers with differential cocaine analog binding affinities*. J Neurochem, 2015. **133**(2): p. 167-73.
214. Schmid, J.A., P. Scholze, O. Kudlacek, M. Freissmuth, E.A. Singer, and H.H. Sitte, *Oligomerization of the human serotonin transporter and of the rat GABA transporter 1 visualized by fluorescence resonance energy transfer microscopy in living cells*. J Biol Chem, 2001. **276**(6): p. 3805-10.
215. Ryl, P.S.J., et al., *In Situ Structural Restraints from Cross-Linking Mass Spectrometry in Human Mitochondria*. J Proteome Res, 2020. **19**(1): p. 327-336.
216. Spector, A.A. and M.A. Yorek, *Membrane lipid composition and cellular function*. J Lipid Res, 1985. **26**(9): p. 1015-35.
217. Khatun, J., K. Ramkissoon, and M.C. Giddings, *Fragmentation characteristics of collision-induced dissociation in MALDI TOF/TOF mass spectrometry*. Anal Chem, 2007. **79**(8): p. 3032-40.
218. Brodbelt, J.S., *Ion Activation Methods for Peptides and Proteins*. Anal Chem, 2016. **88**(1): p. 30-51.

Appendix

MS studies from 3 independent sample preparations were run in triplicate. Mass shifted peptides reported in tables 4.1-4.5 were only reported if observed in at least 2 replicates. Peptides were observed with varying modifications such as acrylamide, oxidation and alkylation. Below are detailed versions of tables 4.1-4.5:

Table A.1: A109C Dimer Crosslinks

Peptide	Modifications	Structural Location
¹ <u>M</u> ETTP <u>L</u> NSQK <u>V</u> LSEAK <u>D</u> R ¹⁸	1-18XL, Acry (2X)/ ¹⁻¹⁸ Alk XL, Acry/ ¹¹⁻¹⁶ XL	N-terminal
¹⁵ AKDREDA <u>Q</u> ENGVLQK ²⁹	15-29XL (3X)/ ¹⁷⁻²⁹ Alk XL/ ¹⁹⁻²⁹ XL, Acry	
²⁰ DAQENGVLQKGVPTADR ³⁷	²⁰⁻³⁷ Alk XL/ ²⁴⁻³⁹ XL	
⁵⁹ ASHSIPAA <u>T</u> TLVAEIR <u>Q</u> GER ⁷⁹	⁵⁹⁻⁷⁹ XL (2X)	
¹⁴⁵ NGAIS <u>I</u> WRKIAPIFK ¹⁵⁹	¹⁴⁵⁻¹⁵⁹ Alk XL, Acry (5X)/ ¹⁴⁵⁻¹⁵² XL, Oxi/ ¹³⁷⁻¹⁵³ XL, Acry, Oxi/ ¹³⁷⁻¹⁵² XL	TM2-TM3 IC Loop
²⁷³ <u>G</u> VKTSGKVVVWTATFPYIVLSVLLVRGATLP <u>G</u> AWR ³⁰⁷	²⁷³⁻²⁹⁸ XL/ ²⁷⁶⁻³⁰⁷ XL	TM5/TM5-TM6 EC Loop
²⁹⁹ GATLP <u>G</u> AWRGVV <u>F</u> LKPNWQKLE ³²²	²⁹⁹⁻³¹⁹ Alk XL, Oxi/ ²⁹⁹⁻³²² Alk XL/ ²⁹⁹⁻³¹⁹ XL, Oxi, Acry/ ²⁰⁹⁻³⁰⁷ XL, Oxi (6X) ³⁰⁸⁻³²² Alk XL	TM5-TM6 EC Loop
⁴⁴⁵ GVITAVLDEF <u>P</u> HIWAKR ⁴⁶¹	⁴⁴⁵⁻⁴⁶¹ XL, Acry (2X)/ ⁴⁵⁴⁻⁴⁶² XL, Acry/ ⁴⁴⁵⁻⁴⁶¹ Alk XL, Acry	TM8/TM8-TM9 IC Loop
⁵⁹⁷ L <u>I</u> STPGTLKER ⁶⁰⁷	⁵⁹⁷⁻⁶⁰⁷ Alk XL, Acry/ ⁵⁹⁷⁻⁶⁰⁷ XL, Acry	TM12/C-Terminal
⁶⁰⁶ ERIIKSIT <u>P</u> ETPTE ⁶¹⁹	⁶⁰⁶⁻⁶¹⁹ Alk XL (3X)/ ⁶⁰⁸⁻⁶¹⁵ XL	C-Terminal

Identified mass-shifted peptides (within 10ppm error) observed in the dimer study in mutation A109C shown in the left column. Specific sites of covalent crosslink identified via CID fragmentation analysis are bolded and underlined. Boxed peptide was observed in the dimer study only, thus suggest an intermolecular crosslink. Parenthesized numbers in the “modifications” column represent the number of times a precursor ion was observed with the given modification.

Table A.2: A109C Monomer Crosslinks

Peptide	Modifications	Structural Location
¹ <u>M</u> ETTP <u>L</u> NSQK <u>V</u> LSEAK <u>D</u> R ¹⁸	1-18XL, Acry (2X)/ ³⁻¹⁸ XL/ ¹¹⁻¹⁸ XL	N-Terminal
¹¹ <u>V</u> LSE ¹⁴	¹¹⁻¹⁴ XL (2X)	
⁵⁹ ASHSIPAA <u>T</u> TLVAEIRQGERETW <u>G</u> K ⁸⁵	⁵⁹⁻⁷⁹ XL/ ⁵⁹⁻⁷⁵ XL/ ⁷⁶⁻⁸⁵ XL, Acry	
¹⁴⁵ NGAIS <u>I</u> WRKIAPIFK ¹⁵⁹	¹⁴⁵⁻¹⁵⁹ Alk XL, Acry (4X)/ ¹⁵⁴⁻¹⁵⁹ XL	TM2-TM3 IC Loop
²⁹⁹ GATLP <u>G</u> AWRGV <u>V</u> FYLKPNWQK ³¹⁹	²⁹⁹⁻³¹⁹ Alk XL, Oxi (2X)/ ²⁹⁹⁻³¹⁹ XL, Oxi, Acry/ ²⁹⁹⁻³⁰⁷ XL, Oxi (4X)	TM5-TM6 EC Loop
⁴⁴⁵ <u>G</u> VITAVLDEF <u>P</u> HIWAKR ⁴⁶¹	⁴⁴⁵⁻⁴⁶¹ Alk XL, Acry (2X)/ ⁴⁴⁵⁻⁴⁶¹ XL, Acry (2X)/ ⁴⁵⁴⁻⁴⁶⁰ XL, Acry, Oxi	TM8/TM8-TM9 IC Loop
⁴⁵⁴ <u>F</u> PHIWAKRR ⁴⁶²	⁴⁵⁴⁻⁴⁶² XL, Acry (2)/ ⁴⁵⁴⁻⁴⁶² Alk XL (2)	TM8-TM9 IC Loop
⁵⁹⁷ L <u>I</u> STPG <u>T</u> LKERIIK ⁶¹⁰	⁵⁹⁷⁻⁶⁰⁷ Alk XL, Acry/ ⁵⁹⁷⁻⁶¹⁰ Alk XL, Acry/ ⁵⁹⁷⁻⁶⁰⁵ XL	TM12/C-Terminal
⁶⁰⁶ ERIIKSIT <u>P</u> E ⁶¹⁵	⁶⁰⁶⁻⁶¹⁰ XL, Acry/ ⁶⁰⁷⁻⁶¹⁰ XL, Acry/ ⁶⁰⁷⁻⁶¹⁵ Alk XL	C-Terminal
⁶⁰⁸ <u>I</u> IKSITPETPTEI <u>P</u> AGDIR ⁶²⁶	⁶¹¹⁻⁶²⁶ Alk XL/ ⁶⁰⁸⁻⁶²⁶ Alk XL/ ⁶⁰⁸⁻⁶²⁶ XL	

Identified mass-shifted peptides in the monomer study in mutation A109C. Description of columns as described in table A.1.

Table A.3: S190C Dimer Crosslinks

Peptide	Modifications	Structural Location
¹ METPLNSQKVLSEAK ¹⁶	3-16Alk XL, Acry/ ¹⁻¹⁴ Alk XL/ ¹⁻¹⁶ Alk XL (2X)/ ¹¹⁻¹⁹ Alk XL/ ¹⁻¹⁶ XL, Acry/ ¹⁻¹⁰ XL/ ¹⁻¹⁶ XL/ ³⁻¹⁶ XL (3X)/ ³⁻¹⁸ XL/ ¹¹⁻¹⁶ XL	N-Terminal
¹⁵ AKDREDAQENGVLQK ²⁹	11-23Alk XL/ ¹⁵⁻²⁹ Alk XL (2X)/ ²⁰⁻²⁹ Alk XL/ ¹⁵⁻²⁹ Alk XL, Acry/ ¹⁷⁻²⁹ Alk XL, Acry/ ¹⁵⁻²⁹ XL, Acry/ ¹⁷⁻²⁹ XL, Acry/ ¹⁵⁻²³ XL/ ²⁰⁻³⁷ XL/ ²⁴⁻³⁷ XL (2X)	
²⁴ NGVLQKGVPTTADRAE ³⁹	²⁴⁻³⁹ XL (2X)/ ³⁰⁻³⁷ XL	
⁵⁹ ASHSIPAATTLVAEIROQGER ⁷⁹	⁵⁹⁻⁷⁵ Alk XL/ ⁷⁴⁻⁸⁰ Alk XL/ ⁵⁹⁻⁷⁹ XL	
⁷⁶ QGERETWGGK ⁸⁵	⁷⁹⁻⁸⁴ Alk XL, Oxi, Acry/ ⁷⁶⁻⁸⁵ Alk XL, Acry (₂)/ ⁸⁰⁻¹⁰⁴ Alk XL/ ⁷⁶⁻⁸⁵ XL, Oxi, Acry/ ⁸⁰⁻⁸⁴ XL, Oxi/ ⁸¹⁻⁸⁵ XL	
¹³⁷ LALGQYHRNGAISIWRRK ¹⁵³	¹³⁷⁻¹⁵³ Alk XL, Acry/ ¹³⁷⁻¹⁵³ Alk XL, Acry, Oxi/ ¹³⁷⁻¹⁵² Alk XL/ ¹³⁷⁻¹⁵³ XL, Acry	TM2/TM2-TM3 IC Loop
¹⁴⁵ NGAISIWRRKIPIFK ¹⁵⁹	¹⁴⁵⁻¹⁵⁹ Alk XL/ ¹⁵³⁻¹⁵⁹ Alk XL/ ¹⁵⁴⁻¹⁵⁹ Alk XL, Acry/ ¹⁴⁵⁻¹⁵³ Alk XL, Oxi/ ¹⁴⁵⁻¹⁵³ XL, Oxi, Acry/ ¹⁵³⁻¹⁵⁹ XL, Acry/ ¹⁵³⁻¹⁵⁹ XL	TM2-TM3 IC Loop
²³⁰ EFYLRHVLQIHQSK ²⁴³	²³¹⁻²⁴³ Alk XL, Acry/ ²³⁰⁻²⁴³ XL, Acry	TM3-TM4 EC Loop
²⁹⁹ GATLPGAWRGVVFYLPKNWQK ³¹⁹	³⁰⁸⁻³¹⁹ Alk XL, Acry/ ³⁰⁸⁻³²² Alk XL, Acry/ ³⁰⁸⁻³¹⁹ Alk XL, Acry, Oxi/ ²⁹⁹⁻³⁰⁷ Alk XL, Oxi/ ²⁹⁹⁻³¹⁹ Alk XL, Oxi/ ³⁰⁸⁻³²² XL, Acry/ ²⁹⁹⁻³⁰⁷ XL, Oxi (2X)/ ²⁹⁹⁻³¹⁹ XL, Oxi (3X)/ ³⁰⁸⁻³²² XL	TM5-TM6 EC Loop
⁵⁹⁷ LSTPGTLKERIIK ⁶¹⁰	⁵⁹⁷⁻⁶⁰⁶ Alk XL/ ⁵⁹⁷⁻⁶⁰⁷ Alk XL (2X)/ ⁵⁹⁷⁻⁶⁰⁶ Alk XL, Acry/ ⁵⁹⁷⁻⁶⁰⁷ Alk XL, Acry/ ⁵⁹⁷⁻⁶¹⁰ XL, Acry (₂)/ ⁵⁹⁷⁻⁶⁰⁷ XL (2X)/ ⁵⁹⁷⁻⁶¹⁰ XL	TM12/C-Terminal
⁶⁰⁶ ERIIKSITPE ⁶¹⁵	⁶⁰⁶⁻⁶¹⁵ XL/ ⁶⁰⁶⁻⁶¹⁹ XL/ ⁶⁰⁶⁻⁶¹⁰ Alk XL, Acry/ ⁶⁰⁶⁻⁶¹⁵ Alk XL/ ⁶⁰⁶⁻⁶¹⁹ Alk XL	C-Terminal
⁶⁰⁷ RIIKSITPETPTEIPAGDIR ⁶²⁶	⁶⁰⁸⁻⁶¹⁵ Alk XL/ ⁶¹⁶⁻⁶²⁶ Alk XL/ ⁶²⁰⁻⁶²⁶ Alk XL/ ⁶⁰⁷⁻⁶¹⁹ Alk XL (2X)/ ⁶⁰⁷⁻⁶²⁶ XL/ ⁶⁰⁸⁻⁶¹⁵ XL/ ⁶⁰⁸⁻⁶¹⁹ XL (3X)/ ⁶⁰⁸⁻⁶²⁶ XL	
⁶²⁰ IPAGDIRMNAV ⁶³⁰	⁶²⁰⁻⁶³⁰ Alk XL/ ⁶²⁰⁻⁶³⁰ XL	

Identified mass-shifted peptides in the dimer study in mutation S190C. Description of columns as described in table A.1.

Table A.4: S190C Monomer Crosslinks

Peptide	Modification	Structural Location
¹ METPLNSQKVLSEAK ¹⁶	¹⁻¹⁴ XL/ ¹⁻¹⁶ XL (2X)/ ³⁻¹⁰ XL/ ³⁻¹⁶ XL/ ¹⁻¹⁶ Alk XL (2X)/ ³⁻¹⁶ Alk XL/ ¹⁻¹⁶ Alk XL, Acry	N-Terminal
³ TPLNSQKVLSEAKDR ¹⁸	¹¹⁻¹⁶ Alk XL/ ³⁻¹⁸ Alk XL, Acry/ ¹¹⁻¹⁹ XL, Acry (2X)/ ³⁻¹⁸ XL/ ¹¹⁻¹⁸ XL/ ¹⁵⁻¹⁹ XL	
¹⁵ AKDREDAQENGVLQK ²⁹	¹⁷⁻²⁹ Alk XL, Acry/ ¹⁵⁻²⁹ XL/ ¹⁹⁻²⁹ XL	
¹⁹ EDAQENGVLQKGVPTTADR ³⁷	²⁰⁻²⁹ Alk XL (2X)/ ¹⁹⁻³⁷ XL/ ²⁰⁻³⁷ XL/ ²⁴⁻³⁷ XL	
²⁴ NGVLQKGVPTTADRAE ³⁹	²⁴⁻³⁹ Alk XL/ ³⁰⁻³⁷ Alk XL/ ²⁴⁻³⁹ XL (3X)	
⁵⁹ ASHSIPAATTLVAEIROQGER ⁷⁹	⁵⁹⁻⁷⁸ Alk XL/ ⁵⁹⁻⁷⁸ XL (2X)/ ⁵⁹⁻⁷⁹ XL/ ⁵⁹⁻⁸⁰ XL	TM2/TM2-TM3 IC Loop
⁷⁴ IROGERETWGGK ⁸⁴	⁷⁴⁻⁸⁴ Alk XL, Oxi (2X)/ ⁷⁴⁻⁷⁹ Alk XL (2X)/ ⁷⁴⁻⁸⁴ Alk XL (2X)	
⁷⁹ RETWGGK ⁸⁵	⁷⁶⁻⁸⁴ Alk XL/ ⁷⁶⁻⁸⁵ Alk XL/ ⁷⁹⁻⁸⁵ Alk XL (2X)/ ⁷⁶⁻⁸⁴ XL, Acry/ ⁸⁰⁻⁸⁴ XL, Oxi/ ⁷⁹⁻⁸⁵ XL/ ⁸¹⁻⁸⁴ XL	
¹³⁷ LALGQYHRNGAISIWRRK ¹⁵³	¹³⁷⁻¹⁵³ Alk XL/ ¹³⁷⁻¹⁵³ Alk XL, Oxi/ ¹³⁷⁻¹⁵³ Alk XL, Oxi, Acry/ ¹³⁷⁻¹⁵² XL	
¹⁴⁵ NGAISIWRRKIPIFK ¹⁵⁹	¹⁴⁵⁻¹⁵⁹ Alk XL, Acry (2X)/ ¹⁴⁵⁻¹⁵³ Alk XL, Acry, Oxi/ ¹⁴⁵⁻¹⁵³ XL, Acry, Oxi/ ¹⁴⁵⁻¹⁵³ XL, Acry	
¹⁵³ KIPIFK ¹⁵⁹	¹⁵⁴⁻¹⁵⁹ Alk XL, Acry/ ¹⁵³⁻¹⁵⁹ Alk XL/ ¹⁵³⁻¹⁵⁹ XL	TM3-TM4 EC Loop
²³¹ FYLRHVLQIHQSK ²⁴³	²³¹⁻²⁴³ Alk XL, Acry (4X)	
²⁹⁹ GATLPGAWRGVVFYLPKNWQKLE ³²²	²⁹⁹⁻³²² XL, Acry/ ²⁹⁹⁻³⁰⁷ XL, Oxi	
³⁰⁸ GVVFYLPKNWQKLE ³²²	³⁰⁸⁻³¹⁹ Alk XL, Acry, Oxi/ ³⁰⁸⁻³¹⁹ Alk XL, Oxi/ ³⁰⁸⁻³²² XL, Acry/ ³⁰⁸⁻³¹⁹ XL	TM8-TM9 IC Loop
⁴⁴⁵ GVTAVLDEFPHWAK ⁴⁶⁰	⁴⁴⁵⁻⁴⁶⁰ Alk XL, Acry, Oxy (2X)/ ⁴⁴⁵⁻⁴⁶⁰ Alk XL, Acry/ ⁴⁴⁵⁻⁴⁶⁰ XL, Oxi/ ⁴⁴⁵⁻⁴⁶⁰ XL (3X)	
⁴⁵⁴ FPHIWA ⁴⁶²	⁴⁵⁴⁻⁴⁶² Alk XL, Acry/ ⁴⁵⁴⁻⁴⁶¹ Alk XL/ ⁴⁵⁴⁻⁴⁶⁰ XL, Oxi, Acry/ ⁴⁵⁴⁻⁴⁶¹ XL, Acry/ ⁴⁵⁴⁻⁴⁶⁰ XL, Oxi/ ⁴⁵⁴⁻⁴⁶² XL	TM12/C-Terminal
⁵⁹⁷ LSTPGTLKERIIK ⁶¹⁰	⁵⁹⁷⁻⁶¹⁰ Alk XL/ ⁵⁹⁷⁻⁶⁰⁶ Alk XL/ ⁵⁹⁷⁻⁶⁰⁷ Alk XL (3X)/ ⁵⁹⁷⁻⁶⁰⁶ XL/ ⁵⁹⁷⁻⁶¹⁰ XL, Acry (₂)	
⁶⁰⁶ ERIIKSITPE ⁶¹⁵	⁶⁰⁶⁻⁶¹⁰ Alk XL/ ⁶⁰⁶⁻⁶¹⁰ Alk XL, Acry/ ⁶⁰⁷⁻⁶¹⁰ XL, Acry/ ⁶⁰⁶⁻⁶¹⁵ XL	
⁶⁰⁷ RIIKSITPETPTEIPAGDIR ⁶²⁶	⁶⁰⁶⁻⁶¹⁹ Alk XL/ ⁶⁰⁶⁻⁶¹⁵ Alk XL/ ⁶⁰⁷⁻⁶¹⁹ Alk XL/ ⁶⁰⁷⁻⁶²⁶ Alk XL/ ⁶⁰⁶⁻⁶¹⁹ XL/ ⁶⁰⁸⁻⁶¹⁹ XL	
⁶²⁰ IPAGDIRMNAV ⁶³⁰	⁶²⁰⁻⁶²⁶ Alk XL (2X)/ ⁶²⁰⁻⁶³⁰ Alk XL	

Identified mass-shifted peptides in the monomer study in mutation S190C. Description of columns as described in table A.1.

Table A.5: Y232C Dimer Crosslinks

Peptide	Modification	Structural Location
¹ METPLNSQKVLSEAKDR ¹⁸	¹⁻¹⁰ Alk XL/ ¹⁻¹⁴ Alk XL/ ¹⁻¹⁸ XL, Acry (3X)/ ¹⁻¹⁰ XL	N-Terminal
¹⁵ AKDRE ¹⁹	³⁻¹⁶ XL, Acry/ ¹⁵⁻¹⁸ XL, Acry/ ¹⁵⁻¹⁸ XL/ ¹⁵⁻¹⁹ XL (2X)	
²⁰ DAQENGLVQKGVPTTADRAE ³⁹	²⁴⁻³⁹ Alk XL/ ²⁰⁻³⁹ XL	
⁵⁹ ASHSJPAATTTLVAEIRQGER ⁷⁹	⁵⁹⁻⁷⁹ XL (3X)	
⁷⁶ QGERETWGGK ⁸⁵	⁷⁶⁻⁸⁵ Alk XL, Acry/ ⁷⁹⁻⁸⁴ Alk XL, Acry, Oxi/ ⁷⁶⁻⁸⁵ XL/ ⁷⁹⁻⁸⁴ XL/ ⁷⁴⁻⁸⁴ XL, Acry/ ⁷⁶⁻⁸⁵ XL, Acry	TM5-TM6 EC Loop
²⁹⁹ GATLPGAWRGVVFYLPKNWQK ³¹⁹	²⁹⁹⁻³¹⁹ Alk XL, Oxi (2X)	
⁴⁴⁵ GVITAVLDEFPHIWAQR ⁴⁶⁰	⁴⁴⁵⁻⁴⁶⁰ XL, Oxi (2X)/ ⁴⁴⁵⁻⁴⁶⁰ XL, Oxi, Acry	TM8/TM8-TM9 IC Loop
⁴⁴⁵ GVITAVLDEFPHIWAQR ⁴⁶¹	⁴⁴⁵⁻⁴⁶¹ Alk XL, Acry (3X)/ ⁴⁴⁵⁻⁴⁶¹ XL, Acry/ ⁴⁴⁵⁻⁴⁶¹ XL (2X)	
⁴⁵⁴ FPHIWAQR ⁴⁶²	⁴⁵⁴⁻⁴⁶¹ Alk XL, Acry/ ⁴⁵⁴⁻⁴⁶¹ Alk XL/ ⁴⁵⁴⁻⁴⁶² Alk XL (7X)/ ⁴⁵⁴⁻⁴⁶² XL, Acry (7X)/ ⁴⁵⁴⁻⁴⁶⁰ XL, Acry, Oxi/ ⁴⁵⁴⁻⁴⁶⁰ XL, Oxi (2X)	TM8-TM9 IC Loop
⁵⁹⁷ LISPTGLKER ⁶⁰⁷	⁵⁹⁷⁻⁶⁰⁷ Alk XL/ ⁵⁹⁷⁻⁶⁰⁶ XL, Acry/ ⁶⁰⁶⁻⁶¹⁰ XL, Acry	TM12/C-Terminal
⁶⁰⁶ ERIISITPETPTE ⁶¹⁹	⁶⁰⁶⁻⁶¹⁵ Alk XL/ ⁶⁰⁶⁻⁶¹⁹ Alk XL (8X)/ ⁶⁰⁶⁻⁶¹⁹ XL/ ⁶⁰⁸⁻⁶¹⁹ XL	C-Terminal
⁶⁰⁸ IISITPETPTEIPAGDIRMNAV ⁶³⁰	⁶⁰⁸⁻⁶²⁶ XL (4X)/ ⁶¹⁶⁻⁶³⁰ XL	

Identified mass-shifted peptides in the dimer study in mutation Y232C. Description of columns as described in table A.1.

Table A.6: Y232C Monomer Crosslinks

Peptide	Modification	Structural Location
³ TPPLNSQKVLSEAK ¹⁶	³⁻¹⁰ Alk XL, Acry/ ¹⁻¹⁶ Alk XL/ ³⁻¹⁶ Alk XL (5X)/ ³⁻¹⁶ XL, Acry (5X)/ ³⁻¹⁰ XL/ ³⁻¹⁶ XL	N-Terminal
⁷⁴ IRQGERETWGGK ⁸⁴	⁷⁴⁻⁸⁴ Alk XL/ ⁷⁴⁻⁸⁴ XL/ ⁵⁹⁻⁷⁹ XL	
⁷⁹ RETWGGK ⁸⁵	⁷⁹⁻⁸⁵ Alk XL/ ⁷⁹⁻⁸⁵ XL, Acry	
⁸⁶ MDFLLSVIGYAVDLGNIWR ¹⁰⁴	⁸⁶⁻¹⁰⁴ Alk XL (3X)/ ⁸⁶⁻¹⁰⁴ XL, Oxi	TM1
¹⁴⁵ NGAISIWRIAPIFK ¹⁵⁹	¹⁴⁵⁻¹⁵⁹ Alk XL, Acry (2X)/ ¹⁵³⁻¹⁵⁹ Alk XL, Acry/ ¹⁵³⁻¹⁵⁹ XL, Acry/ ¹⁴⁵⁻¹⁵³ XL, Oxi/ ¹⁴⁵⁻¹⁵³ XL/ ¹⁴⁵⁻¹⁵⁹ XL	TM2-TM3 IC Loop
²⁷³ GVKTSQK ²⁷⁹	²⁷³⁻²⁷⁹ XL, Acry/ ²⁷³⁻²⁷⁹ Alk XL, Acry/ ²⁷⁶⁻²⁷⁹ Alk XL, Acry	TM4-TM5 IC Loop
²⁹⁹ GATLPGAWRGVVFYLPKNWQK ³¹⁹	³⁰⁸⁻³²² Alk XL, Acry/ ²⁹⁹⁻³¹⁹ Alk XL, Oxi (2X)/ ³⁰⁸⁻³¹⁹ Alk XL, Oxi/ ²⁹⁹⁻³⁰⁷ Alk XL/ ²⁹⁹⁻³⁰⁷ XL, Oxi (3X)	TM5-TM6 EC Loop
⁴⁴⁵ GVITAVLDEFPHIWAQR ⁴⁶¹	⁴⁴⁵⁻⁴⁶¹ Alk XL, Acry (3X)/ ⁴⁴⁵⁻⁴⁶¹ XL	TM8/TM8-TM9 IC Loop
⁴⁵⁴ FPHIWAQR ⁴⁶²	⁴⁵⁴⁻⁴⁶² Alk XL, Acry/ ⁴⁵⁴⁻⁴⁶⁰ Alk XL/ ⁴⁵⁴⁻⁴⁶² Alk XL (6X)/ ⁴⁵⁴⁻⁴⁶² XL, Acry (7X)/ ⁴⁵⁴⁻⁴⁶⁰ XL, Oxi (2X)	TM8-TM9 IC Loop
⁵⁹⁷ LISPTGLKER ⁶⁰⁷	⁵⁹⁷⁻⁶⁰⁷ Alk XL, Acry/ ⁵⁹⁷⁻⁶⁰⁷ XL	TM12/C-Terminus
⁶⁰⁶ ERIISITPETPTE ⁶¹⁹	⁶⁰⁶⁻⁶¹⁹ Alk XL (6X)/ ⁶⁰⁷⁻⁶¹⁰ XL, Acry	C-Terminus
⁶⁰⁸ IISITPETPTEIPAGDIR ⁶²⁶	⁶⁰⁸⁻⁶¹⁹ Alk XL/ ⁶⁰⁸⁻⁶²⁶ XL (2X)	

Identified mass-shifted peptides in the monomer study in mutation Y232C. Description of columns as described in table A.1.

Table A.7: S252C Dimer Crosslinks

Peptide	Modifications	Structural Location
¹ METTP ¹ NSQK ¹⁶ VLSEAK ¹⁶	¹⁻¹⁶ Alk XL, Acry/ ¹⁻¹⁶ XL, Acry/ ³⁻¹⁸ XL/ ¹⁻¹⁶ XL	N-Terminal
¹ MET ¹ PLNSQK ¹⁶ VLSEAK ¹⁸ D ¹⁸ R	¹⁻¹⁸ Alk XL, Acry/ ³⁻¹⁶ Alk XL (4X)/ ¹¹⁻¹⁸ Alk XL (2X)/ ¹⁻¹⁴ XL, Acry/ ³⁻¹⁶ XL, Acry/ ³⁻¹⁶ XL (3X)/ ¹⁵⁻²³ XL	
⁵⁹ ASHSIPAA ¹ TTTLVAEIR ⁷⁹ QGER ⁷⁹	⁵⁹⁻⁷⁹ XL (4X)	
⁷⁶ QGERET ⁷⁶ WGK ⁸⁵ K ⁸⁵	⁷⁹⁻⁸⁵ Alk XL (3X)/ ⁷⁹⁻⁸⁵ XL, Acry (2X)/ ⁸¹⁻⁸⁴ XL, Acry, Oxi/ ⁷⁶⁻⁸⁰ XL/ ⁷⁶⁻⁸⁵ XL	
⁸¹ TWGKK ¹ MD ¹ FLLSVIGYAVDLGNIWR ¹⁰⁴	⁸¹⁻¹⁰⁴ Alk XL, Oxi (2X)	N-Terminal/TM1
¹³⁷ LALGQYHRNGA ¹⁵² IS ¹⁵² W ¹⁵² R	¹³⁷⁻¹⁴⁴ Alk XL/ ¹³⁷⁻¹⁵² Alk XL, Oxi (4X)	TM2/TM2-TM3 IC Loop
¹⁴⁵ NGA ¹⁴⁵ IS ¹⁴⁵ W ¹⁴⁵ R ¹⁴⁵ KIAP ¹⁴⁵ IFK ¹⁵⁹	¹⁴⁵⁻¹⁵⁹ Alk XL, Acry, Oxi/ ¹⁵⁴⁻¹⁵⁹ Alk XL, Acry/ ¹⁴⁵⁻¹⁵³ Alk XL, Oxi/ ¹⁴⁵⁻¹⁵³ Alk XL/ ¹⁴⁵⁻¹⁵⁹ XL	TM2-TM3 IC Loop
²³¹ FYLR ²³¹ HVLQ ²⁴³ IHQSK ²⁴³	²³¹⁻²⁴³ Alk XL/ ²³⁰⁻²⁴³ XL, Acry/ ²³¹⁻²⁴³ XL, Acry	TM3-TM4 EC Loop
²⁹⁹ GATLP ²⁹⁹ GAWR ³¹⁹ GVV ³¹⁹ FY ³¹⁹ LKPNW ³¹⁹ QK ³¹⁹	²⁹⁹⁻³¹⁹ Alk XL/ ²⁹⁹⁻³⁰⁷ XL, Oxi (7X)/ ²⁹⁹⁻³⁰⁷ XL (4X)/ ²⁹⁹⁻³¹⁹ XL	TM5-TM6 EC Loop
³⁰⁸ GVV ³⁰⁸ FY ³⁰⁸ LKPNW ³²² QK ³²² L ³²² E	³⁰⁸⁻³¹⁹ Alk XL (2X)/ ³⁰⁸⁻³²² XL	TM7-TM8 EC Loop
³⁸⁹ MRNE ³⁹²	³⁸⁹⁻³⁹² XL (2X)	
⁴⁴⁵ GVITAVLDEFPHI ⁴⁶¹ WAKR ⁴⁶¹	⁴⁴⁵⁻⁴⁶¹ Alk XL, Acry (5X)/ ⁴⁴⁵⁻⁴⁶⁰ XL	TM8/TM8-TM9 IC Loop
⁴⁵⁴ FPHI ⁴⁵⁴ WAKRR ⁴⁶²	⁴⁵⁴⁻⁴⁶² Alk XL (2X)/ ⁴⁵⁴⁻⁴⁶² XL, Acry (3X)/ ⁴⁵⁴⁻⁴⁶¹ XL (2X)	TM8-TM9 IC Loop
⁵⁹⁷ LSTPGTLKERI ⁶¹⁰	⁵⁹⁷⁻⁶⁰⁶ Alk XL, Acry/ ⁵⁹⁷⁻⁶⁰⁷ Alk XL, Acry/ ⁵⁹⁷⁻⁶⁰⁷ Alk XL (2X)/ ⁵⁹⁷⁻⁶¹⁰ Alk XL/ ⁵⁹⁷⁻⁶¹⁰ XL, Acry (2X)	TM12/C-Terminal
⁶⁰⁶ ERIKSITPETPTE ⁶¹⁹	⁶⁰⁶⁻⁶¹⁵ Alk XL/ ⁶⁰⁶⁻⁶¹⁹ Alk XL (4X)/ ⁶⁰⁸⁻⁶¹⁵ Alk XL/ ⁶⁰⁸⁻⁶¹⁹ Alk XL/ ⁶⁰⁷⁻⁶²⁶ XL/ ⁶⁰⁸⁻⁶¹⁵ XL/ ⁶⁰⁸⁻⁶²⁶ XL	C-Terminal

Identified mass-shifted peptides in the dimer study in mutation S252C. Description of columns as described in table A.1.

Table A.8: S252C Monomer Crosslinks

Peptide	Modification	Structural Location
¹ METTP ¹ NSQK ¹⁶ VLSEAK ¹⁸ D ¹⁸ R	¹⁻¹⁴ Alk XL, Acry/ ¹⁻¹⁶ Alk XL, Acry/ ¹⁻¹⁸ Alk XL, Acry/ ¹⁻¹⁸ Alk XL, Oxi/ ¹⁻¹⁸ Alk XL/ ¹⁻¹⁴ XL, Acry/ ¹⁻¹⁴ XL	N-Terminal
³ TTPLNSQK ¹⁶ VLSEAK ¹⁶	³⁻¹⁶ Alk XL (4X)/ ³⁻¹⁸ XL, Acry/ ³⁻¹⁸ XL/ ¹¹⁻¹⁴ XL	
¹⁷ DREDAQENGVLQK ²⁹	¹⁷⁻²⁹ Alk XL, Acry/ ²⁴⁻³⁷ Alk XL	
⁵⁹ ASHSIPAA ¹ TTTLVAEIR ⁷⁹ QGER ⁷⁹	⁵⁹⁻⁷⁹ XL (2X)	
⁷⁹ RET ⁷⁹ WGK ⁸⁵ K ⁸⁵	⁷⁹⁻⁸⁵ Alk XL (2X)/ ⁷⁹⁻⁸⁴ XL, Oxi/ ⁷⁹⁻⁸⁵ XL	N-Terminal/TM1
⁸¹ TWGKK ¹ MD ¹ FLLSVIGYAVDLGNIWR ¹⁰⁴	⁸¹⁻¹⁰⁴ XL/ ⁸¹⁻¹⁰⁴ Alk XL, Oxi (2X)/ ⁸⁵⁻¹⁰⁴ Alk XL, Oxi/ ⁸⁵⁻¹⁰⁴ Alk XL	
¹³⁷ LALGQYHRNGA ¹⁵² IS ¹⁵² W ¹⁵² R	¹⁴⁵⁻¹⁵⁹ Alk XL, Acry/ ¹³⁷⁻¹⁵² Alk XL, Oxi/ ¹⁴⁵⁻¹⁵⁹ Alk XL/ ¹³⁷⁻¹⁵² XL, Oxi	TM2/TM2-TM3 IC Loop
²⁷³ GVKTS ²⁷⁹ GK ²⁷⁹	²⁷⁶⁻²⁷⁹ Alk XL, Acry/ ²⁷³⁻²⁷⁹ Alk XL/ ²⁷³⁻²⁷⁹ XL/ ²⁷⁶⁻²⁷⁹ XL	TM4-TM5 IC Loop/TM5
²⁹⁹ GATLP ²⁹⁹ GAWR ³¹⁹ GVV ³¹⁹ FY ³¹⁹ LKPNW ³¹⁹ QK ³¹⁹	²⁹⁹⁻³¹⁹ Alk XL, Oxi/ ²⁹⁹⁻³⁰⁷ XL, Oxi (8X)/ ²⁹⁹⁻³¹⁹ XL	TM5-TM6 EC Loop
³⁸⁹ MRNE ³⁹² DVSEVAKDAGPSLLFIT ⁴¹² YAE ⁴¹²	³⁸⁹⁻⁴¹² Alk XL/ ³⁸⁹⁻³⁹² XL/ ³⁹¹⁻⁴¹² XL	TM7-TM8 EC Loop
⁴⁴⁵ GVITAVLDEFPHI ⁴⁶¹ WAKR ⁴⁶¹	⁴⁴⁵⁻⁴⁶¹ Alk XL, Acry, Oxi/ ⁴⁴⁵⁻⁴⁶¹ Alk XL, Oxi (₂)/ ⁴⁴⁵⁻⁴⁶¹ Alk XL, Acry (5X)	TM8/TM8-TM9 IC Loop
⁴⁵⁴ FPHI ⁴⁵⁴ WAKRR ⁴⁶²	⁴⁵⁴⁻⁴⁶² XL, Acry (2X)/ ⁴⁵⁴⁻⁴⁶² Alk XL (2X)/ ⁴⁵⁴⁻⁴⁶² XL	TM8-TM9 IC Loop
⁶⁰⁶ ERIKSITPETPTE ⁶¹⁹	⁶⁰⁶⁻⁶¹⁹ Alk XL (3X)/ ⁶⁰⁷⁻⁶¹⁹ Alk XL, Acry/ ⁶⁰⁷⁻⁶¹⁰ XL, Acry/ ⁶⁰⁷⁻⁶¹⁵ XL	C-Terminal
⁶⁰⁷ RIK ⁶⁰⁷ SIT ⁶⁰⁷ PET ⁶¹⁹ PTE ⁶¹⁹ PAGDIR ⁶²⁶	⁶⁰⁷⁻⁶²⁶ XL/ ⁶⁰⁸⁻⁶¹⁹ XL (2X)/ ⁶⁰⁸⁻⁶²⁶ XL	

Identified mass-shifted peptides in the monomer study in mutation S252C. Description of columns as described in table A.1.

Table A.9: R564C Dimer Crosslinks

Peptide	Modifications	Structural Location
³ TTPLNSQKVLSEAKDR ¹⁸	³⁻¹⁸ Alk XL/ ³⁻¹⁸ Alk XL, Acry/ ¹⁻¹⁶ Alk XL, Acry/ ³⁻¹⁰ XL, Acry (2X)/ ³⁻¹⁶ XL, Acry/ ³⁻¹⁶ XL (2X)	N-Terminal
¹¹ VLSEAKDREDAQE ²³	¹⁵⁻²³ Alk XL/ ¹¹⁻¹⁶ Alk XL, Acry/ ¹¹⁻²³ XL (2X)/ ¹¹⁻¹⁸ XL	
¹⁷ DREDAQENGVLQKGVPTTADR ³⁷	¹⁷⁻²⁹ Alk XL/ ¹⁹⁻³⁷ Alk XL/ ²⁰⁻³⁷ Alk XL/ ¹⁷⁻²⁹ Alk XL, Acry (3X)/ ¹⁷⁻²⁹ XL/ ¹⁵⁻²⁹ XL/ ¹⁹⁻²⁹ XL/ ¹⁹⁻³⁷ XL/ ³⁰⁻³⁷ Alk XL	
⁵⁹ ASHSIPAATITLVAEIRQGERETWGGK ⁸⁵	⁵⁹⁻⁷⁵ Alk XL/ ⁵⁹⁻⁷⁹ Alk XL/ ⁵⁹⁻⁸⁰ Alk XL/ ⁷⁴⁻⁸⁴ Alk XL/ ⁵⁹⁻⁷⁹ XL (3X)/ ⁷⁶⁻⁸⁵ XL	
⁸⁵ KMDFLLSVIGYAVDLGNIWR ¹⁰⁴	⁸⁵⁻¹⁰⁴ Alk XL/ ⁸⁶⁻¹⁰⁴ Alk XL	TM1
¹⁴⁵ NGAISIWRK ¹⁵³	¹⁴⁵⁻¹⁵³ Alk XL, Oxi (3X)/ ¹⁴⁵⁻¹⁵³ XL, Oxi (2X)/ ¹³⁷⁻¹⁵³ XL, Acry	TM2-TM3 IC Loop
¹⁵³ KIAPIFK ¹⁵⁹	¹⁴⁵⁻¹⁵⁹ Alk XL, Acry/ ¹⁵³⁻¹⁵⁹ XL, Acry (3X)/ ¹⁵⁴⁻¹⁵⁹ XL	
²³⁰ EFYLRHVLQHQHQS ²⁴³	²³⁰⁻²⁴³ XL, Acry/ ²³¹⁻²⁴³ Alk XL, Acry	TM3-TM4 EC Loop
²³⁵ HVLQIHQSK ²⁴³	²³⁵⁻²⁴³ XL (3X)	
³⁰⁸ GVVYFLKPNWQK ³¹⁹	³⁰⁸⁻³¹⁹ Alk XL, Oxi (2X)/ ²⁹⁹⁻³¹⁹ XL, Oxi, Acry/ ³⁰⁸⁻³¹⁹ XL, Oxi, Acry/ ²⁹⁹⁻³¹⁹ XL, Oxi/ ³⁰⁸⁻³¹⁹ XL	TM5-TM6 EC Loop
⁴⁴⁵ GVITAVLDFEPHIWAK ⁴⁶⁰	⁴⁴⁵⁻⁴⁶⁰ Alk XL, Acry (3X)/ ⁴⁴⁵⁻⁴⁶⁰ XL, Acry/ ⁴⁵⁴⁻⁴⁶⁰ XL, Acry (2X)/ ⁴⁵⁴⁻⁴⁶¹ XL, Acry/ ⁴⁵⁴⁻⁴⁶² XL, Acry (2X) ⁴⁴⁵⁻⁴⁶¹ Alk XL/ ⁴⁵⁴⁻⁴⁶² XL	TM8/TM8-TM9 IC Loop
⁵⁹⁷ LITSPGTLKER ⁶⁰⁷	⁵⁹⁷⁻⁶⁰⁶ Alk XL/ ⁵⁹⁷⁻⁶⁰⁷ Alk XL/ ⁵⁹⁷⁻⁶⁰⁶ Alk XL, Acry/ ⁵⁹⁷⁻⁶⁰⁷ XL, Acry (2X)/ ⁵⁹⁷⁻⁶⁰⁵ XL/ ⁵⁹⁷⁻⁶⁰⁶ XL/ ⁵⁹⁷⁻⁶⁰⁷ XL	TM12/C-Terminal
⁶⁰⁸ IKSITPETPTEIPAGDIRMNAV ⁶³⁰	⁶⁰⁶⁻⁶¹⁵ Alk XL/ ⁶⁰⁷⁻⁶¹⁵ Alk XL/ ⁶²⁰⁻⁶²⁶ Alk XL/ ⁶⁰⁷⁻⁶¹⁰ Alk XL, Acry/ ⁶⁰⁸⁻⁶³⁰ XL, Oxi/ ⁶¹¹⁻⁶³⁰ XL, Oxi/ ⁶⁰⁶⁻⁶¹⁵ XL ⁶⁰⁷⁻⁶¹⁵ XL/ ⁶⁰⁸⁻⁶²⁶ XL/ ⁶¹¹⁻⁶²⁶ XL(2X)	C-Terminal

Identified mass-shifted peptides in the dimer study in mutation R564C. Description of columns as described in table A.1.

Table A.10: R564C Monomer Crosslinks

Peptide	Modifications	Structural Location
¹ METPLNSQKVLSEAK ¹⁶	¹⁻¹⁶ XL (2X)/ ³⁻¹⁶ XL (2X)/ ³⁻¹⁸ XL/ ³⁻¹⁰ XL, Acry/ ³⁻¹⁶ XL, Acry	N-Terminal
¹¹ VLSEAKDREDAQE ²³	¹¹⁻²³ XL (2X)	
¹⁵ AKDREDAQENGVLQK ²⁹	¹⁷⁻²⁹ Alk XL, Acry/ ¹⁵⁻²⁹ Alk XL/ ¹⁵⁻¹⁸ XL/ ¹⁵⁻²⁹ XL (2X)/ ²⁰⁻³⁷ XL	
¹⁹ EDAQENGVLQKGVPTTADR ³⁷	²⁰⁻³⁹ Alk XL/ ¹⁹⁻³⁷ XL (2X)/ ²⁴⁻³⁷ XL	
⁵⁹ ASHSIPAATITLVAEIRQGE ⁷⁸	⁵⁹⁻⁷⁸ Alk XL/ ⁵⁹⁻⁸⁰ Alk XL/ ⁵⁹⁻⁷⁹ XL (2X)	
⁷⁶ QGERETWGGK ⁸⁵	⁷⁶⁻⁸⁵ Alk XL, Acry(₂)/ ⁷⁹⁻⁸⁵ Alk XL, Acry(₂)/ ⁷⁶⁻⁸⁴ Alk XL, Oxi/ ⁷⁹⁻⁸⁴ Alk XL/ ⁷⁹⁻⁸⁵ Alk XL/ ⁷⁶⁻⁸⁵ XL	
⁸¹ TWGGKMDFFLLSVIGYAVDLGNIWR ¹⁰⁴	⁸⁶⁻¹⁰⁴ Alk XL, Oxi/ ⁸⁰⁻⁸⁵ Alk XL/ ⁸¹⁻⁸⁵ XL	TM1
¹³⁷ LALGQYHRNGAISIWRK ¹⁵³	¹⁵³⁻¹⁵⁹ Alk XL, Acry/ ¹³⁷⁻¹⁵² Alk XL, Oxi/ ¹⁴⁵⁻¹⁵³ Alk XL, Oxi (3X)/ ¹³⁷⁻¹⁵³ XL/ ¹⁴⁵⁻¹⁵³ XL	TM2/TM2-TM3 IC Loop
¹⁵³ KIAPIFK ¹⁵⁹	¹⁵⁴⁻¹⁵⁹ Alk XL, Acry/ ¹⁵³⁻¹⁵⁹ Alk XL, Acry/ ¹⁵³⁻¹⁵⁹ XL, Acry/ ¹⁵³⁻¹⁵⁹ XL	TM2-TM3 IC Loop
²³¹ FYLRHVLQIHQS ²⁴³	²³⁵⁻²⁴³ XL (3X)/ ²³¹⁻²⁴³ Alk XL	TM3-TM4 EC Loop
³⁰⁸ GVVYFLKPNWQK ³¹⁹	³⁰⁸⁻³¹⁹ Alk XL, Oxi, Acry/ ³⁰⁸⁻³¹⁹ Alk XL, Oxi/ ³⁰⁸⁻³²² Alk XL/ ³⁰⁸⁻³²² XL, Acry/ ³⁰⁸⁻³¹⁹ XL	TM5-TM6 EC Loop
⁴⁴⁵ GVITAVLDFEPHIWAKR ⁴⁶¹	⁴⁴⁵⁻⁴⁶¹ Alk XL, Acry (4X)/ ⁴⁴⁵⁻⁴⁶⁰ Alk XL, Acry (2X)/ ⁴⁴⁵⁻⁴⁶² XL, Acry	TM8/TM8-TM9 IC Loop
⁴⁵⁴ FPHIWAKRR ⁴⁶²	⁴⁵⁴⁻⁵⁶² XL, Acry/ ⁴⁵⁴⁻⁴⁶¹ XL	TM8-TM9 IC Loop
⁵⁹⁷ LITSPGTLKE ⁶⁰⁶	⁵⁹⁷⁻⁶⁰⁵ Alk XL/ ⁵⁹⁷⁻⁶⁰⁷ Alk XL/ ⁵⁹⁷⁻⁶⁰⁶ XL/ ⁵⁹⁷⁻⁶⁰⁷ XL	TM12/C-Terminal
⁶⁰⁸ IKSITPETPTEIPAGDIRMNAV ⁶³⁰	⁶⁰⁶⁻⁶¹⁹ Alk XL/ ⁶⁰⁸⁻⁶²⁶ XL/ ⁶¹¹⁻⁶²⁶ XL (2X)/ ⁶²⁰⁻⁶³⁰ Alk XL	C-Terminal

Identified mass-shifted peptides in the monomer study in mutation R564C. Description of columns as described in table A.1.

Each peptide reported in tables A1-A10, is the result of the analysis of multiple spectras at different retention times. The following MSMS chromatograms illustrate the fragmentation analysis performed in this study for peptide FPHIWAKRR in Y232C Dimer.

N1 Trial 1

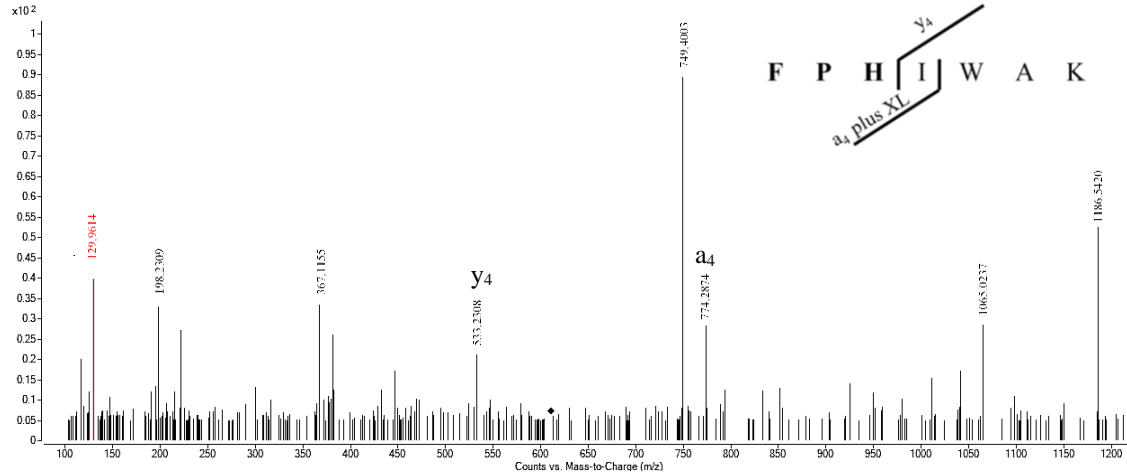


Figure A.1: ESI-QTOF-MSMS spectra of FPHIWAK crosslinked peptide at retention time 3.477. The asterisk represents the precursor ion. The double charged ion was seen at m/z 611.2839 and fragmented by CID. The fragmentation pattern is shown, with possible sites of crosslink in bold. Red peak represents an internal fragment

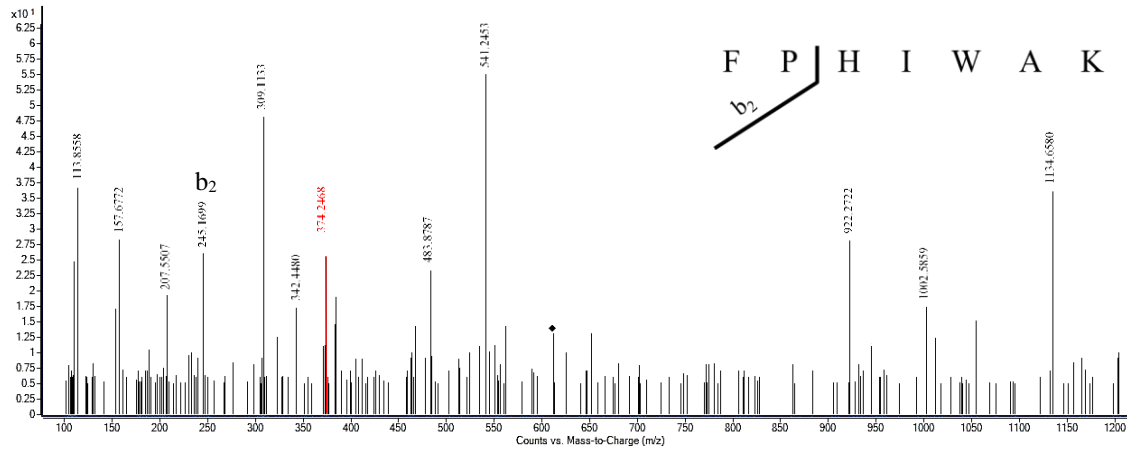


Figure A.2: ESI-QTOF-MSMS spectra of FPHIWAK crosslinked peptide at retention time 3.557. Description same as in Figure A.1.

Final result reported as FPHIWAK

N1 Trial 2

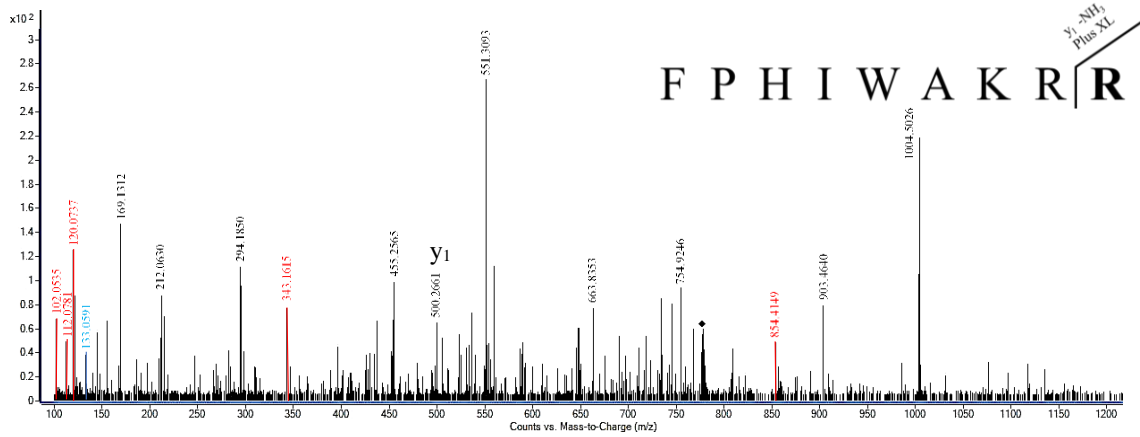


Figure A.3: ESI-QTOF-MSMS spectra of FPHIWAKRR crosslinked peptide at retention time 3.733. The asterisk represents the precursor ion. The double charged ion was seen at m/z 777.4138 and fragmented by CID. The fragmentation pattern is shown, with possible sites of crosslink in bold. Peaks shown in red represent internal ions, blue peak represents a fragment of the crosslinker.

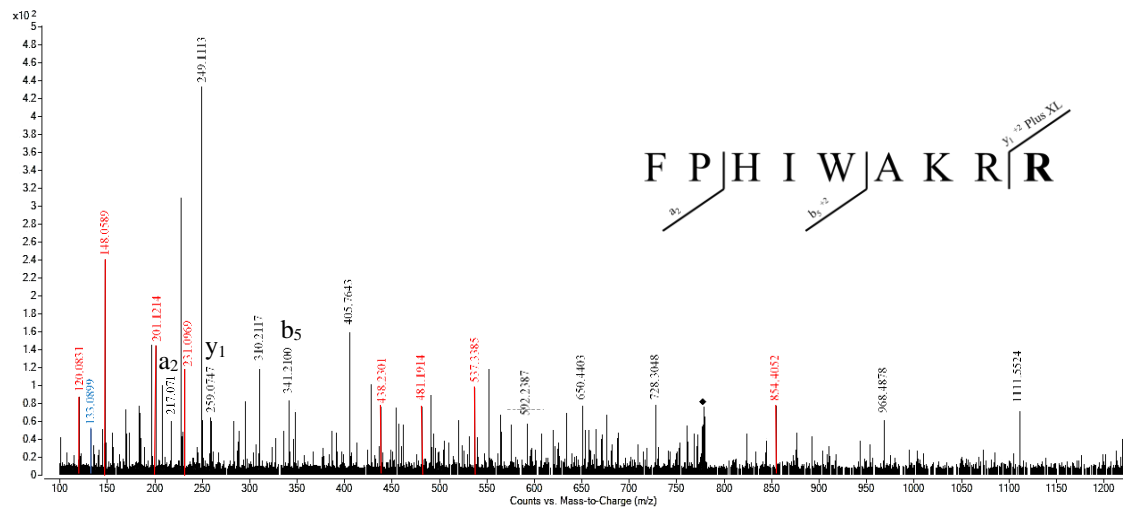


Figure A.4: ESI-QTOF-MSMS spectra of FPHIWAKRR crosslinked peptide at retention time 3.822. Description same as in Figure A.3.

Final result reported as FPHIWAKRR

N1 Trial 3

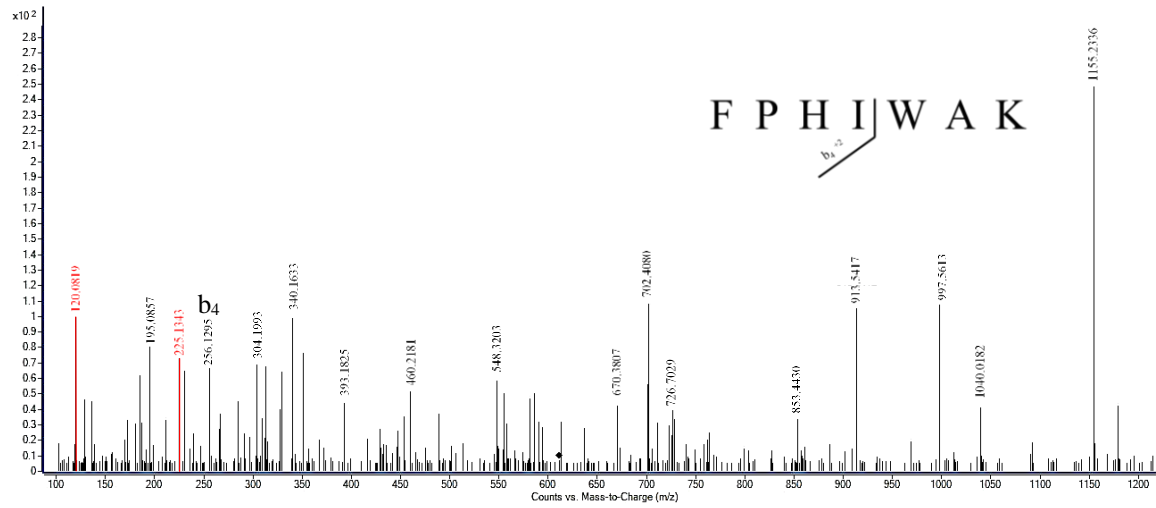


Figure A.5: ESI-QTOF-MSMS spectra of FPHIWAK crosslinked peptide at retention time 3.47. The asterisk represents the precursor ion. The double charged ion was seen at m/z 611.2855 and fragmented by CID. The fragmentation pattern is shown, with possible sites of crosslink in bold. Red peaks represent internal ions.

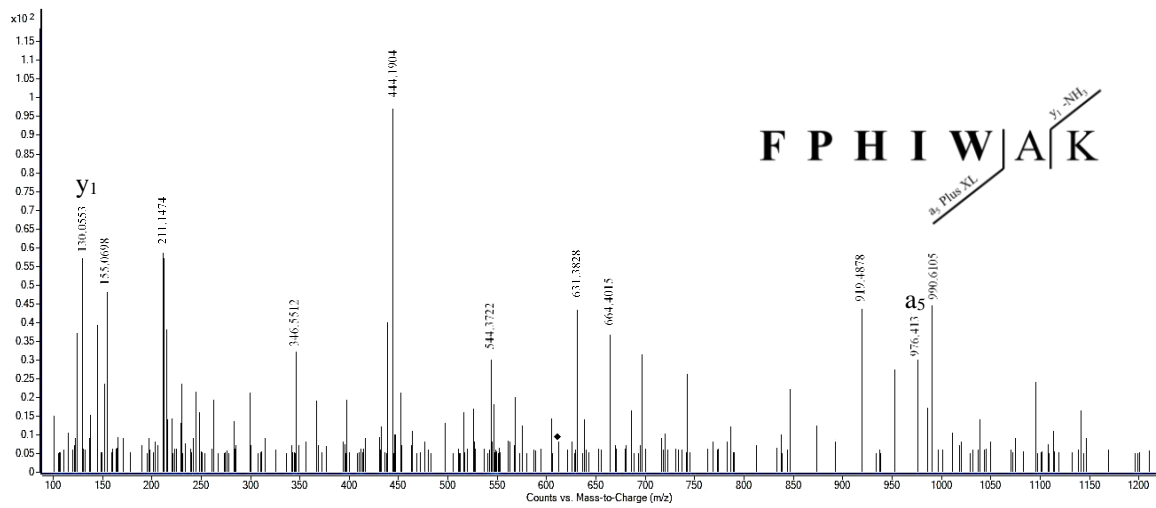


Figure A.6: ESI-QTOF-MSMS spectra of FPHIWAK crosslinked peptide at retention time 3.62. Description same as in Figure A.5.

Final result reported as FPHIWAK

N1 Trial 3

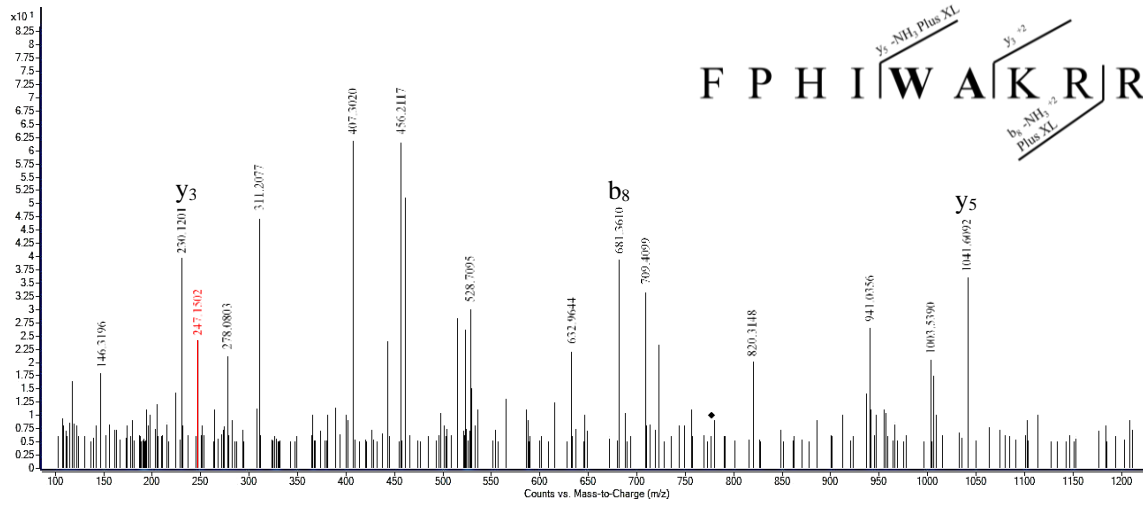


Figure A.7: ESI-QTOF-MSMS spectra of FPHIWAKRR crosslinked peptide at retention time 3.735. The asterisk represents the precursor ion. The double charged ion was seen at m/z 777.4149 and fragmented by CID. The fragmentation pattern is shown, with possible sites of crosslink in bold. Red peak represents an internal ion.

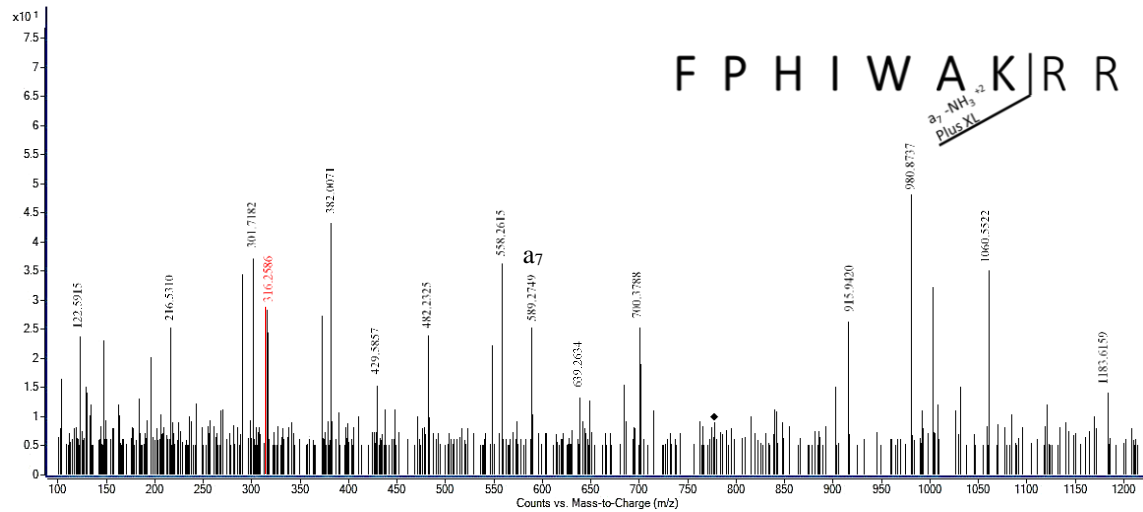


Figure A.8: ESI-QTOF-MSMS spectra of FPHIWAKRR crosslinked peptide at retention time 3.873. Description same as in Figure A.7.

Final result reported as FPHIWAKRR

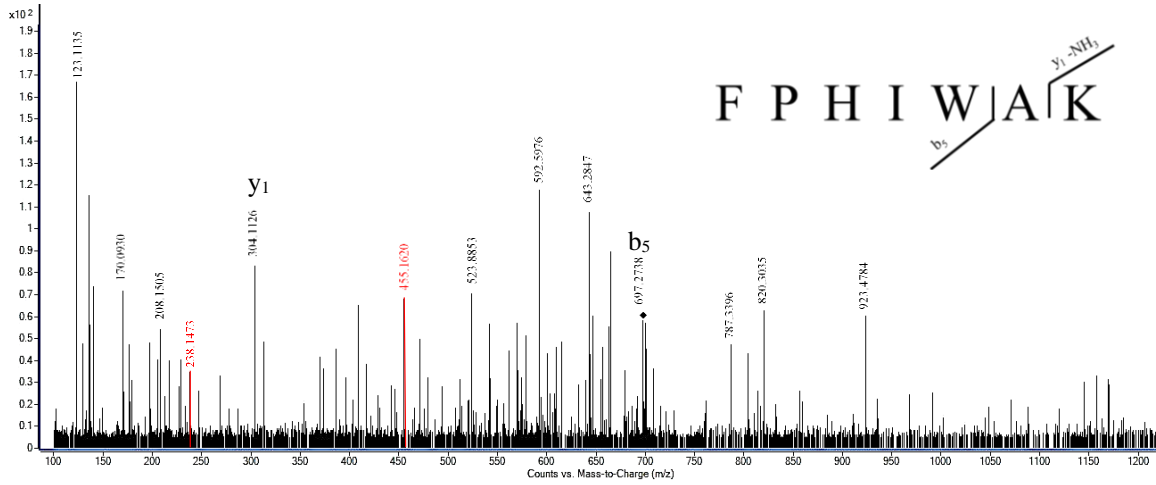


Figure A.9: ESI-QTOF-MSMS spectra of FPHIWAK crosslinked peptide at retention time 3.855. The asterisk represents the precursor ion. The double charged ion was seen at m/z 698.3000 and fragmented by CID. The fragmentation pattern is shown, with possible sites of crosslink in bold. Red peaks represent internal ions

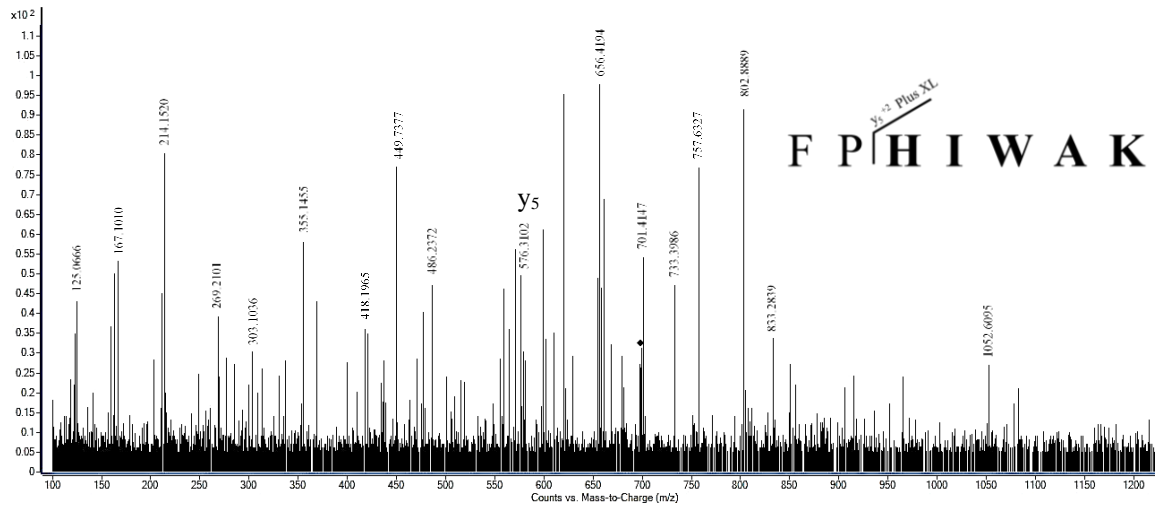


Figure A.10: ESI-QTOF-MSMS spectra of FPHIWAK crosslinked peptide at retention time 4.035. Description same as in Figure A.9.

Final result reported as FPHIWAK

N2 Trial 3

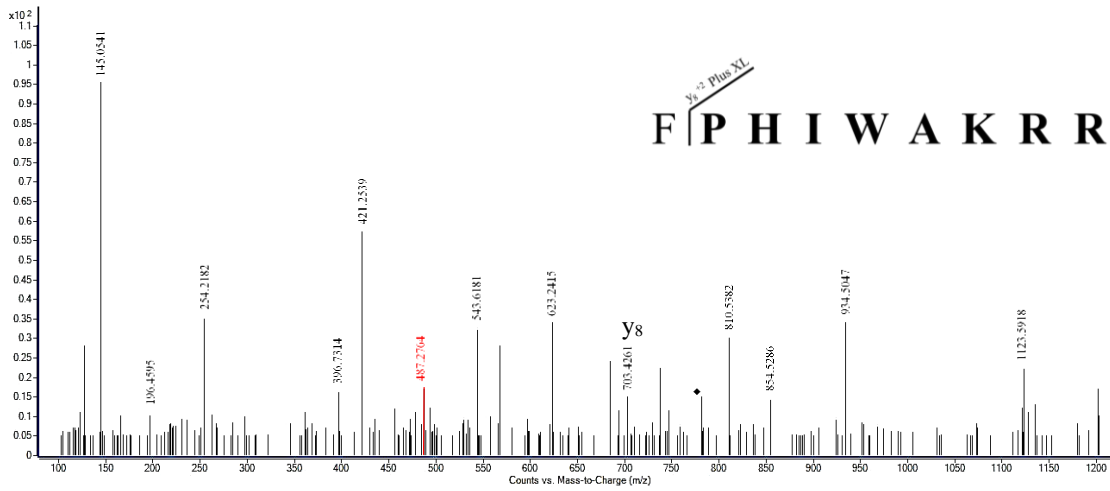


Figure A.11: ESI-QTOF-MSMS spectra of FPHIWAKRR crosslinked peptide at retention time 3.765. The asterisk represents the precursor ion. The double charged ion was seen at m/z 777.4088 and fragmented by CID. The fragmentation pattern is shown, with possible sites of crosslink in bold. Read peak represents an internal ion.

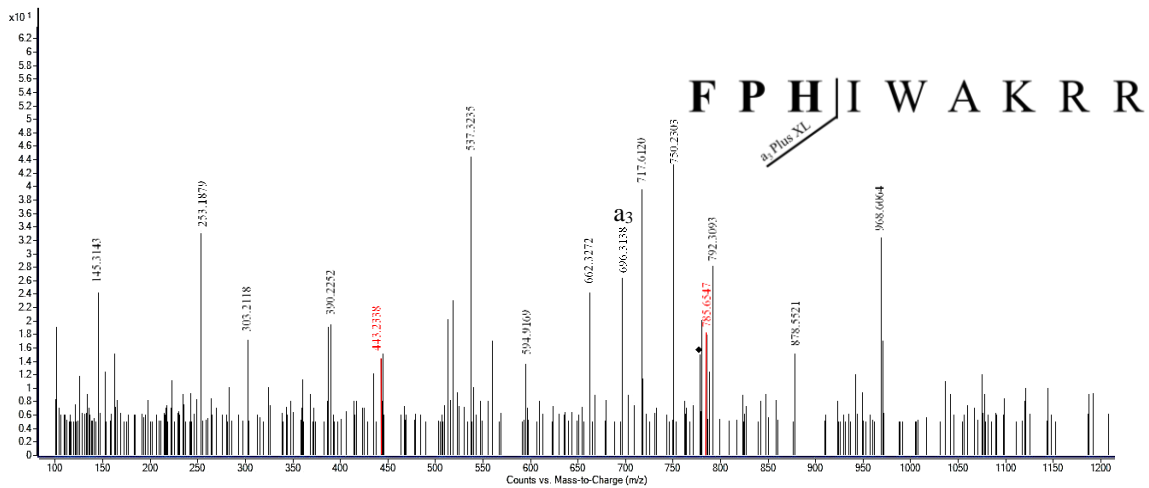


Figure A.12: ESI-QTOF-MSMS spectra of FPHIWAKRR crosslinked peptide at retention time 3.796. Description same as in Figure A.11.

Final result reported as **FPHIWAKRR**

N3 Trial 1

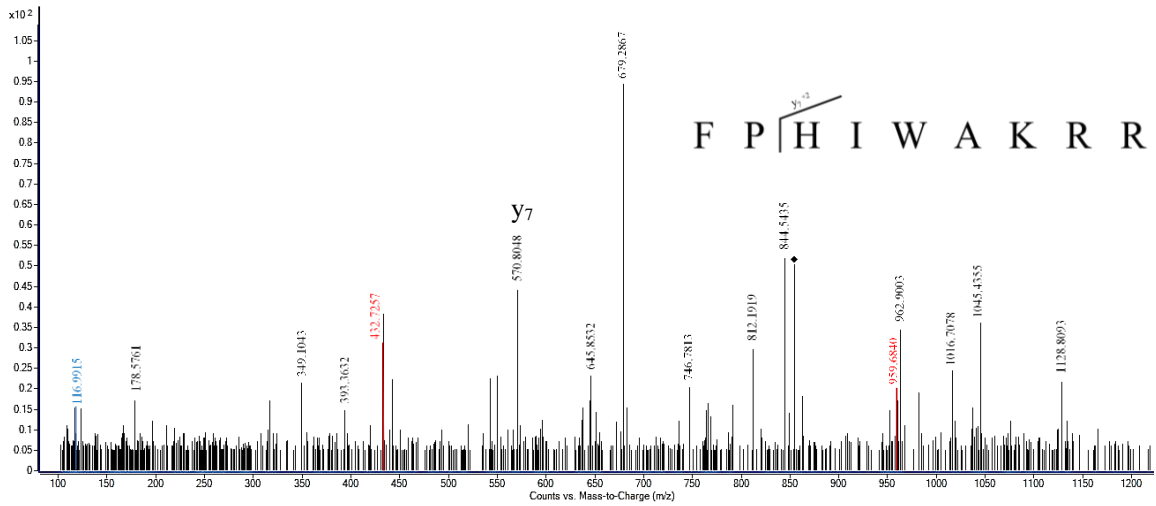


Figure A.13: ESI-QTOF-MSMS spectra of FPHIWAKRR crosslinked peptide at retention time 3.385. The asterisk represents the precursor ion. The double charged ion was seen at m/z 854.3923 and fragmented by CID. The fragmentation pattern is shown, with possible sites of crosslink in bold. Red peaks represent internal ions, blue peak represents a fragment on the crosslinker.

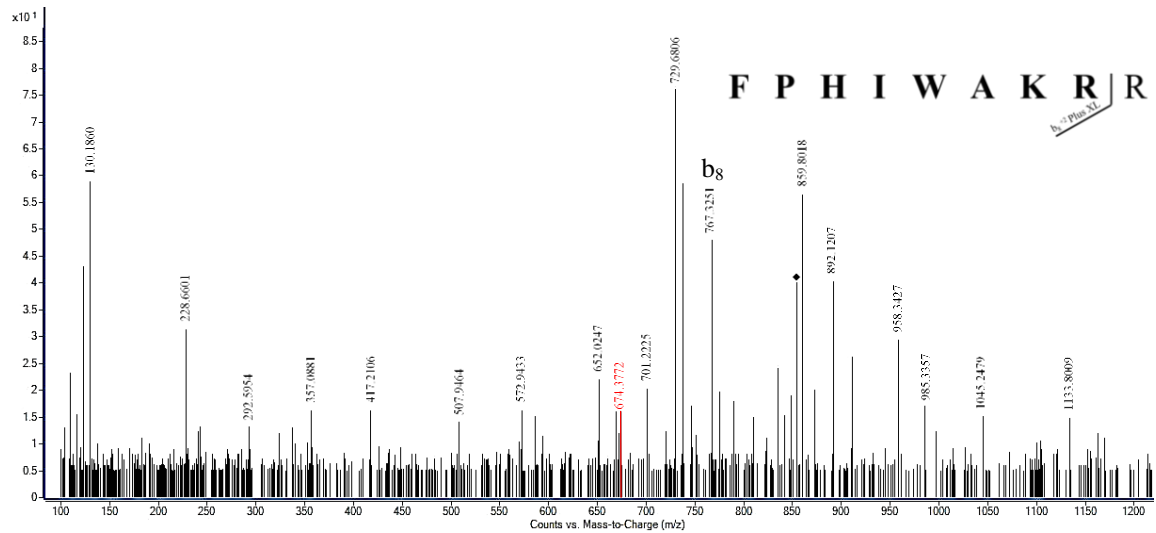


Figure A.14: ESI-QTOF-MSMS spectra of FPHIWAKRR crosslinked peptide at retention time 3.518. Description same as in Figure A.13.

Final result reported as **FPHIWAKRR**

N3 Trial 2

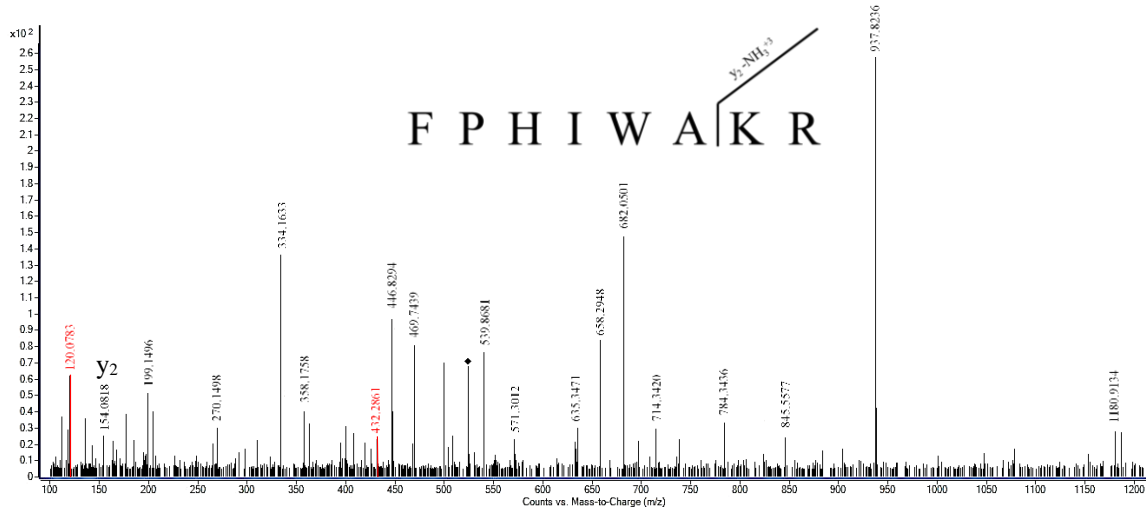


Figure A.15: ESI-QTOF-MSMS spectra of FPHIWAKR crosslinked peptide at retention time 3.445. The asterisk represents the precursor ion. The triply charged ion was seen at m/z 524.5932 and fragmented by CID. The fragmentation pattern is shown, with possible sites of crosslink in bold. Red peaks represent internal ions.

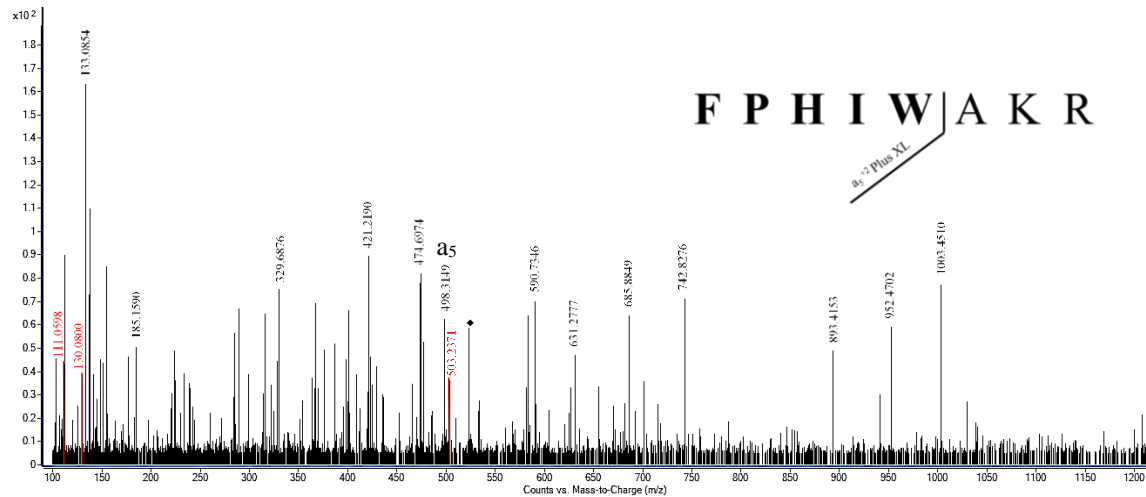


Figure A.16: ESI-QTOF-MSMS spectra of FPHIWAKR crosslinked peptide at retention time 3.557. Description same as in Figure A.15.

Final result reported as **FPHIWAKR**

N3 Trial 3

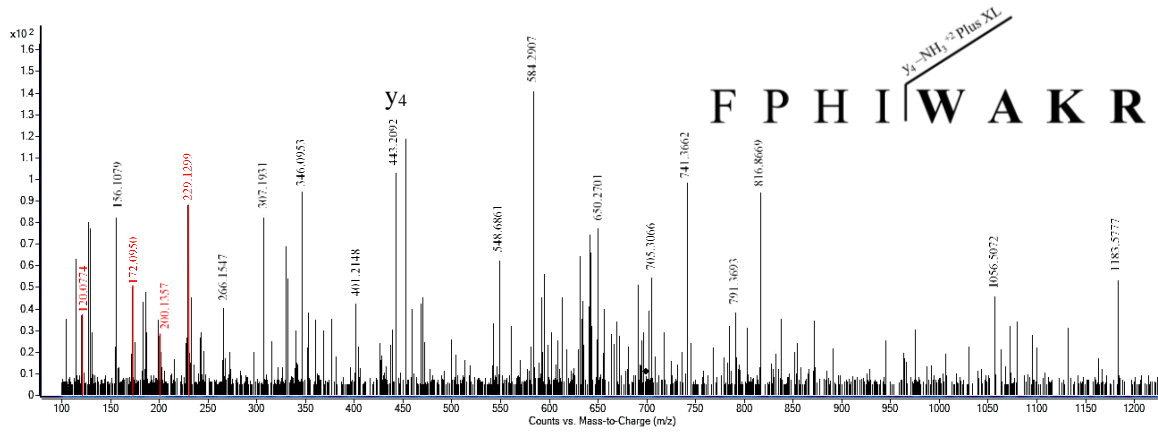


Figure A.17: ESI-QTOF-MSMS spectra of FPHIWAKR crosslinked peptide at retention time 3.6. The asterisk represents the precursor ion. The double charged ion was seen at m/z 699.3506 and fragmented by CID. The fragmentation pattern is shown, with possible sites of crosslink in bold. Red peaks represent internal ions.

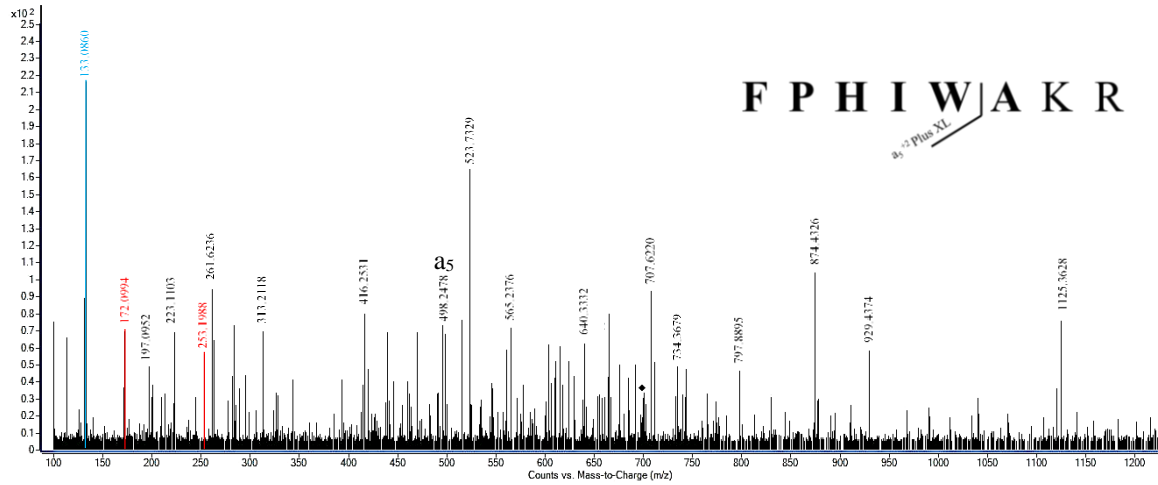


Figure A.18: ESI-QTOF-MSMS spectra of FPHIWAKR crosslinked peptide at retention time 3.741. Description same as in Figure A.17.

Final result reported as FPHIWAKR

N3 Trial 3

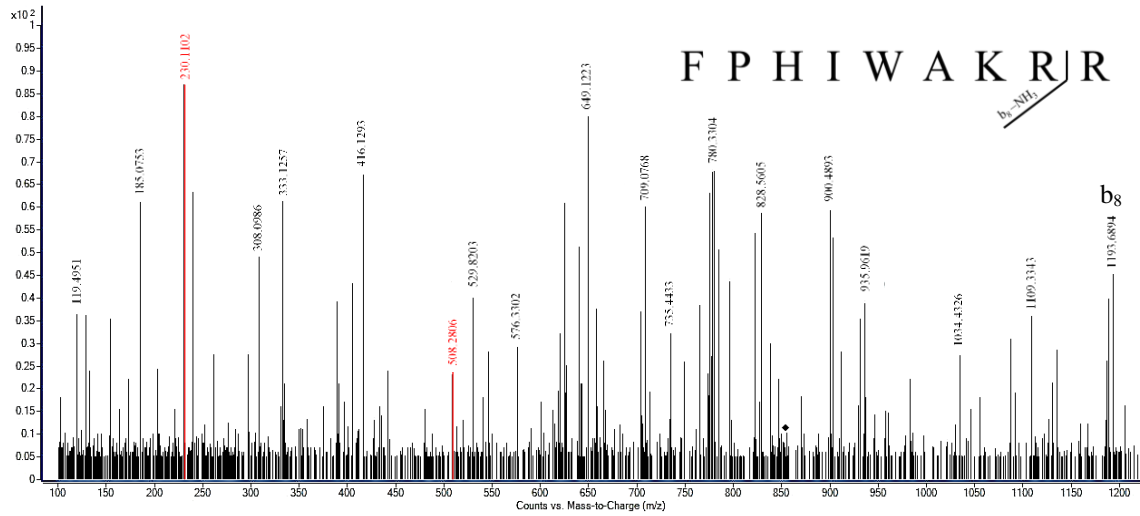


Figure A.19: ESI-QTOF-MSMS spectra of FPHIWAKRR crosslinked peptide at retention time 3.483. The asterisk represents the precursor ion. The double charged ion was seen at m/z 854.3964 and fragmented by CID. The fragmentation pattern is shown, with possible sites of crosslink in bold. Red peaks represent internal ions.

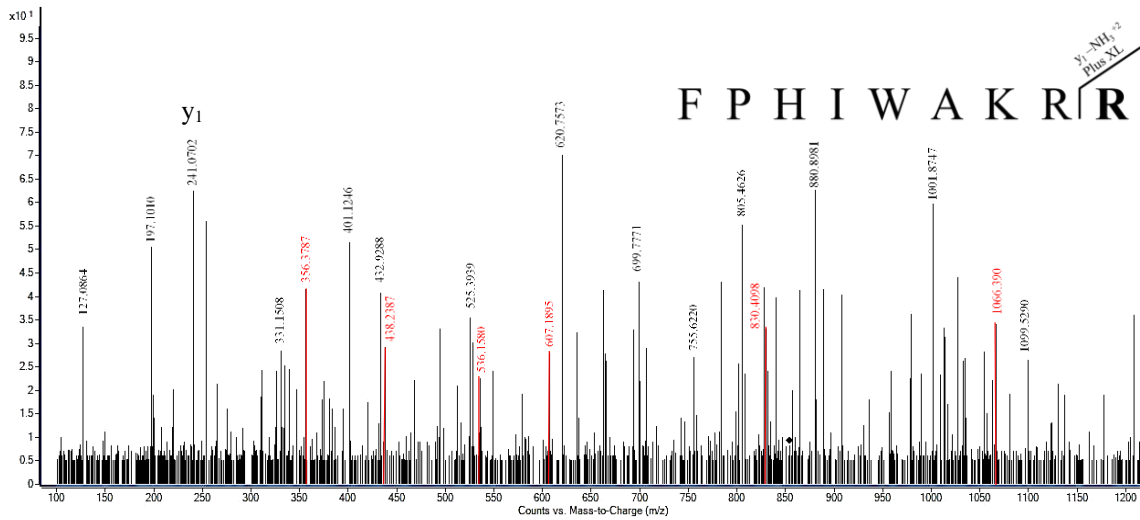
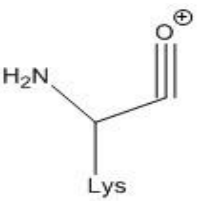
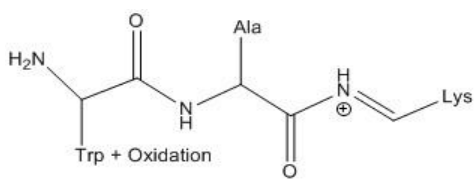
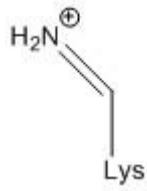
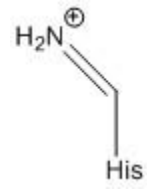


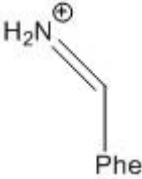
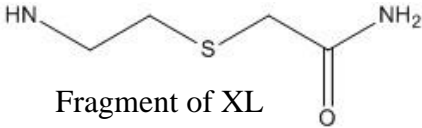
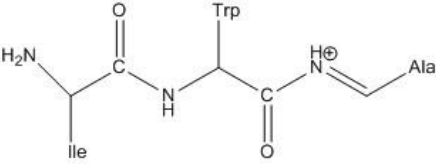
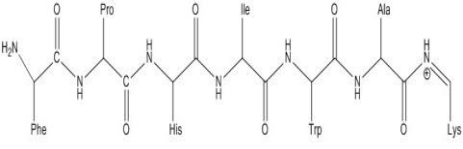
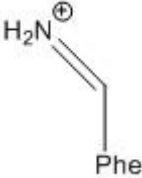
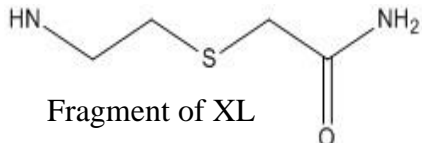
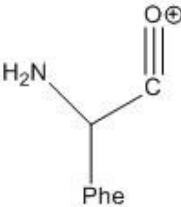
Figure A.20: ESI-QTOF-MSMS spectra of FPHIWAKRR crosslinked peptide at retention time 3.515. Description same as in Figure A.19.

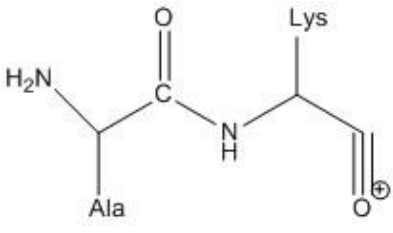
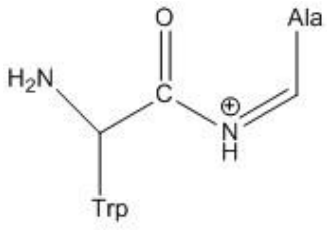
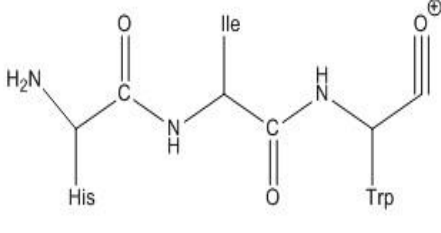
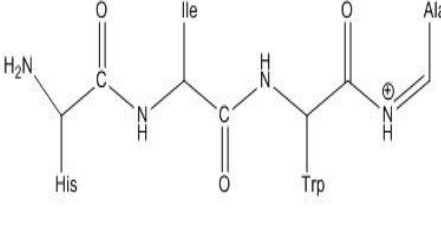
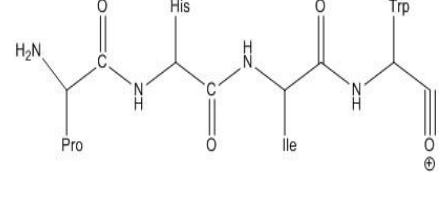
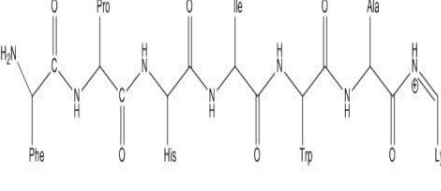
Final result reported as FPHIWAKRR

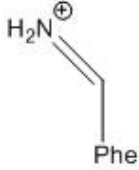
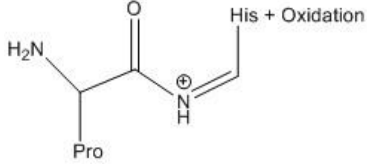
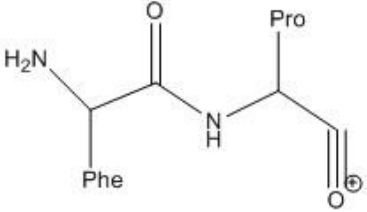
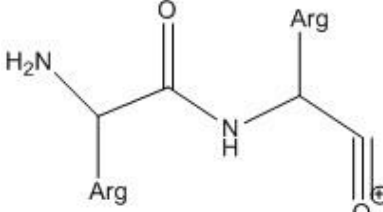
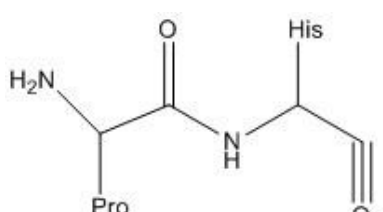
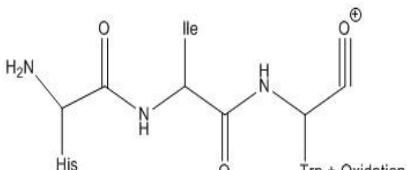
Internal ions were observed in most spectras. They result from subsequent collisions and continuing absorption of energy by “y” and “b” ions after the first bond breakage. Typically, under CID “a”, “b” and “y” ions are produced. However, a CID fragmentation study by Khatun et al. showed that high energy CID can produce a, x, c and z ions [217]. In this study, we observed immonium ions and internal ions produced by the neutral loss of water or ammonia. As well as unlikely internal ions but which were possible due to high energy CID, as described by Khatun et al. These internal ions have been reported before [217, 218] and a list of all internal ions found are reported in table A.11.

Table A.11: Internal ion fragments

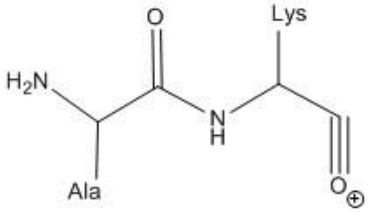
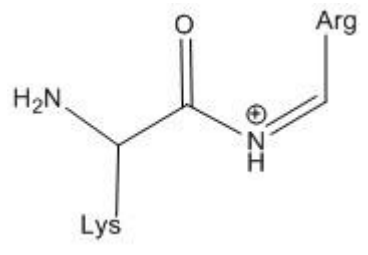
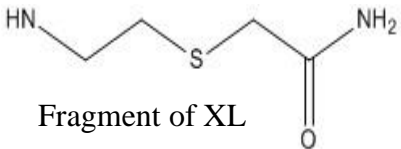
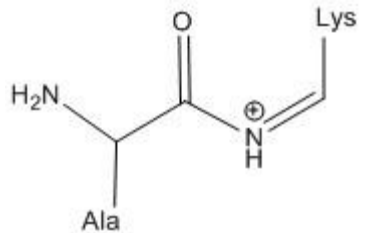
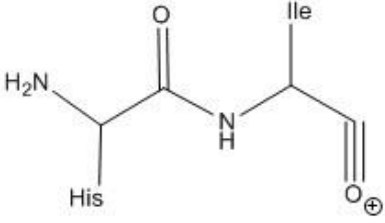
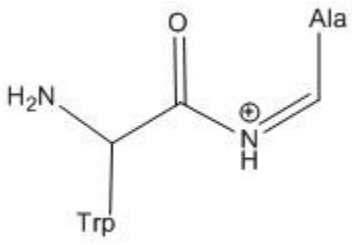
Internal Ion Fragment	Theoretical m/z	Observed m/z	Trial	Retention Time
	129.102788	129.9614	N1T1	3.477
	374.219215	374.2468	N1T1	3.557
	101.107873	102.0535	N1T2	3.733
	111.079647	112.0781		

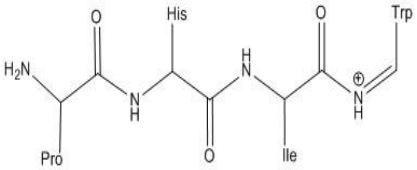
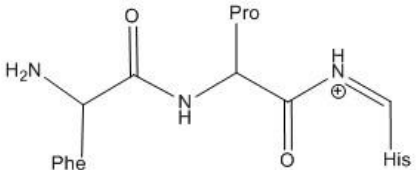
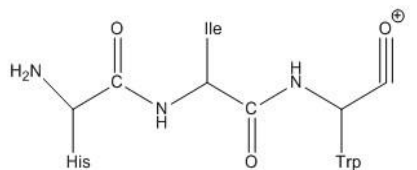
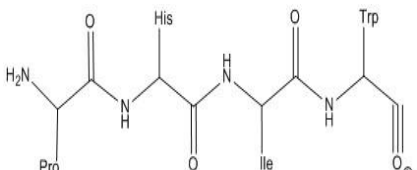
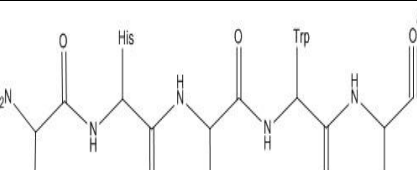
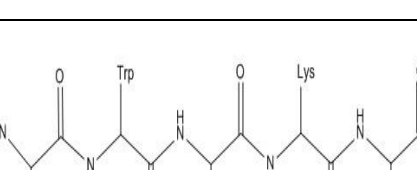
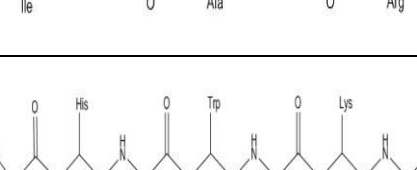
	120.081324	120.0737		
 <p>Fragment of XL</p>	133.043559	133.0591		
	343.213401	343.1615		
	854.504104	854.4149		
	120.081324	120.0831	N1T2	3.822
 <p>Fragment of XL</p>	133.043559	133.0899		
	148.076239	148.0589		

	200.139902	201.1214		
	230.129337	231.0969		
	438.237939	438.2301		
	481.280138	481.1914		
	536.298528	537.3385		
	854.504104	854.4052		

	120.081324	120.0819	N1T3	3.47
	225.135151	225.1343		
	246.136828	247.1502	N1T3	3.735
	315.225697	316.2586	N1T3	3.873
	237.135151	238.1473	N2T2	3.855
	454.232854	455.1620		

	486.362859	487.2764	N2T3	3.765
	443.32066	443.2338	N2T3	3.796
	785.526236	785.6547		
<p>Lys + Acrylamide</p>	432.263108	432.7257	N3T1	3.385
	959.572535	959.6840	N3T1	3.385
	673.349578	674.3772	N3T1	3.518
	120.081324	120.0783	N3T2	3.445

	200.139902	200.1357		
	229.202836	229.1299		
 <p>Fragment of XL</p>	133.043559	133.0860	N3T3	3.741
	172.144987	172.0994		
	252.158626	253.1988		
	230.129337	230.1102	N3T3	3.483

	508.303613	508.2806		
	356.20865	356.3787	N3T3	3.515
	438.237939	438.2387		
	536.298528	536.1580		
	607.335642	607.1895		
	830.458514	830.4098		
	1066.58584	1066.3902		

Internal ion fragments observed in chromatograms A.1-A.20 from peptide FPHIWAKRR (at times observed as FPHIWAKR or FPHIWAK due to miss cleavages) for the dimer study on mutation Y232C.